University of Bergen

Department of physics and technology

Master thesis in
Measurements Science and Instrumentation

Evaluation of the Field Kelvin Probe for non-intrusive condition monitoring of concrete reinforcements

Simen Kaasa Hellner
Spring 2020

Abstract

Early detection of corrosion in reinforced concrete is of great importance for safe operation of the concrete based infrastructure we rely on such as bridges and large buildings. Undetected corrosion in the steel reinforcements can prove costly, both in terms of repair costs and in the worst case scenario, loss of human lives as was recently seen in Genoa, Italy. New and improved inspection techniques can potentially drastically improve the detection rate, thus reducing costs, and even save lives.

In this thesis a novel instrument, the Field Kelvin Probe (FKP), a handheld field instrument operating on the same principle as the original Kelvin Probe, has been evaluated for the first time with for the purpose of using it as a tool for inspection of reinforced concrete. Multiple test samples have been designed and constructed from scratch over the course of the project to evaluate the capabilities of the FKP, from the detection of embedded metal to detection of imitated corrosion in rebars. Using these test samples, it was shown that the FKP can locate the embedded steel and detect potential gradients matching those one would expect during active rebar corrosion, even beneath coated surfaces. A simple model was created to describe the results, with very good agreement between theory and experiments. The results presented in this thesis indicate that the FKP has the potential to be a powerful handheld no-contact inspection tool that could eventually become the trusted technique for inspection of reinforced concrete.

Supervisors:

Bodil Holst[1], Eugen Florin Turcu[2], Sylvia Keßler[3]

[1]University of Bergen (Bergen, Norway)
[2]NORCE Norwegian Research Center AS (Bergen, Norway)
[3]Helmut Schmidt University (Hamburg, Germany)

Acknowledgements

First, a huge thank you to my supervisors, Bodil and Florin. To Bodil, for invaluable guidance and patience during the writing process. To Florin, for great advice and motivation during the thesis work and for really making me feel like a member of the team. The time spent in the lab at NORCE has been way more enjoyable and inspiring than I ever imagined. For this, the rest of the people at NORCE also deserve a shout, thank you to Kjetil, Inge, Gaute, and Frank for all help and support I received during my project. I also want to thank my co-supervisor Sylvia for providing a different perspective to the project and helping with the idea for the final experiment.

I want to thank the staff, professors, and fellow students and friends at the Department of Physics and Technology for a great sense of community. A very special thank you goes out to Odin and Alex for your friendship and moral support over the last five years and for always being available whenever I needed a distraction.

Last, but certainly not least, I want to thank all my family and friends for your support. A very special thank you to my parents and my sisters, for always supporting and encouraging me. Thank you, I could never have done any of this without you!

Simen Kaasa Hellner

23.03.2020

List of abbreviations

NDT	Non-Destructive Testing
NII	Non-Intrusive Inspection
CSE	Copper Sulphate Electrode
KP	Kelvin Probe
FKP	Field Kelvin Probe
SKP	Scanning Kelvin Probe
CPD	Contact Potential Difference

List of figures

Table of contents

1 Introduction

1.1 Motivation

Figure 1: Genoa bridge collapse, August 14th, 2018. Corrosion is a possible cause. [1]

Concrete structures are a vital part of the infrastructure we rely on. Many large load-bearing structures are built using concrete, examples include road bridges, storage tanks, offshore oil rigs, and many more. To enhance the structural strength of these structures, reinforcing steel bars (rebars) are usually placed inside the concrete. The condition of the concrete reinforcements is critical for the safe operation of these structures and undetected deterioration can prove costly, either by repair costs or, in the worst case scenario, collapse and loss of human lives[1]. An important source of deterioration is chloride induced corrosion of the reinforcements. Structures exposed to de-icing salt or in coastal and marine environments are therefore particularly at risk. Norway alone has around 18000 road bridges, many of them concrete based [2]. With a large portion of Norwegian roads being situated in a coastal climate, and de-icing salts being a widespread method for removing snow and ice from roads, corrosion is inevitable.

In 2016, the National Association of Corrosion Engineers (NACE) released the two-year global study “International Measures of Prevention, Application and Economics of Corrosion Technology (IMPACT)”, in which they estimated the annual global cost of corrosion damages to be US$2.5 trillion, equivalent to roughly 3.4% of the global GDP at the time[3]. By improving how corrosion is dealt with, they estimated that the global cost could be improved by between 15-35%.

"The IMPACT study reinforces what recent news headlines have made all too clear: there needs to be a change in how corrosion decisions are made," said Bob Chalker, CEO of NACE International. "Whether it is a pipeline, an airplane, a water treatment plant or highway bridge, corrosion prevention and control is essential to avoiding catastrophic events before it’s too late."[4]

The challenge then lies in the detection of ongoing corrosion in the concrete reinforcement, so that preemptive measures can be taken. Many of the current inspection methods have one or more of the following drawbacks: slow, unreliable, imprecise and costly, both in terms of man-hours and due to interrupted operation while the inspections take place. A new approach to corrosion monitoring of concrete reinforcements is needed. In this thesis work the Field Kelvin Probe, a novel technology developed by one of my supervisors (Dr. Eugen Florin Turcu, NORCE), is evaluated for the first time as a new technique for monitoring corrosion in concrete reinforcements.

Parts of the work presented in this thesis was presented as an oral contribution at Eurocorr 2019 is Seville, Spain, and also as a poster at Overflate 2019 in Bergen, Norway (See Appendix II).

1.2 Corrosion

The main topic of this thesis is related to the testing of new instrumentation, however a basic understanding of the corrosion process, and how it relates to electric potentials (more on this in chapter 2.1), is necessary to describe the Field Kelvin Probe (FKP). A brief introduction to corrosion is therefore presented here, while a more thorough explanation of how corrosion is measured is discussed in the theory chapter (section 2.1).

1.2.1 What is corrosion?

Most metals are found in nature in various chemical compounds, or ores. Ore is natural rock or sediment containing minerals, typically metals that can be extracted [5]. For example, iron is usually found in iron ore as various types of iron oxide. Corrosion of metals is a natural consequence of the smelting process, where the metal is separated from its natural compounds and reaches a metallic state. The natural compounds represent low energy states and the energy required to extract metallic iron from iron ore through smelting, is returned to the environment when the metallic iron converts back to iron oxide by corrosion [6]. Corrosion of iron is an electrochemical process that begins with the transfer of electrons from iron to oxygen (oxygen reduction) [7]. The iron acts as the reducing agent, giving up electrons, while the oxygen acts as the oxidising agent, absorbing electrons. While dry corrosion (without the presence of water) is possible, the corrosion rate is affected by the presence of water. In the case of rebar corrosion, water is involved in the reaction. The reduction of oxygen follows the following formula:

$$O_2 + 4e^- + 2H_2O \rightarrow 4OH^-$$

The oxidation of iron provides the electrons for the above process:

$$2Fe \rightarrow 2Fe^{2+} + 4e^{-}$$

Corrosion occurs when these two processes (reduction and oxidation) happen simultaneously. The complete reaction is then:

$$2Fe + O_2 + 4e^{-} + 2H_2O \rightarrow 2Fe^{2+} + 4e^{-} + 4OH^{-}$$

The iron and hydroxide ions then react, forming iron hydroxide:

$$2Fe^{2+} + 4OH^{-} \rightarrow 2Fe(OH)_2$$

All corroding systems are comprised of four components: an electrolyte to allow movements of ions, an anodic reaction, a cathodic reaction, and an electrolytic path through which electrons can move between the anodic and cathodic regions. The anodic region is where the metal is effectively dissolved, and the cathodic region consumes the electrons from the anodic reaction. If corrosion occurs in a rebar, the concrete pore structure (which is filled with pore solution) provides the electrolytic path, while the rebar itself provides a path for the electrons[8], as shown in Figure 2.

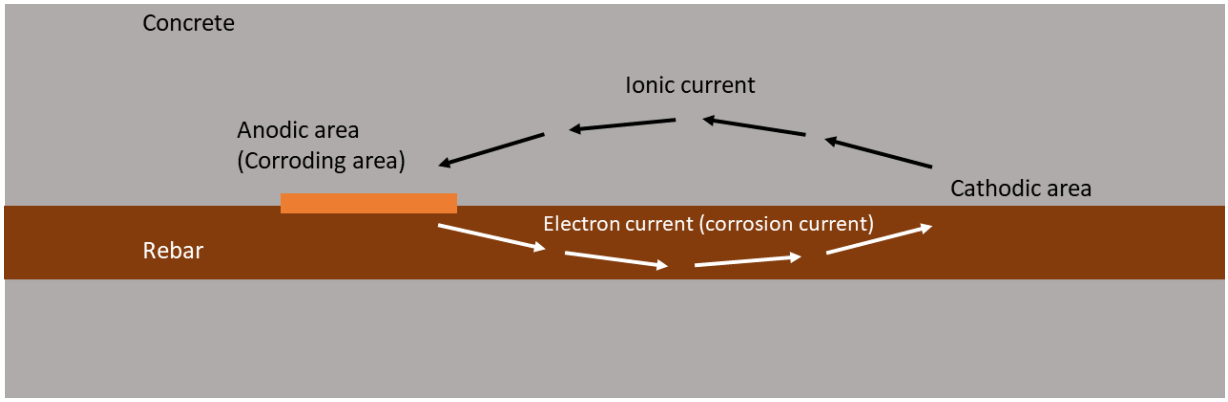

Figure 2: A corroding rebar. The metal is corroding at the anodic area. The electrons produced in the anodic reaction are consumed in the cathodic reaction.

When a rebar corrodes in a concrete structure, the first easily visible sign is usually cracking or spalling of the concrete surface, as shown in Figure 3. If the corrosion process continues, the rebar will over time corrode until the complete loss of cross section, severely compromising the structural strength of the construction.

Figure 3: Corrosion-induced cracking has exposed a rebar and resulted in spalling of the concrete wall.

Due to the chemical properties of the concrete mixture, a thin iron oxide layer, or passive layer, is formed on the rebar during concrete casting, in a process called passivation [9]. If a critical amount (critical threshold) of saltwater (chlorides) reaches the rebar, de-passivation of the rebar occurs, and the passive layer breaks down. The main sources of chloride attack on concrete structures are de-icing salts and saltwater spray in marine environments[10]. The key reactions for the chloride induced breakdown of the passive layer are as follows:

$$Fe^{2+} + 2Cl^{-} \rightarrow FeCl_2$$

$$FeCl_2 + 2H_2O \rightarrow Fe(OH)_2 + 2HCl$$

This is when corrosion can occur, and why concrete structures in marine environments are particularly at risk.

1.3 State-of-the-art NII methods and the technology gap

Several methods for Non-Invasive Inspection (NII) of concrete reinforcements are available on the market, all with advantages and disadvantages. It is important to note that in many cases, especially in marine environments, a coating is applied to the concrete surface for corrosion

protection. In this chapter, two NII-methods will be discussed briefly in an attempt to highlight the technology gap and explain why a new approach is needed.

1.3.1 The half-cell potential method

Half-cell potential measurements is the most common method for corrosion inspection of concrete structures[11]. Using a reference electrode, often a copper/copper sulphate ($Cu/CuSO_4$) electrode (CSE), and connecting it through a voltmeter to an exposed piece of rebar, the inspector can read out the potential difference between the reference electrode and the rebar.

Figure 4 shows a schematic of a half-cell potential measurement.

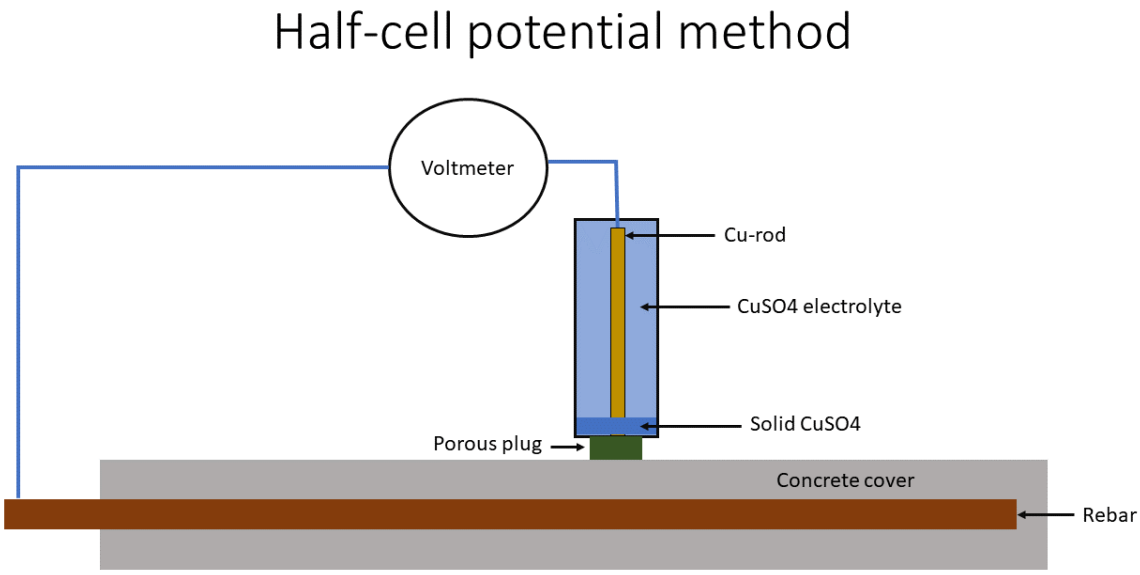

Figure 4: Schematic of the half-cell potential measurement method on a rebar embedded in concrete. The $CuSO_4$ electrode forms one half-cell and the rebar forms the other half-cell

Since the electric potential of the first half-cell, the reference electrode, is fixed and known (ca. +0.317V with respect to the normal hydrogen electrode[12], this is an industry standard), the potential of the other half-cell, the steel in the concrete, can be found by measuring the potential difference between the two. The inspector can create a potential map of the steel and concrete surface by repeating the measurements in a grid across the surface. An example of such a potential map (often called equipotential plot) is shown in Figure 5, where the axes represent distance in mm and the colour scale represents the half-cell potential reading in mV [13]. The probability of active corrosion can be assessed by looking at the most negative potential readings in combination with pronounced potential gradients of 100mV or more.

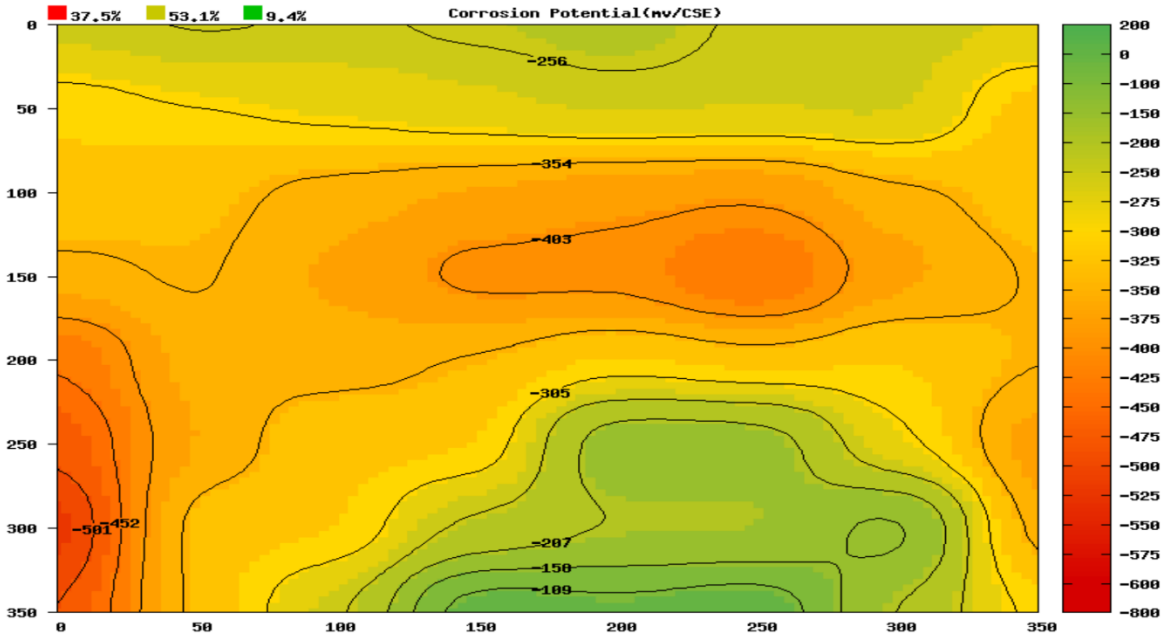

Figure 5: Example of a potential map (equipotential plot) obtained from half-cell measurements. The axes represent distance in mm and the colour scale represents the half-cell potential reading in mV. Measurements were carried out in 50mm steps in both directions. [13]

As mentioned, the half-cell potential method requires connection with the embedded rebar. This may or may not mean that the inspector will have to dig into the concrete to expose the rebar. Measurements with the reference electrode also requires pre-wetting of the concrete surface with an electrolyte (e.g. tap water), and a stabilisation period of at least a few minutes per measurement, as the electrolytes of the electrode and the concrete bulk need to mix and stabilise. Additionally, as discussed in section 3.3.4, evidence has emerged during the work on this thesis suggesting that the copper leaking from the CSE permanently alters the chemistry (and electric potential) of the concrete, meaning it might not be truly non-destructive. As a final remark on the half-cell potential method, since the reference electrode requires direct electric contact with the concrete surface in order to perform measurements, it is unable to measure through a non-conducting coating.

1.3.2 Four-probe Wenner array

Another possible approach to condition assessment of concrete reinforcements that avoids several of the hurdles encountered with the half-cell method is using a four-probe Wenner array configuration, shown in Figure 6. By applying a varying AC current between the outer two electrodes, and measuring the potential drop response between the inner electrodes, the instrument can extract the impedance response of the rebar, which can be used to determine the

corrosion conditions including corrosion rate and concrete resistivity[14, 15]. This method is non-destructive in the sense that it does not require contact with an exposed rebar and it only requires electric contact to the surface to apply the current. The measurement resolution is only limited by the distances between the probes and such an instrument could, in principle, be built in any size.

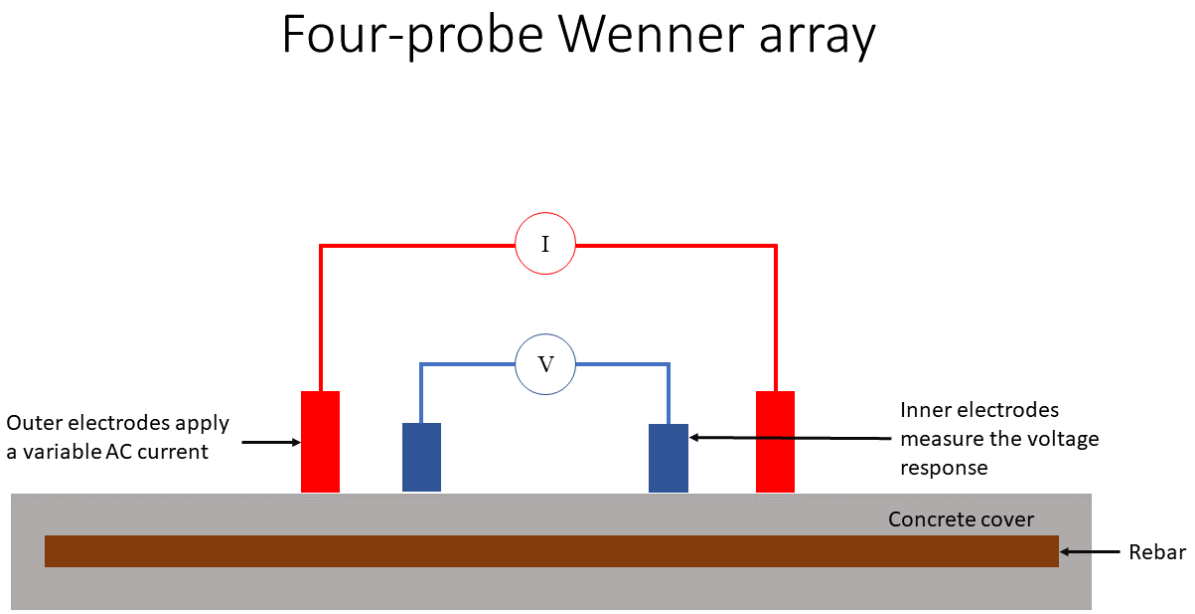

Figure 6: Schematic of the four-probe Wenner array configuration for measurements on concrete.

While this method is a good approach to condition assessment of uncoated concrete, it has one of the same drawbacks as the half-cell method. Since direct electric contact with the concrete surface is required, a coating will render it unusable.

1.3.3 The technology gap

In Summary, the current methods for corrosion condition inspection of concrete reinforcements available on the market are lacking in certain aspects. Corrosion potentials can be measured using the half-cell potential method, but not necessarily in a quick, accurate, and non-destructive manner. The four-probe allows quick measurements of corrosion rate and the creation of potential maps. The main hurdle is that a protective coating will prevent these methods from being used. In this thesis, a new approach, the Field Kelvin Probe (FKP), is presented and evaluated. The FKP is non-intrusive, works on coated surfaces, and may prove to be the answer to many issues encountered by the industry, academia, and institutions dealing with corrosion in concrete reinforcements.

2 Background and theory

2.1 Electric potentials and corrosion

Arbitrary electric potential differences, dependent on the charge distribution, exist between two pieces of metal, metal 1 and metal 2, that are insulated from one another. If the two pieces of metal are brought into mutual electric contact the charges will redistribute, making the electric potentials of the two metals, and hence the potential difference between the two, well defined. If the two pieces are different materials, a certain potential will be established at the junction. This potential is known as the Galvani potential, $\phi_G^{(1,2)}$ of the junction.

Now, consider two conductors in mutual contact in vacuum. See Figure 7 for the following descriptions. They will have surface potentials $\chi^{(1)}$ and $\chi^{(2)}$, meaning the potential difference between a point just outside the conductor (a, b) and a point inside the conductor (A, B). The Galvani potential, $\phi_G^{(1,2)}$, is established between the two conductors. The potential difference between points a and b, located just outside the conductor is known as the Volta potential, $\phi_V^{(1,2)}$, or the contact potential difference (CPD). The relation between the three potentials is the following:

$$\phi_V^{(1,2)} = \chi^{(1)} - \chi^{(2)} + \phi_G^{(1,2)} \quad (1)$$

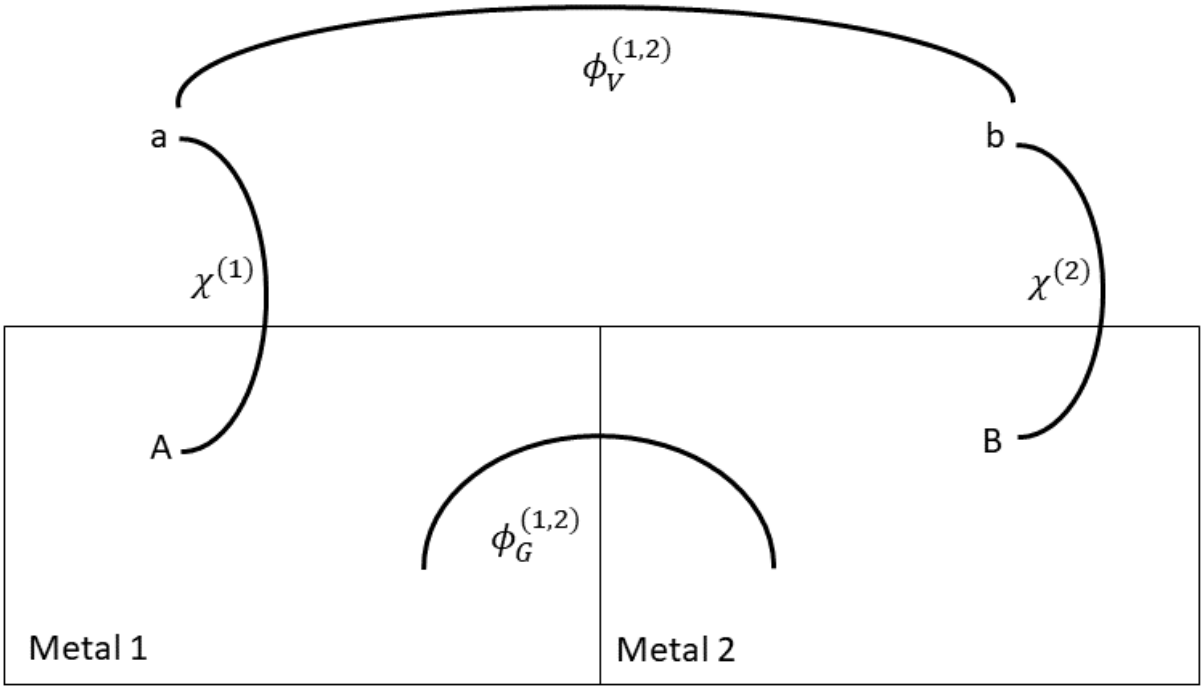

Figure 7: Two metals in electric contact in vacuum. The Galvani potential, $\phi_G^{(1,2)}$, is the electric potential difference between the two metals. The surface potentials, $\chi^{(\ )}$, is the potential difference between a point just outside the conductor surface (a,b) and a point inside the conductor (A,B). The Volta potential, $\phi_V^{(1,2)}$, or contact potential difference (CPD) is the potential difference between points a and b.

Because points a and b are in the same medium (vacuum in this case), the Volta potential can be measured, which is not the case for the Galvani potential. The Volta potential between two metals is directly related to the work functions of these two metals[16]. The work function of a material is defined as the minimum amount of work required to remove an electron from the material to a point just outside the surface. Both chemical and electrostatic work is considered. The work function Φ can be written as:

$$\Phi = -\mu_e + e\chi \tag{2}$$

Where μ_e is the chemical potential of the material, i.e. the chemical work required to transfer an electron from infinitely far away, into the sample and e is the elementary charge. As will be explained in section 2.2.2, the work function, and hence the contact potential, is directly measurable with the Kelvin Probe (and the Field Kelvin Probe). Since the work function is a defining property of a material, different materials can then be distinguished with a KP.

In the case of corrosion of the metal, it would no longer be sensible to talk about work functions, as the work function of a metal does not change when the metal corrodes. Corrosion, in most cases, is not uniform but rather dispersed over several active spots. When steel embedded in concrete undergoes active corrosion, it develops a relatively high negative electric potential in comparison to the surrounding concrete, which is can be measured with a reference electrode such as a CSE or Kelvin Probe. The potential difference between the steel and the concrete can be in the order of several hundred millivolts. During active rebar corrosion, as mentioned in section 1.2.1, anodic and cathodic regions will form on the rebar. Two main reactions are responsible for this[17]:

i) Iron oxidation, which represents the anodic area and liberates electrons from the steel in the following way: $2Fe \rightarrow 2Fe^{2+} + 4e^{-}$

ii) Oxygen reduction, which consume the electrons from the anodic reaction in the following way: $O_2 + 2H_2O + 4e^{-} \rightarrow 4OH^{-}$

In the absence of additional electron sources, under steady conditions without external influences, the two reaction rates are equal.

For the description of corrosion, it is customary to talk in terms of current densities, not reaction rates. For a particular reaction, the current density, j, can be described by relating the current generated over time to the number of electrons that have been transferred in the reaction:

$$j = nFR \tag{3}$$

Where n is the number of valence electrons for the particular material (e.g. 2 for iron), F is Faraday's constant ($F = 96500\ C/mol\ of\ electrons$), and R is the reaction rate. Under steady state conditions, the relationship between the anodic and cathodic reactions can be described by $j_c = -j_a$, where j_c and j_a are the cathodic and anodic current densities, respectively. Plotting both reactions in terms of current density with respect to the electric potential of the steel yields a so-called polarization diagram, as shown in Figure 8.

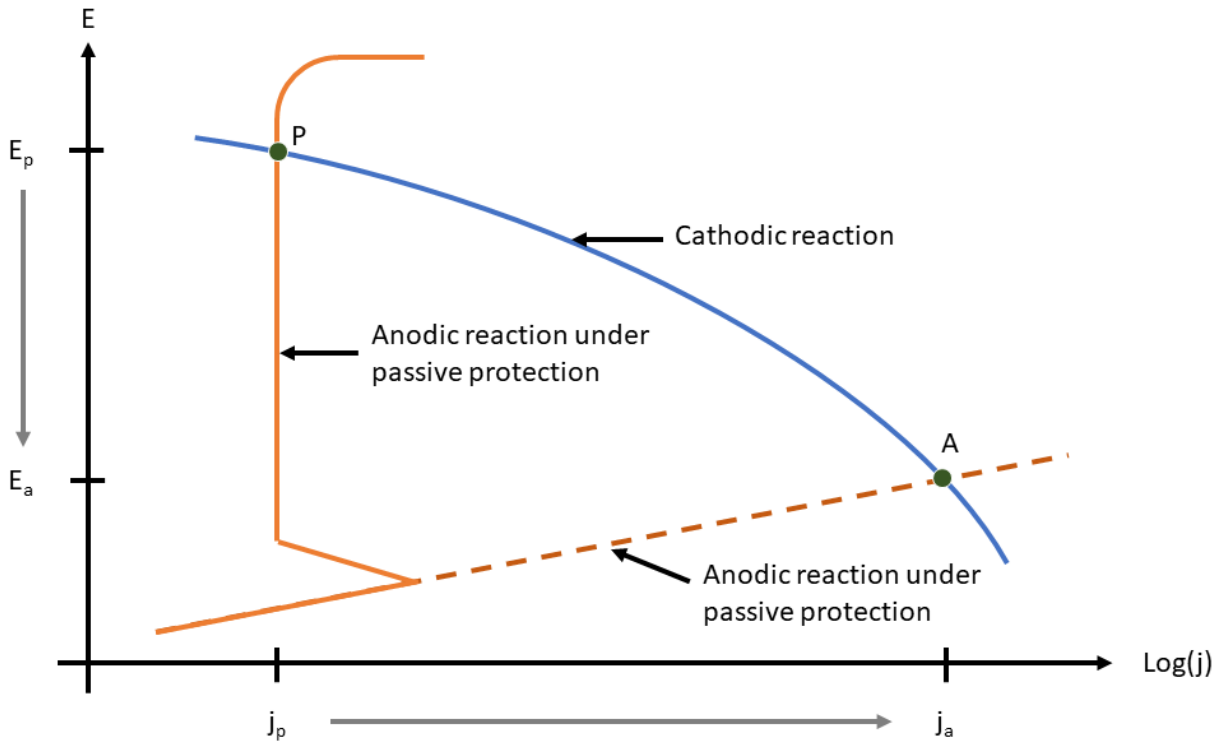

Figure 8: Polarization diagram showing the relationship between the anodic and cathodic reactions in terms of current density vs. the potential of the steel. Log scale, arbitrary units.[17]

When the steel is protected by the passive layer (discussed in section 1.2.1), and there is no corrosion, the two current densities intersect at a higher (less negative) potential. When the passive layer breaks down, the anodic current density increases and intersects the cathodic current density at a much lower (more negative) potential. In an actively corroding system, localized corrosion can be detected by looking for spots of relative potential difference (CPD) compared to the surrounding environment.

2.2 The Kelvin Probe (KP)

The Field Kelvin Probe (FKP) is based on the original Kelvin Probe design, with some key differences making it more suitable for field work. This section will give a brief overview of the history and principle of operation of the Kelvin Probe, its advantages as well as the instruments limitations making it unsuited for field work.

2.2.1 A Brief history of the Kelvin Probe

The Kelvin Probe (KP) was introduced by Sir William Thomson, better known as Lord Kelvin. He published his idea in the scientific journal "Nature" in 1881, as a method to measure the

contact potential (he called it contact electricity) of metals[18]. A drawing of Thomson's original design from the same article is shown in Figure 9.

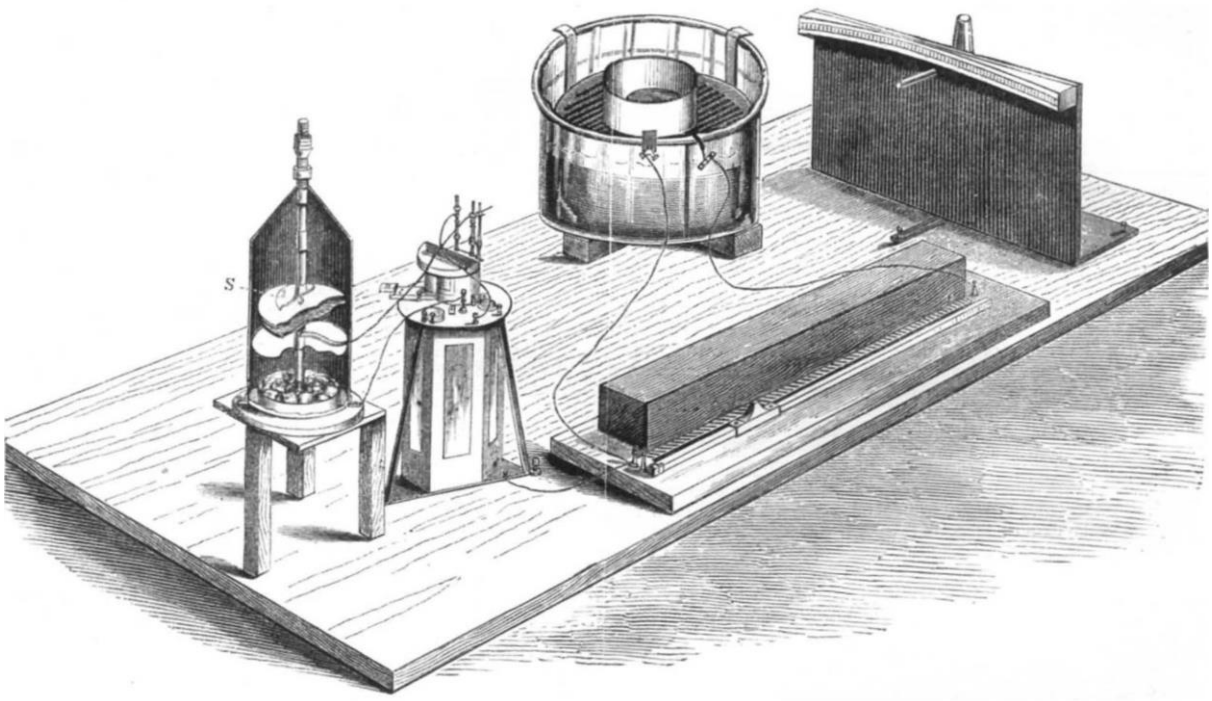

Figure 9: The original design for the Kelvin Probe, introduced in the scientific journal "Nature" by Sir William Thomson in 1881. Drawing taken from "Nature" [18].

In this setup the metal sample surface and the Kelvin probe together form a parallel plate capacitor, where the area of the plates are several orders of magnitude larger than the sample-probe distance. Thomson used the Kelvin Probe (or as he called it, the Volta-condenser) to measure the work functions of metals[19]. If the capacitance between the plates is measured, the work function difference of the two metals can be calculated directly. The measurement of charge on the plates is, however, hard to perform. Thomson's solution to this issue was to measure the discharge current produced when the distance between the plates was varied. The work function difference was then measured by manually varying the probe-sample distance and measuring the resulting discharge current.

The technique as it is commonly used today was introduced by W. A. Zisman in 1932[20]. His approach utilized a vibrating capacitor technique, where the probe plate vibrates periodically, causing a steady AC current to flow. The CPD is calculated by applying an AC current that nullifies the flowing current (more on this in the next section). A schematic drawing of Zisman's Kelvin Probe setup is shown in Figure 10.

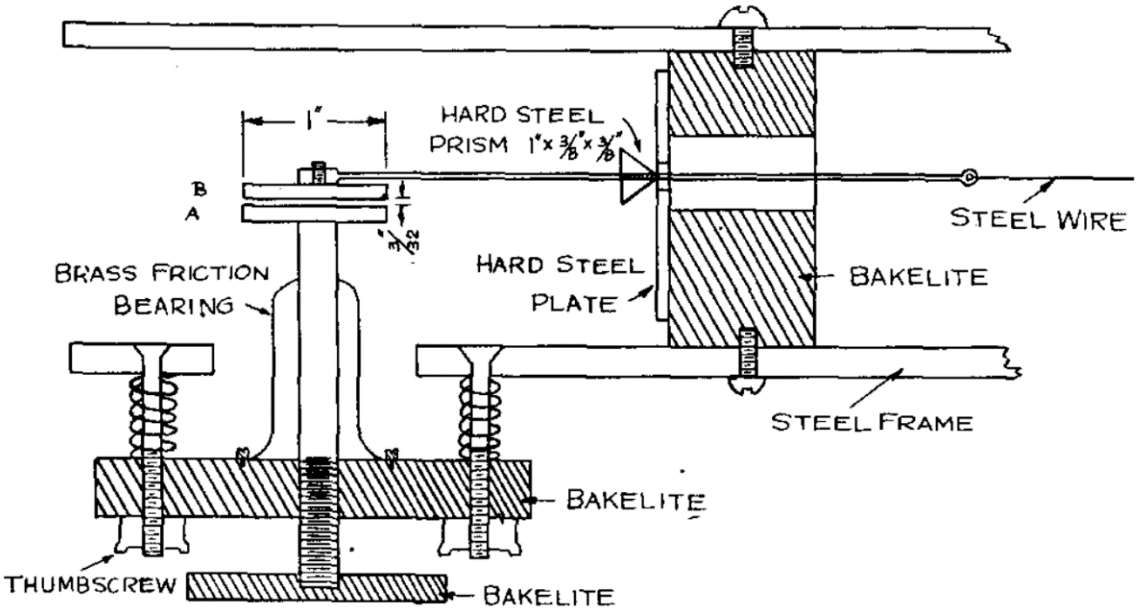

Figure 10: Schematic of W. A. Zisman's Kelvin Probe technique, utilizing a periodically vibrating probe plate setting up an AC current. [20]

A technique to look for variations in contact potential across a surface (Zisman's probe was stationary), the Scanning Kelvin Probe (SKP), was introduced by Parker and Warren in 1962[21]. Using a setup to scan over an area with the Kelvin Probe, they were able to measure local contact potential differences with a resolution of several millimetres. While this method is still in use, the resolution has been greatly improved. By using a 50nm probe-sample distance, a lateral resolution of better than 5µm was achieved in 1992 by Mäckel and Baumgärtner[22]. Pictures of a state-of-the-art SKP, produced by KP Technologies, from the FKP lab at NORCE in Bergen are shown in Figure 11.

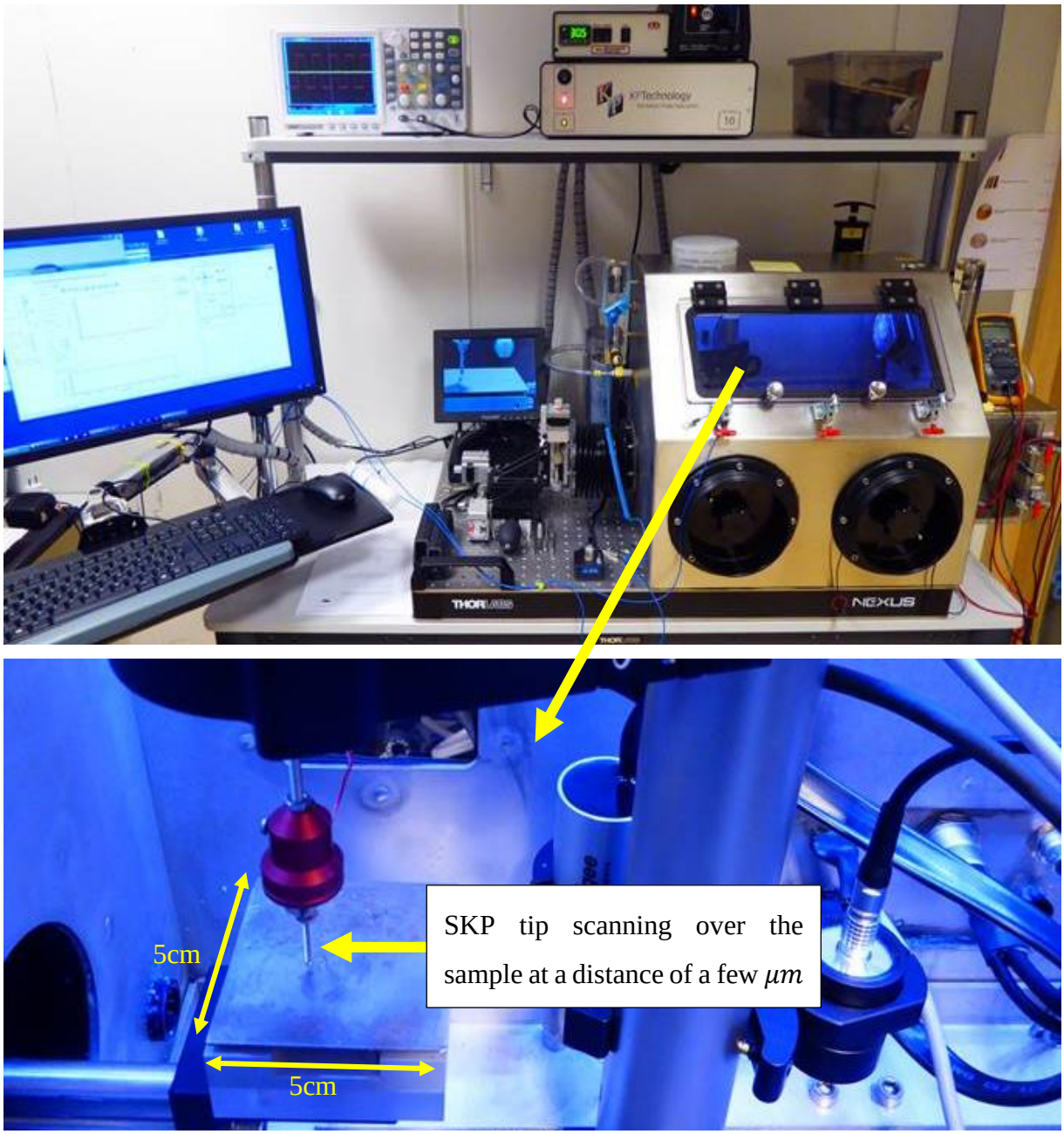

Figure 11: State-of-the-art SKP in the FKP lab at NORCE, Bergen. The top picture shows the whole setup, while the bottom picture shows the probe tip while scanning a 5x5cm^2 carbon steel sample. SKP produced by KP Technologies.

The application of the Kelvin Probe for corrosion science was introduced by the group of Stratmann et al. at Max Planck Institute für Eisenforschung (MPIE) in the 1990's [23, 24]. They showed that the Volta potential between the probe and the sample surface is directly correlated to the corrosion potential of the corroding metal surface.

Finally, and most important for this thesis, the application of the Kelvin Probe for corrosion of concrete steel reinforcements was investigated by Walsh and Sagüés at the University of South

Florida [8]. Using a modified KP, they demonstrated that they were able to measure corrosion potentials that replicated what was measured with established methods. A schematic diagram of this KP, as well as a picture of the probe, is shown in Figure 12. The Kelvin Probe's principle of operation is explained in the next section.

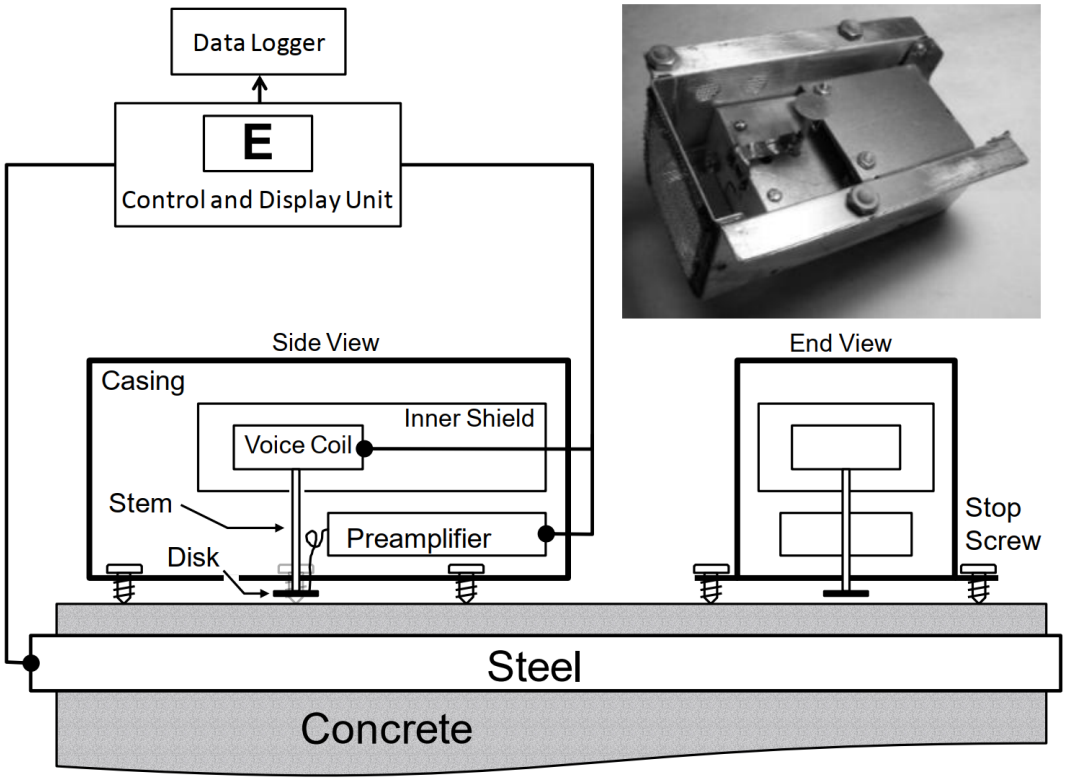

Figure 12: Schematic diagram of Walsh's KP as implemented in the investigation on its application to corrosion in concrete steel reinforcements.[8]

2.2.2 Principle of operation

As previously stated, the probe tip and the sample act as a parallel plate capacitor. The probe tip acts as a reference electrode, separated by a short distance from the sample by a dielectricum (air in most cases), and the two are electrically connected as shown in Figure 13.

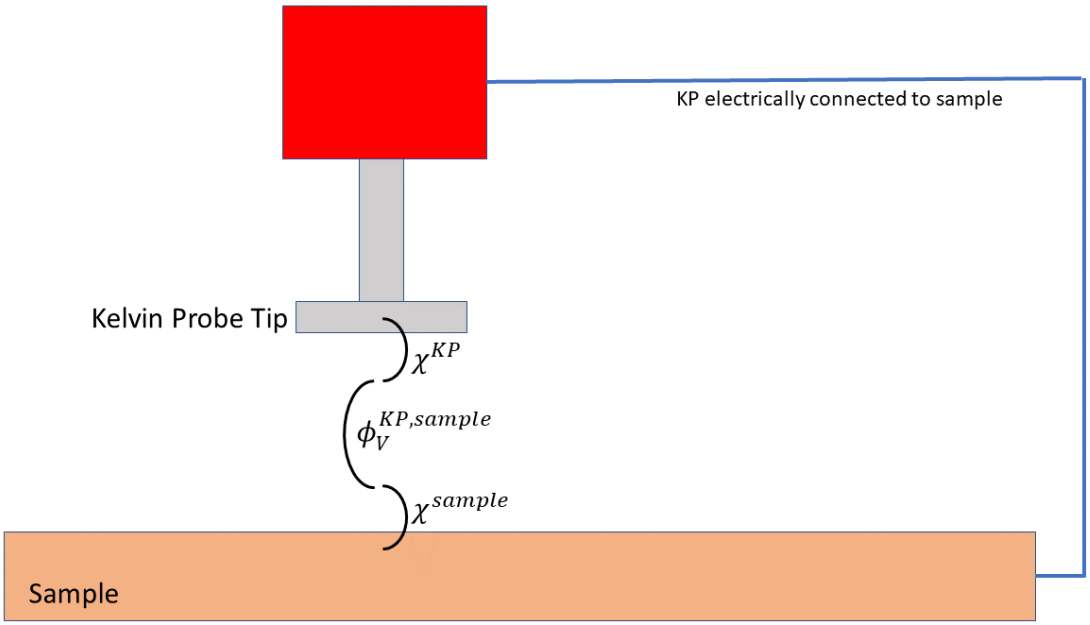

Figure 13: Schematic drawing of the Kelvin Probe tip and the sample, showing the surface potentials and the Volta potential. χ is the surface potential of the sample and tip, and ϕ_V is the CPD (or Volta potential difference).

As in equation (2), the work functions of the Kelvin Probe tip and the sample, Φ^{KP} and Φ^{sample}, can be expressed as:

$$\Phi^{KP} = -\mu_e^{KP} + e\chi^{KP}$$

$$\Phi^{sample} = -\mu_e^{sample} + e\chi^{sample}$$

Since the KP and the sample are electrically connected, the electrochemical potentials μ_e , i.e. both the chemical and electrostatic work required, of the electrons in the two materials will be equalized, resulting in the establishment of the Volta potential between the KP and the sample:

$$\tilde{\mu}_e^{sample,KP} = \mu_e^{sample} - e\phi^{sample} = -\Phi^{sample} - e\phi_V^{sample} = \mu_e^{KP} - e\phi^{KP}$$
$$= -\Phi^{KP} - e\phi_V^{KP}$$

Substituting in equation (1) leads to:

$$e\left(\phi_V^{sample} - \phi_V^{KP}\right) = e\phi_V^{sample,KP} = \Phi^{KP} - \Phi^{sample} \quad (4)$$

The Volta potential has a direct correlation to the charging of the capacitor formed by the KP tip and the sample. When the KP tip is vibrated over the sample surface, i.e. the probe-sample distance is varied periodically, a displacement AC-current is induced. For an ideal parallel plate capacitor, the capacitance can be expressed as:

$$C = \epsilon \frac{A}{d + \Delta d sin(\omega t)}$$

Where ϵ is the dielectric constant of the dielectricum, A is the area of the smallest of the two capacitor plates (usually the probe tip) and $d + \Delta d sin(\omega t)$ is the probe-sample distance at time t. d is the average probe-sample distance, Δd is the displacement, and ω is the vibration frequency. The induced AC-current can then be expressed as:

$$i_{induced} = \phi_V^{sample,KP} \frac{dC}{dt} = e\phi_V^{sample,KP} (\epsilon A \Delta d \omega) \frac{\cos(\omega t)}{d + \Delta d sin(\omega t)}$$

If an external voltage, U_{ext}, is applied between the KP tip and the sample, the induced current becomes:

$$i = \left(\phi_V^{sample,KP} - U_{ext}\right) \frac{dC}{dt} \tag{5}$$

A conventional way to work out the Volta potential is to use a "nulling technique", where U_{ext} is varied until the induced current in equation (5) disappears, i.e. when $\phi_V^{sample,KP} = U_{ext}$. Since the contact potential of the KP tip is known, the contact potential of the sample can be calculated once the Volta potential, from here on referred to as contact potential difference CPD, is known[25].

2.2.3 Limitations/The need for a new instrument

The Scanning Kelvin Probe is a powerful instrument, able to measure local differences in contact potential with high accuracy and lateral resolution. As discussed in section 2.2.1, previous work by scientists at MPIE has demonstrated its uses in corrosion science and work by Walsh and Sagüés has shown that it can also be applied to inspection of corrosion in concrete steel reinforcements[8].

In a lab environment, and with small samples, the SKP is very suited for inspection of corrosion. In the real world, however, bridges and large concrete structures are rarely found inside a lab. The SKP (see Figure 11) is a large and heavy instrument and taking it outside for field measurements on a concrete structure would be highly impractical. The SKP also requires a concealed environment to avoid disturbance of the measurements and is therefore enclosed in a "cage". Finally, the SKP tip is quite fragile and requires a very short probe-sample distance. This means that any irregularities in the concrete surface, in combination with the vibration of the tip, could quite easily cause it to break. In short, the SKP is a great lab instrument, but limited in its application to concrete rebar corrosion, as it is not well suited for field work.

2.3 The Field Kelvin Probe (FKP)

The development of the Field Kelvin probe was inspired by the previous work on the application of Kelvin Probes to corrosion science and was developed in response to the presented limitations of the SKP. This section introduces the FKP as a possible alternative to the current inspection methods for rebar corrosion in concrete. The principle of operation is explained, as well as the FKP's advantage over other inspection methods. Finally, as the FKP has been in constant development during the work presented in this thesis, the current state of the technology is discussed.

2.3.1 Principle of operation

As previously stated, the basic principle of the FKP is the same as any Kelvin Probe. The FKP functions as a variable capacitor inducing a current, by varying the capacitance, which is then used to work out the contact potential of the sample. The main difference between the FKP and the KP is the sensor design, which is shown in Figure 14. Instead of a vibrating tip, as in the KP, the FKP has three metal sensors (brass, in the version presented in this thesis) attached in a wheel configuration, enclosed by a metal casing (here, brass) with a window (about $10x10mm^2$ in this version) facing down towards the sample. The change in capacitance is then mainly produced, not by varying the probe-sample distance as is the case with the KP, but by varying the area of the sensor that is exposed in the window. The fact that there are three separate sensors, not one continuous sensor, also means that the change in capacitance is not continuous throughout the spin cycle. This is circumvented by an LED and photocell aiding with the timing and position of the sensors, making sure that the right measurements are done. The FKP does not rely on the conventional nulling technique, mentioned in section 2.2.2, but

the integrated electronics convert the measured signal into the contact potential difference (CPD) using stepwise bias voltage application and extrapolation.

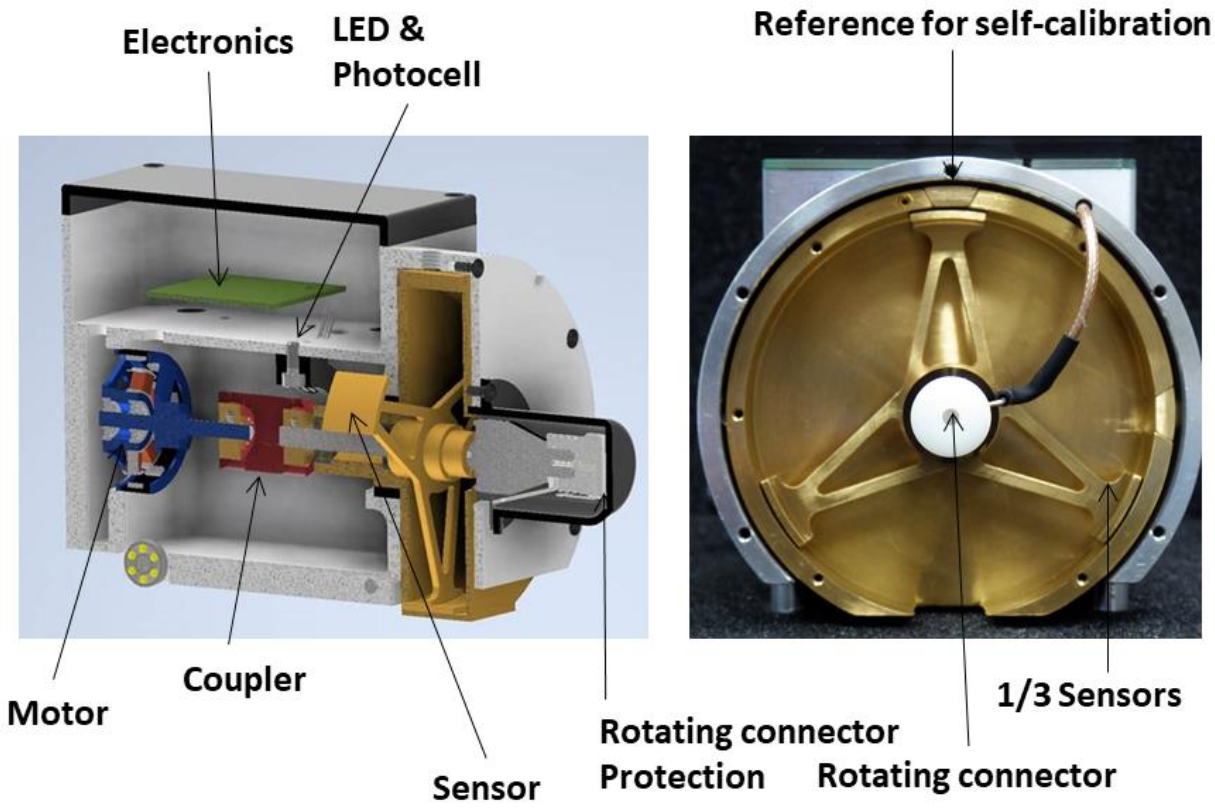

Figure 14: Left: Schematic drawing of the inside of the FKP, seen from the side. Middle: drawing of the rotating sensor, seen from the front. Right: Picture of the rotating sensor, seen from the front [NORCE].

The FKP is small, light, and compact compared to the SKP, making it convenient for field work. It is powered by battery and controlled via Bluetooth from a computer, tablet, or smart phone. The only external connection required for measurements is ground, i.e. there needs to be some common electrical connection between the sample and the instrument. Tests have been done demonstrating that the ground connection can be quite remote and still produce good measurements (see sections 3.4.6 and 4).

There is also a possibility that the FKP can be self-calibrating (although this was not used during the work presented here) by the FKP measuring the potential difference between the sensor and the metal plug labelled "Reference for self-calibration" in Figure 14, at the same time as it is measuring on the sample. The measured potential difference between the sensor and reference plug should be zero (or another fixed value), so calibrations could be done automatically by the electronics or software. Figure 15 shows the FKP in action on a concrete wall with visible cracks and corroded rebars.

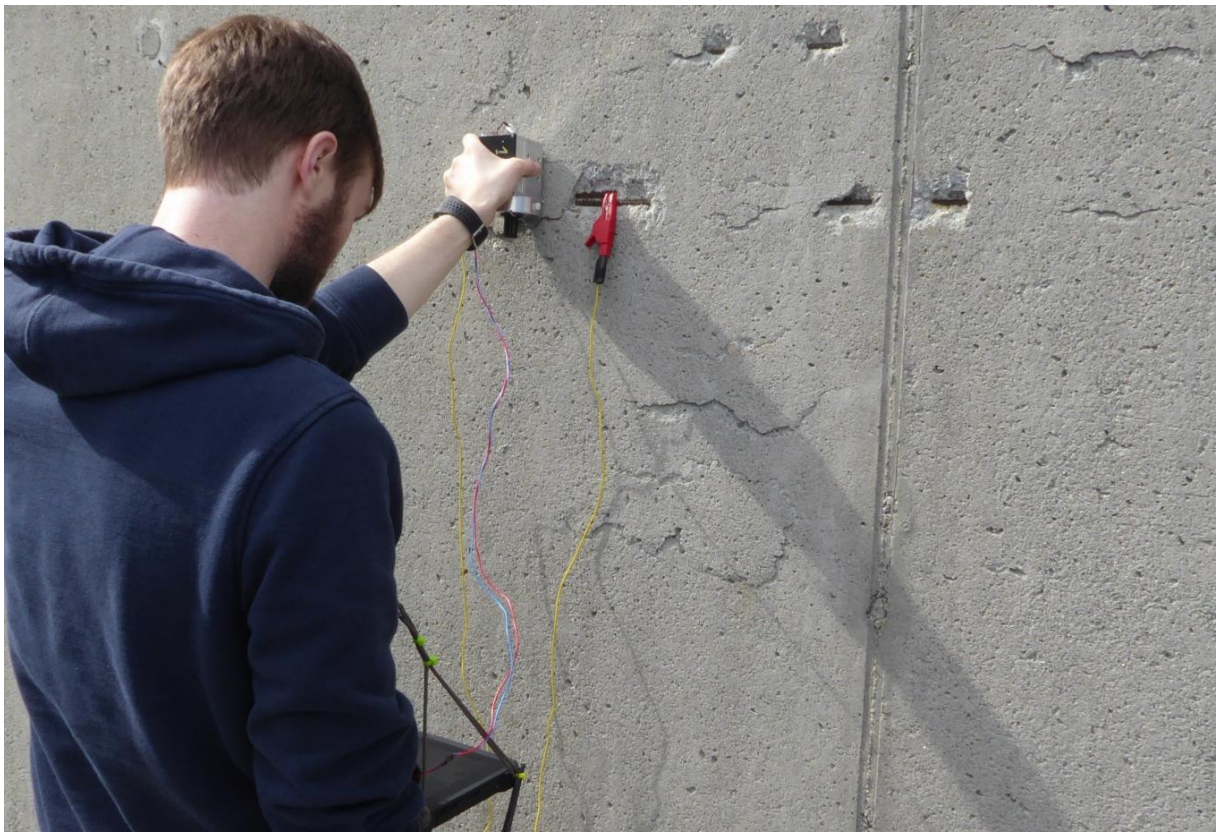

Figure 15: Early field test with the FKP, showing how it may be used. The instrument is powered by batteries and is controlled via Bluetooth from a tablet. Yellow wire used to ground the FKP to an exposed rebar.

2.3.2 FKP on concrete – Parallel plate capacitor model

For the purpose of simulation, a simple model of the FKP scanning over rebars embedded in concrete was created. In the model, the FKP and rebar for the two parts of a parallel plate capacitor, with two different dielectrics in between, concrete and air, as shown in Figure 16.

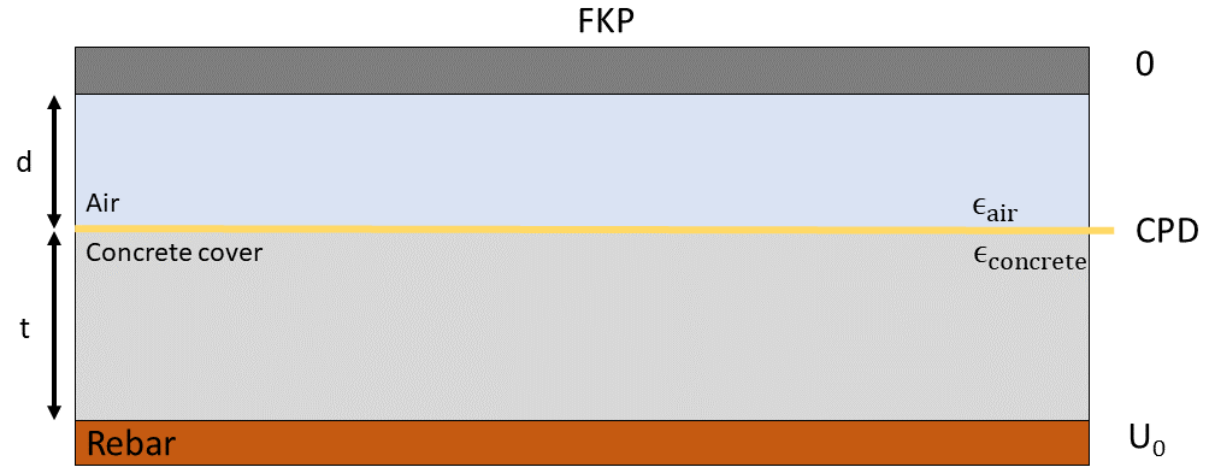

Figure 16: A simple model of the FKP-rebar system. The FKP and rebar form the two parts of a parallel plate capacitor. In between are two different dielectrics, concrete and air. By assuming that the potential difference between the two plates is the applied voltage U_0, i.e. the potential of the FKP is zero, the contact potential difference CPD at the concrete-air interface can be calculated.

This system can be described as two capacitors in series, one for each dielectric medium with permittivity $\epsilon_{concrete}$ and ϵ_{air}. The capacitance of these is $C_1 = \epsilon_{concrete}\frac{A}{t}$ and $C_2 = \epsilon_{air}\frac{A}{d}$ for concrete and air respectively, where A is the area of the plates (the smallest of the two plates), d is the probe-sample distance(work distance), and t is the concrete cover depth. The total capacitance is the given by $\frac{1}{C} = \frac{1}{C_1} + \frac{1}{C_2}$, yielding:

$$C = \frac{\epsilon_{air}\epsilon_{concrete}}{\epsilon_{air}t + \epsilon_{concrete}d} \tag{6}$$

Assuming that the potential of the FKP is zero and that the potential difference between the two capacitor plates is the applied voltage U_0, the charge held by the two plates (positive on one plate and negative on the other) is given by $Q = CU_0$. The surface charge density is then $\sigma = CU_0/A$. The displacement field flux D is equal to the surface charge density in this geometry, i.e. $D = \sigma = CU_0/A = Q/A$ in both mediums, and D is continuous. By then applying $D = \epsilon E$, this gives the following for the electric fields E in the two media:

$$E_{concrete} = \frac{Q}{\epsilon_{concrete} A} \text{ and } E_{air} = \frac{Q}{\epsilon_{air} A} \tag{7}$$

The contact potential difference *CPD* (or interface potential) at the concrete-air boundary is then given by $CPD/d = E_{concrete} = Q/\epsilon_{concrete} A$. By substituting $Q = CU_0$ and equation (6), the final expression for the *CPD* at the concrete-air interface:

$$CPD = \frac{\epsilon_{concrete} d}{\epsilon_{air} t + \epsilon_{concrete} d} U_0 \tag{8}$$

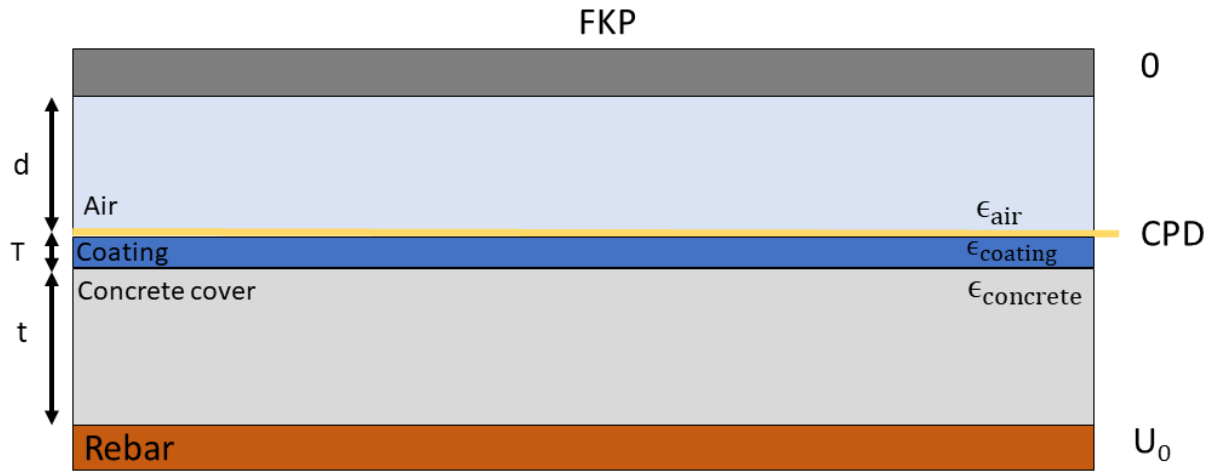

Figure 17:The parallel plate capacitor model(Figure 16) for the FKP-rebar system with a coating added to the concrete surface.

The application of a coating on the concrete can also be added to this model by adding another capacitor, as shown in Figure 17, with capacitance $C_{coating} = \epsilon_{coating} A/T$, where T is the coating thickness. The total capacitance then becomes:

$$C = \frac{\epsilon_{concrete} \epsilon_{coating} \epsilon_{air} A}{\epsilon_{coating} \epsilon_{air} t + \epsilon_{concrete} \epsilon_{air} T + \epsilon_{coating} \epsilon_{concrete} d} \tag{9}$$

Then, by following the same steps as before, the expression for the *CPD* at the coating-air interface becomes:

$$CPD = \frac{\epsilon_{air}\sqrt{\epsilon_{coating}^2 + \epsilon_{concrete}^2}d}{\epsilon_{coating}\epsilon_{air}t + \epsilon_{concrete}\epsilon_{air}T + \epsilon_{coating}\epsilon_{concrete}d}U_0 \quad (10)$$

The parallel plate capacitor model is put to the test in section 3.4.2. According to this model, the FKP will still be able to measure the contact potential difference *CPD* through a protective coating.

2.3.3 Advantages

The differences in the design of the FKP compared to the SKP leads to some convenient advantages for field work. The fact that the FKP is powered by battery and controlled via Bluetooth, making it essentially wireless, combined with the compact size makes it easy to handle in the field. The rotating sensor, which is enclosed in a casing, makes the instrument more robust compared to the conventional vibrating tip. In addition, the work distance of up to a few centimetres, compared to millimetres for the KP, means that measurements with the FKP is less dependent on smooth surfaces.

2.3.4 Current state of the FKP technology

The FKP was in a constant state of development during the year spent on this thesis. This section will give a very brief overview of the state of the technology at this time. The FKP, in its protective 3D-printed plastic casing, is shown in Figure 18. The current version weighs 946g, including the three AA-batteries it runs on. The sensor is made of brass and has a size of 12x10mm^2. The FKP is now run with Bluetooth 5.0, and there are plans to implement a Bluetooth positioning system, which is still being tested. With the positioning system in place, it would be very simple to perform repeated handheld scans of a surface and monitor corrosion progression over time.

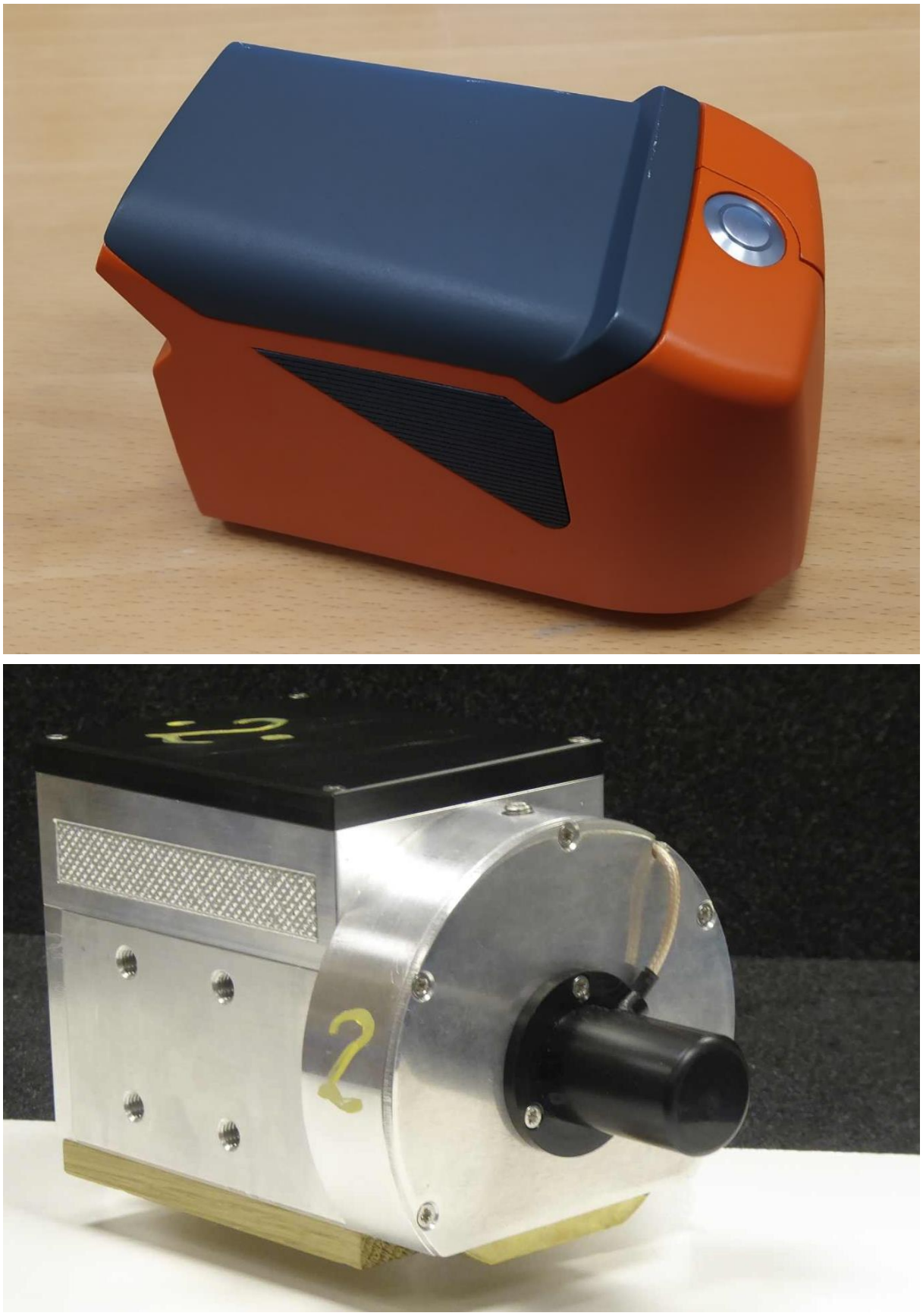

Figure 18: Latest version of the FKP. The probe is protected by a 3D-printed plastic casing shown in the top picture. The bottom picture shows the FKP without the casing.

2.4 On measurement uncertainty using the FKP

The value acquired from a measurement with the FKP is in fact an average of multiple measurements, however there was no access to the raw data in the present version of the electronics. Measurement uncertainty for the results in this thesis can therefore only be acquired by performing several repeated measurements. This point was not clear at the beginning of the work, where it was believed that the individual measurements could be extracted, and error bars calculated. For this reason, some of the measurements are presented without proper error bars. Where this is the case, it is commented on. For the time being, not much is known about the effects of e.g. temperature and humidity (both in the air and in the concrete itself) on the FKP measurements. Given more time than the duration of a MSc. program allows, experiments should have been done in controlled environments to acquire a sense of the effects of these, and other, external factors. Because of this, some of the results are presented without error bars.

One experiment was done specifically to get a sense of the measurement uncertainty (section 3.4.6), showing good stability. It must be noted however that this was a quick test and that a more thorough investigation on the measurement uncertainty should be performed in the future.

3 Method development and results

The subject of this thesis is specifically the application of the FKP for condition monitoring of concrete steel reinforcements. Experiments were also done on non-concrete test samples, such as coated and uncoated metal panels. This was done to show i) that the FKP can be applied on coated surfaces and ii) that it can distinguish between pristine steel and irregularities which could be due to corrosion. These test samples and results from non-concrete testing are shown in section 3.2.

The rest of the chapter (section 3.3- 3.4) concerns experiments done on test samples with steel plates and rebars embedded in cement stone. A distinction is made between concrete, which follows a strict formula and contains aggregates (small stones), and cement stone, which is simply cement mixed with water. Some of these test sample experiments produced valuable and encouraging results, while others did not. To document the full thesis work, all test samples and results are presented and discussed in chronological order. The experience gained from the construction of each test sample, as well as the results, aided in the design of the subsequent samples that led up to the final and successful test setup, which is presented in section 3.4.

3.1 Experimental setup and data analysis

For all but one of the tests described in the following sections, the test samples were scanned with the FKP mounted to a robotic stage, as shown in Figure 19. The robotic stage can accommodate test samples of sizes up to 300x150mm^2.

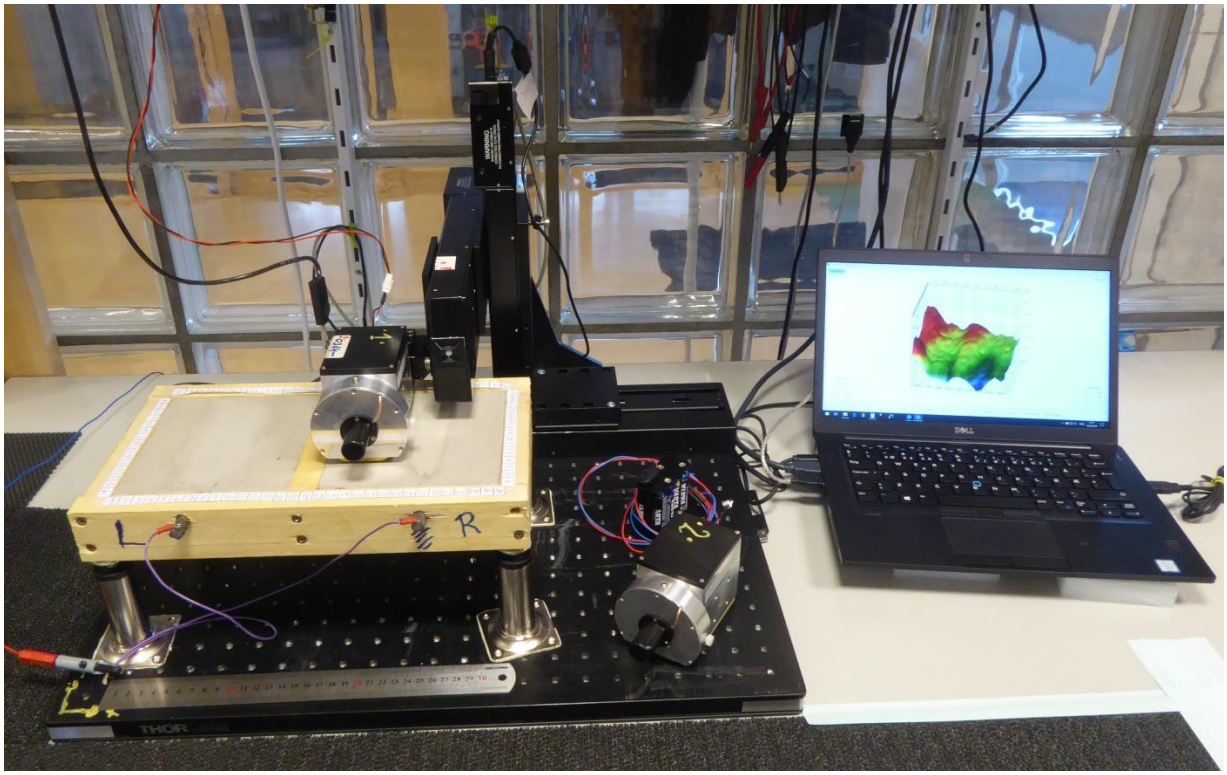

Figure 19: The FKP mounted to a robotic stage, allowing for scans in X and Y direction as well as control over the work distance. Pictured on the stage is cement stone test sample 4, described in section 3.3.5.

In this setup, the FKP and the robotic arm on the stage are synchronized so that the arm moves the FKP between measurements. Measurements are done in a grid of a chosen resolution (distance between measurement points) with about one measurement every two seconds. The resolution can be chosen freely when starting a scan, but improving the resolution naturally increases the scan time. Scans with 1mm resolution were done (Figure 40), but unless otherwise specified the scans were always done with a resolution of 5mm, as this resolution provided a good compromise between resolution and scan time.

The data was imported and plotted using several Matlab scripts and is mainly presented in two different ways: i) Heatmap (example in Figure 22), where the X and Y axes represent the position of the measurement, and the colour represents the contact potential difference (CPD)

value and ii) surface plots (example in Figure 26), where the height on the Z axis as well as the colour represents the CPD value. It must be noted that both the heatmaps and the surface plots were plotted as square surface areas even when this was not the case, but the axes still show the correct values. This was done to make the plots somewhat similar, since a lot of differently sized areas were scanned. To account for this, some of the pictures of the actual test samples that were overlaid have been distorted to match the proportions in the plot. Several line scans were also done, as well as handheld spot measurement, and these are presented in 2D plots.

3.2 Non-concrete testing

Several tests were done on non-concrete test samples, showing that the FKP does compare to the SKP in terms of distinguishing between different metals and between pristine and corroded metal.

To show that the FKP is a viable alternative to the SKP, the first logical step was to do a straight comparison between the two. For the comparison, the two metal plates shown in Figure 20, zinc and copper, were scanned with both instruments.

Figure 20: Zinc (left) and copper (right) that was scanned with both the SKP and FKP to compare the two instruments. The numbers written underneath denote the "expected" CPD values, measured with the SKP.

The results, presented in Figure 21, show a good agreement between the two instruments. The potential difference measured between the two metals is the same (around 500mV). It is worth noting that the resolution of the two is quite different, a few mm for the SKP and 1cm for the

FKP. As previously mentioned, the lateral resolution of the FKP is mostly limited by the step size, which was chosen here to be 1cm as this was only meant as a quick test.

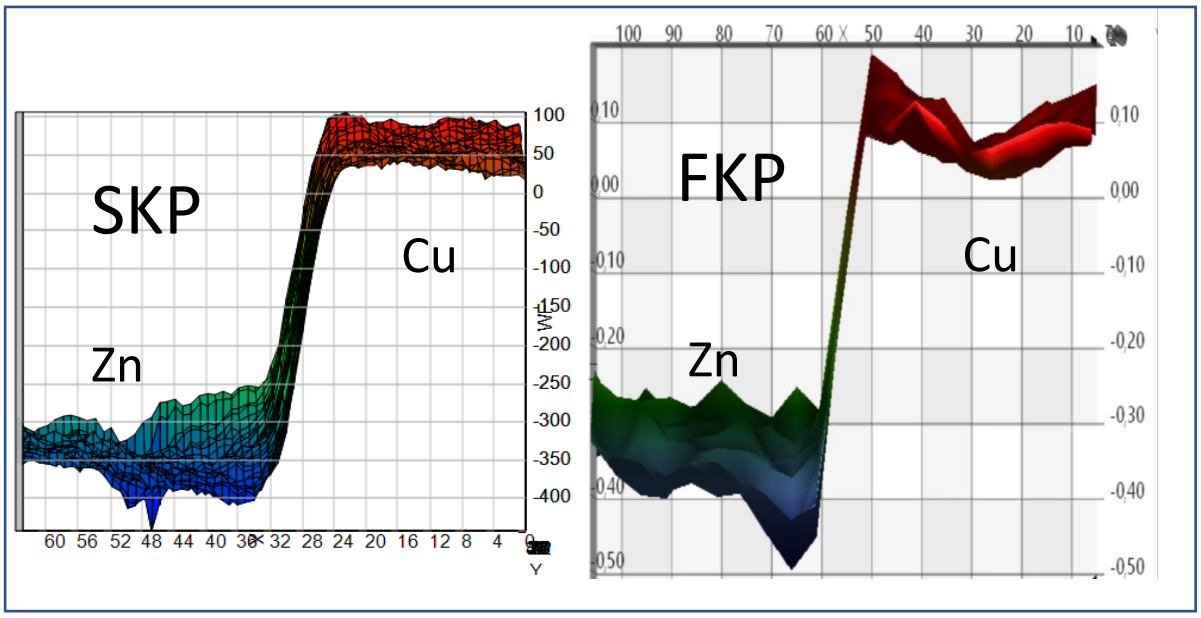

Figure 21:Comparison between the SKP (left) and the FKP (right). Both instruments were used to scan over two metals plates, zinc and copper. The images are screenshots from the dedicated software for the SKP and FKP, respectively. The images have been distorted slightly to match the axes. The y-axis in the SKP picture gives the CPD in millivolts, while the y-axis for the FKP picture gives the CPD in volts.

The result shows that for large differences in the 100mV range, as expected for corrosion measurements, the FKP can reproduce the results obtained with the SKP.

To test the detection of corrosion defects as well as the performance through a coating, a metal panel with severe corrosion damage was coated with Bengaläck (two coats – Dry film thickness, DFT=120 µm) and scanned with the FKP. The panel before and after coating, as well as the heatmap from the scan, is shown in Figure 22.

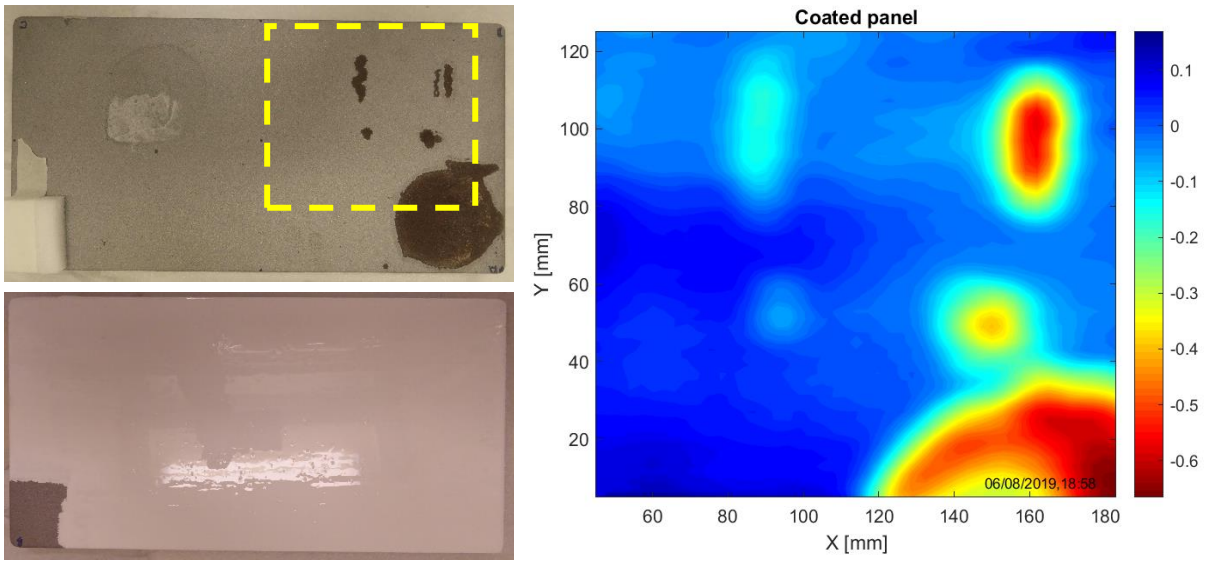

Figure 22:Metal panel with corrosion defects before and after coating with Bengaläck. The yellow square marks the scanned area, with the result shown in the heatmap to the right.

From the results presented in Figure 22, it is clear that the FKP can distinguish between pristine and corroded steel, even through a coating. This is a very major point as discussed in the introduction, because the two other inspection methods discussed cannot measure through a coating. Another test with a coated steel plate was done. This time, the plate had three "regions", as shown in Figure 23, one where tap water was applied, one where salt water was applied, and one where there was a palladium patch. Again, the sample was coated with Bengaläck.

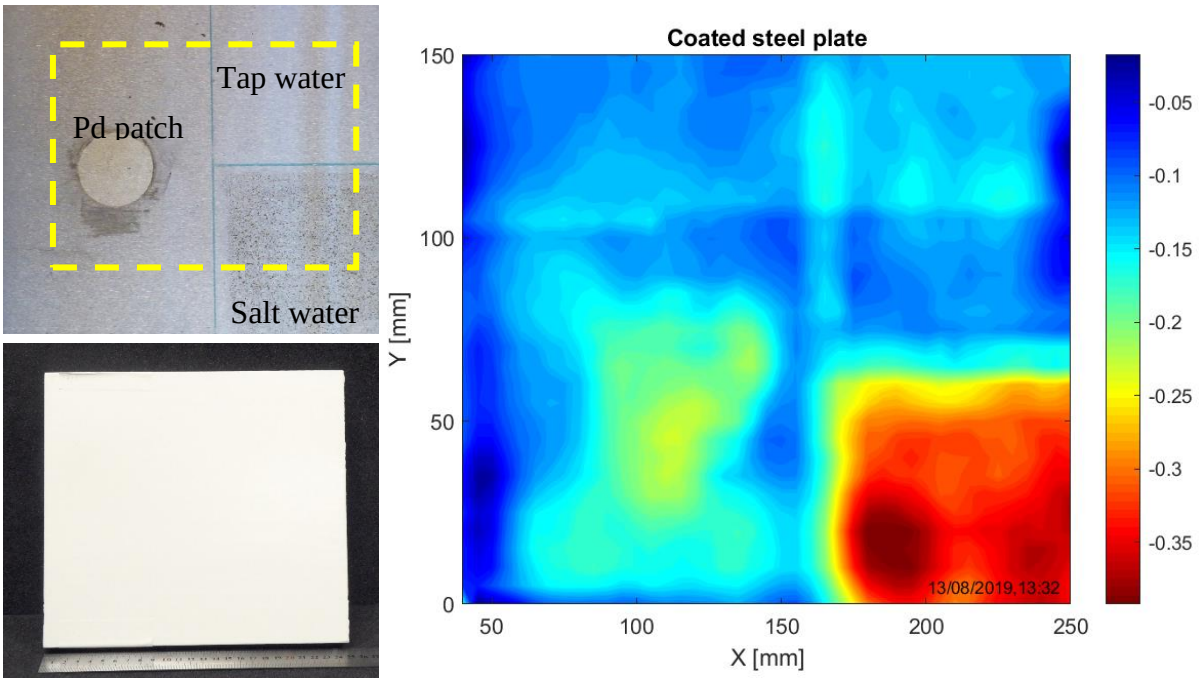

Figure 23:Steel plate with corrosion defects caused by tap water, salt water and Pd electroplating, before and after coating with Bengaläck. The yellow square marks the scanned area shown in the heatmap to the right.

As before, the corrosion defects are clearly visible, especially where salt water was applied. The results presented in this section show that the FKP compares quite well with the SKP and that it can distinguish between pristine and corroded steel through a coating.

3.3 Preliminary concrete testing designs

3.3.1 Cement stone test sample preparation

A total of 10 test sample designs were made and tried out, leading up to the final design. All test samples were made using Infra PLAN cement, pictured in Figure 24, mixed with water. No mixing formula was followed, but water was added until the mixture had reached a suitable consistency. This, in hindsight, was probably not the best approach as knowledge about density and water content would have helped when analysing the data. This mix is not technically regarded as concrete, which would require the addition of aggregates (small stones), and will therefore from this point on be referred to as cement stone.

Figure 24: The cement used for all the cement test samples (Infra PLAN) is pictured on the left-hand side and the manual mixing of the cement with water is pictured in the middle. The right-hand picture is of cement test sample 2(ch.3.3.3) during casting. The back sides of the steel samples and the connecting wires are partly visible.

The frames were all assembled with wooden planks and were placed top-side down on a glass plate covered in a plastic sheet during casting. It is worth noting that in the following sections, some of the test samples are described as too large for a full scan to be possible with the robotic stage. This was a deliberate and accepted trade-off to fit more contents in a single sample. In hindsight, it might have been preferable to design the test samples in a way that allowed for full scans.

3.3.2 Cement stone test sample 1

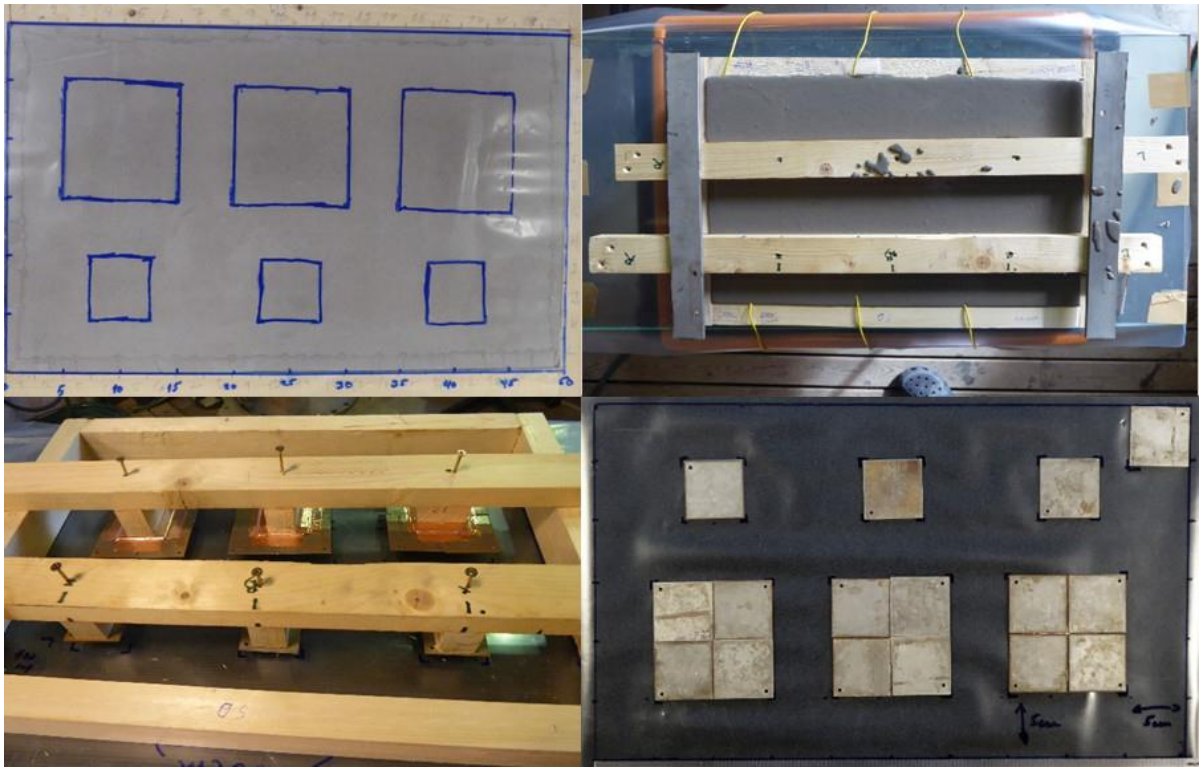

Figure 25: Cement stone test sample 1, before (bottom left), after (top left), and during (top right) casting. The final image (bottom right) show the contents of the test sample laid out on a plastic sheet.

The first step was to test whether the FKP can detect steel embedded in cement stone. To this end, the first cement test sample was designed. A 300x500 mm^2 cement stone slab was cast with a total of fifteen 50x50mm^2 carbons steel plates embedded at three different depths, from 5mm to 10mm as shown in Figure 25. Three larger plates were assembled by combining four of the smaller plates for each and connecting them with copper tape. Tests showed that one of the plates in the shallow large plate assembly (four smaller carbon steel plates connected together) might have disconnected from the rest during the fabrication of the sample, as it does not show up on the scans.

Multiple scans were done on this test sample, showing that the shallowest steel plates were clearly visible, with good contrast from the surrounding environment. Due to the large area of the test sample and the limits of the scanning setup, a full scan of the sample was not possible. The best results were obtained by scanning over the largest shallow plate and half of the small shallow plate. The resulting surface plot and heatmap is shown in Figure 26. As previously mentioned, the top left quadrant of the large steel plate assembly seems to have been disconnected.

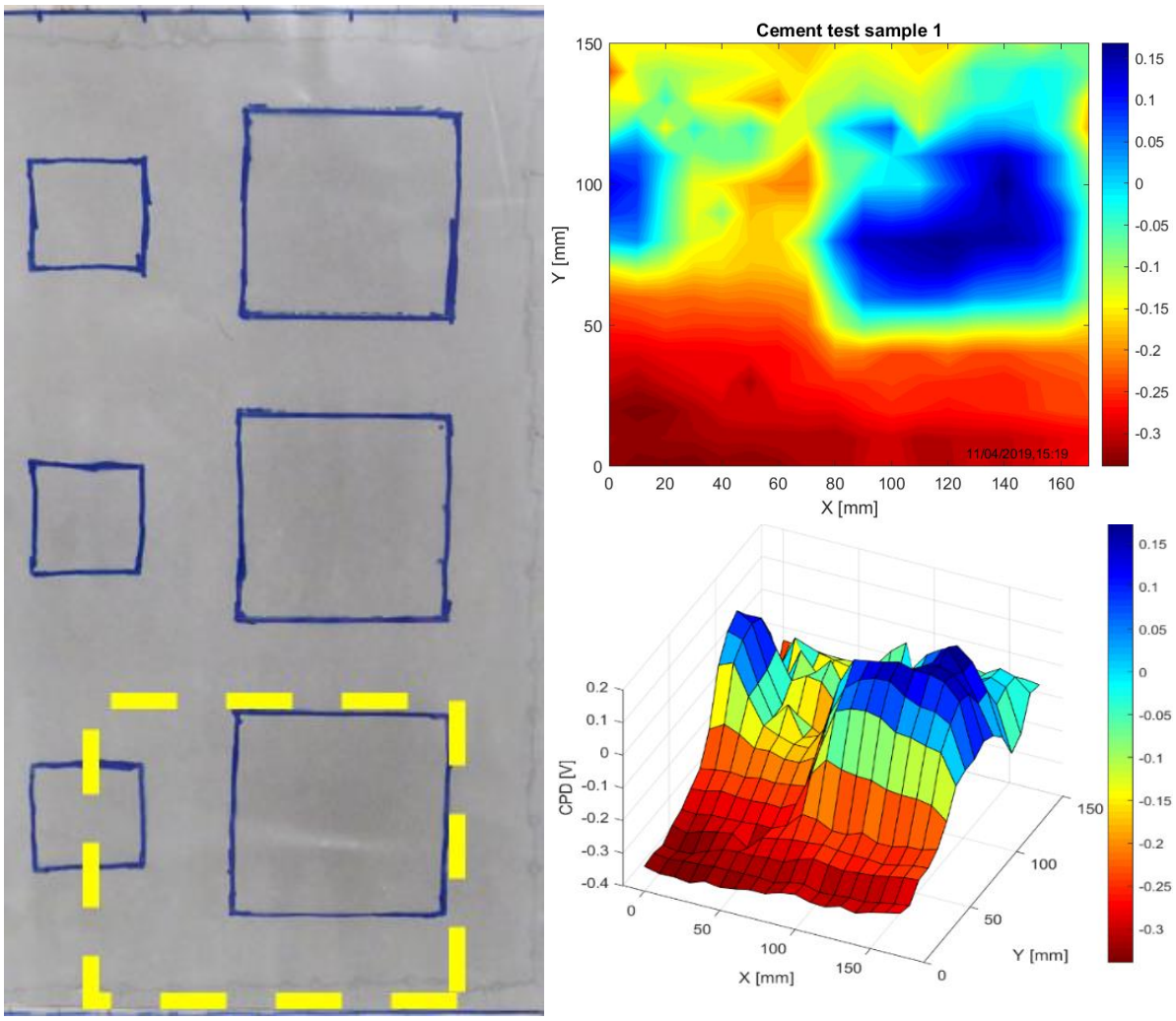

Figure 26: Heat map and surface plot from scanning over the two shallowest steel plates in cement stone test sample 1. The yellow square indicates the scanned area of the sample.

The results from this test sample show that the FKP can indeed detect the embedded steel in cement stone but provide no information on its ability to detect corrosion patterns, which became the next logical step.

3.3.3 Cement stone test sample 2

The second cement stone test sample was designed to test the spatial resolution of the FKP, as well as its ability to detect corrosion patterns. Embedded in the 300x300mm^2 cement stone slab were two steel plates with some rust patterns and a piece of stainless steel with several sharp corners and a roughly 20x10mm^2 hole. The metal samples were embedded at a depth of around 8mm. The contents of cement test sample 2 are shown in Figure 27.

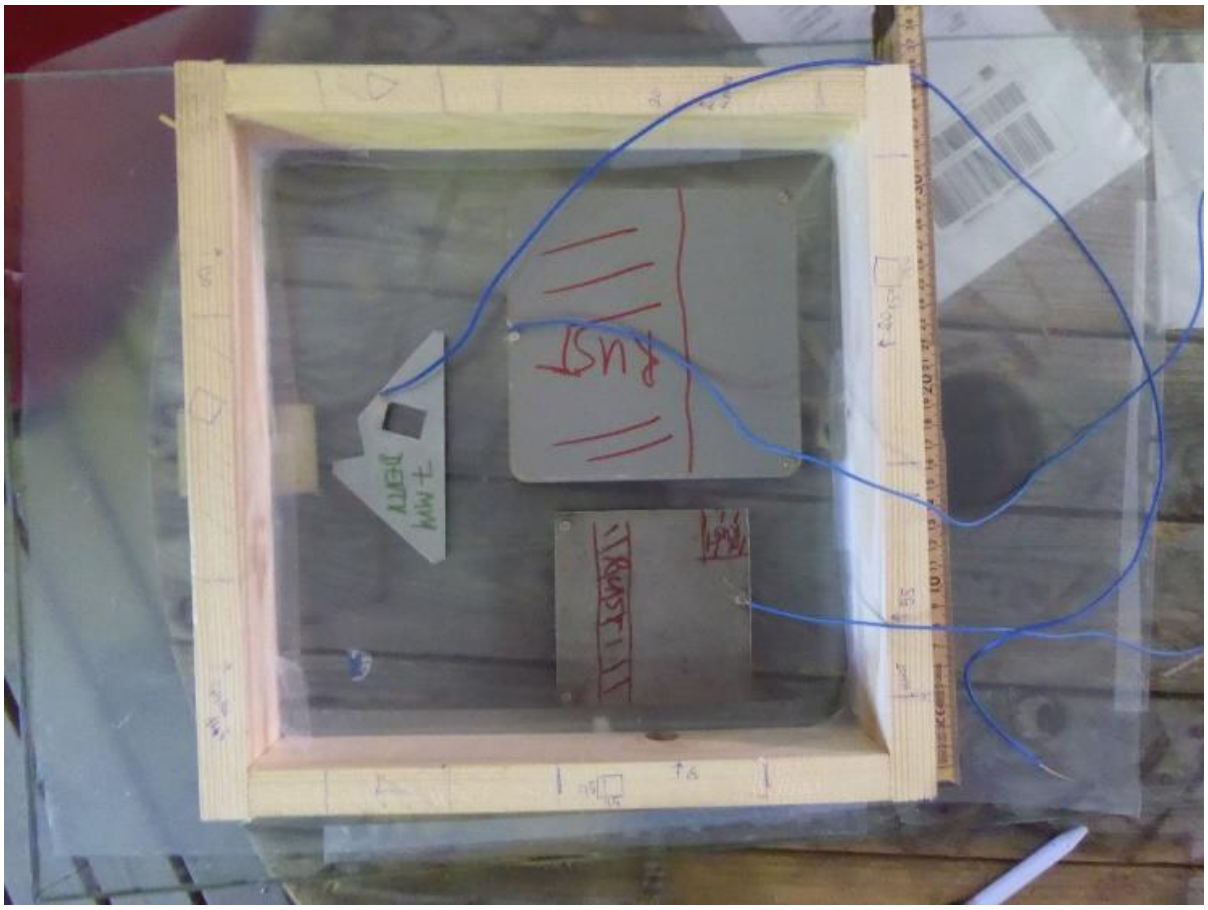

Figure 27: The contents of cement stone test sample 2 prior to casting, seen from the back of the sample. The areas marked "RUST" correspond to rust patterns on the opposite side of the plates.

Again, the test sample was too large for the scanning setup to get a complete scan, so scans were done in two parts. Scans over the two steel plates show that the smaller plate is visible, while the large one is not. It also seems like the rust pattern on the smaller plate is distinguishable from the rest of the plate, although the results are inconclusive. The heatmap from the scan with an overlaid image of the test sample contents is shown in Figure 28. It is not clear why the larger plate was not detected by the FKP.

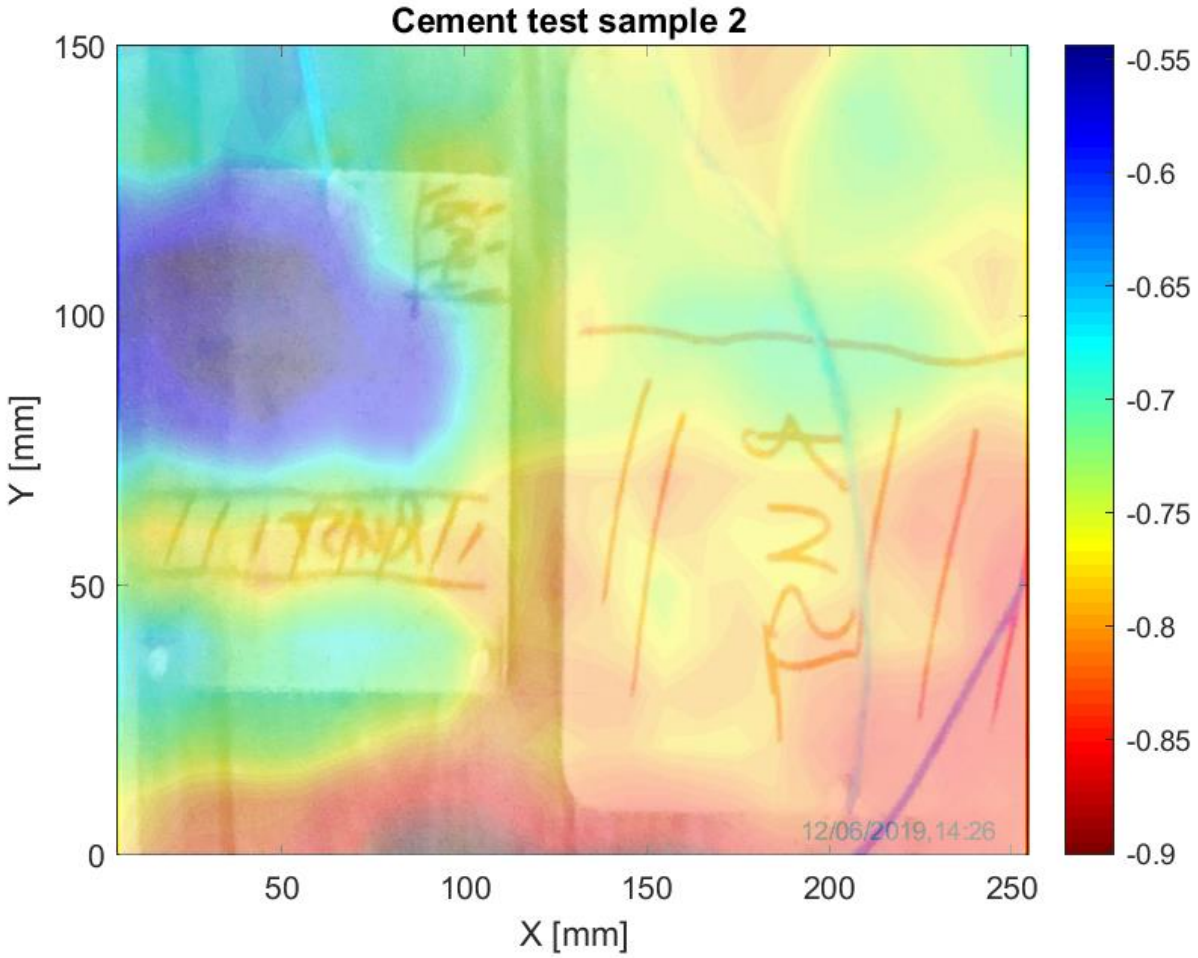

Figure 28: Image of the two steel plates embedded in cement stone test sample 2 overlaid on the heatmap from the scan of the area. The marked areas on the plates indicate a rust pattern on the other (scanned) side.

The scan of the stainless steel shape shows a shape with a spike which coincides with the hole. The edges of the shape, however, are not clearly visible. The heatmap with an overlaid image of the shape is shown in Figure 29.

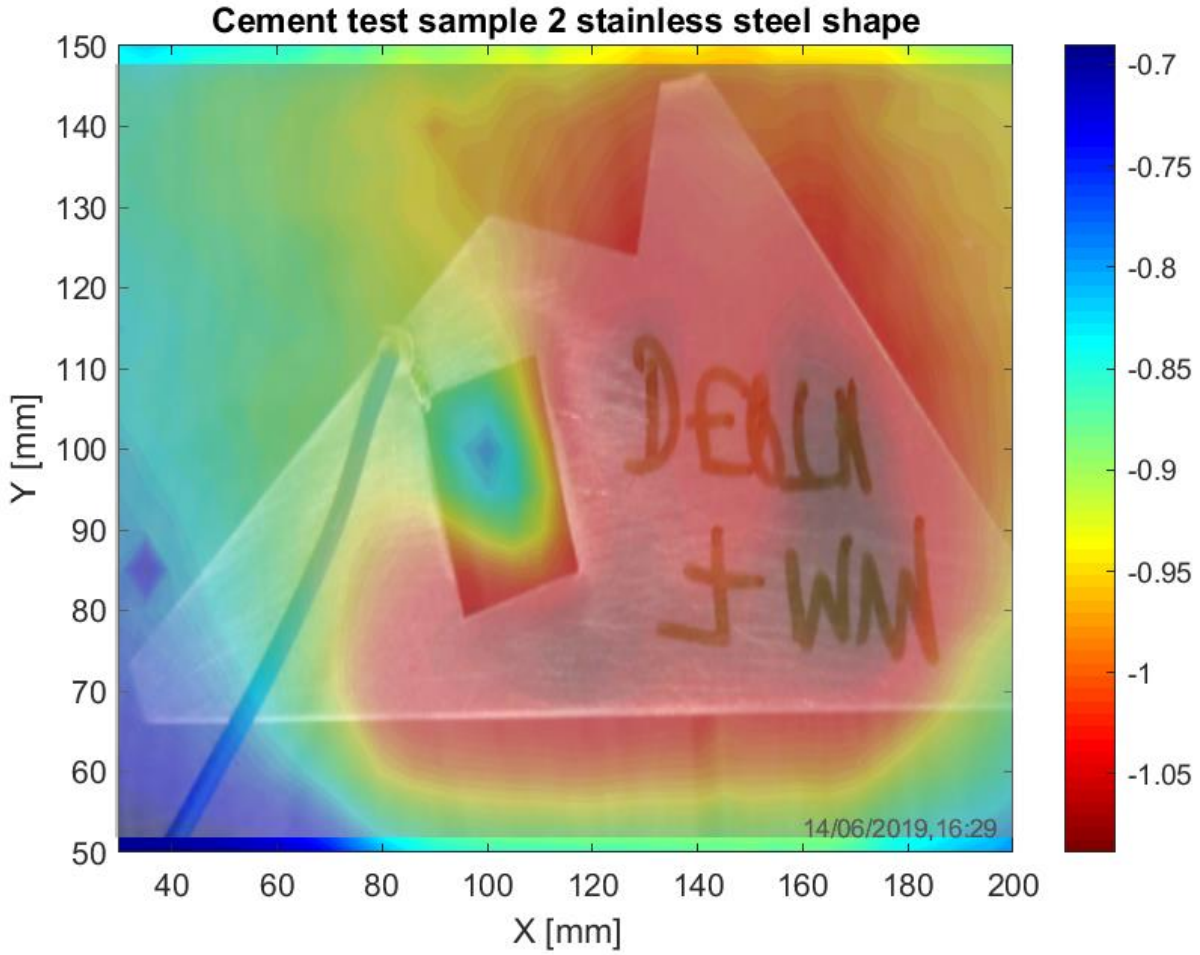

Figure 29: Image of the stainless steel shape embedded in cement test sample 2 overlaid on the heatmap from the scan of the area. Overlaid image of the stainless steel shape has been distorted to match the proportions of the plot.

In short, the results from cement stone test sample 2 gave some indication that the rust pattern on one of the steel plates was detectable by the FKP. Further tests were done to verify this result.

3.3.4 Cement stone test sample 3

The indication that the rust pattern in cement test sample 2 was distinguishable, though inconclusive, was promising and encouraged further investigation. Cement test sample 3 was made with this goal in mind, but this time in a more controlled way. A triangular shape was assembled by cutting and connecting five carbon steel plates as shown in Figure 30. The whole triangle was sandblasted, then half was corroded with 3.5% NaCl solution, before it was embedded in the sample at a depth of 5mm.

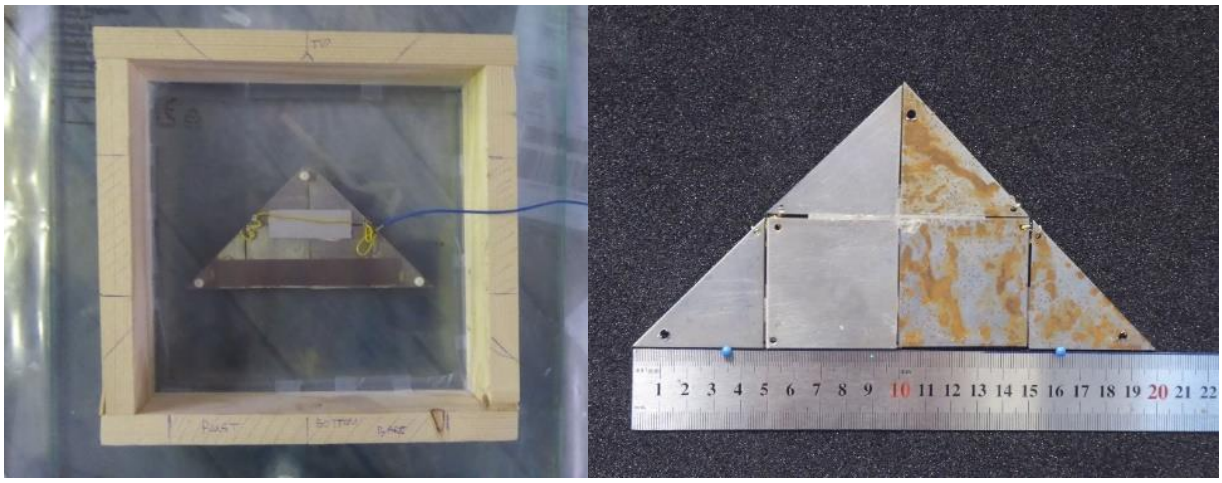

Figure 30: The contents of cement stone test sample 3, seen from both sides.

Scans of this slab again showed a clear contrast between the carbon steel and the surrounding cement stone. A clear distinction between pristine and corroded steel was not seen in the scans, though the steel plate is clearly visible. The heatmap with an image of the contents (Figure 30) overlaid is shown in Figure 31.

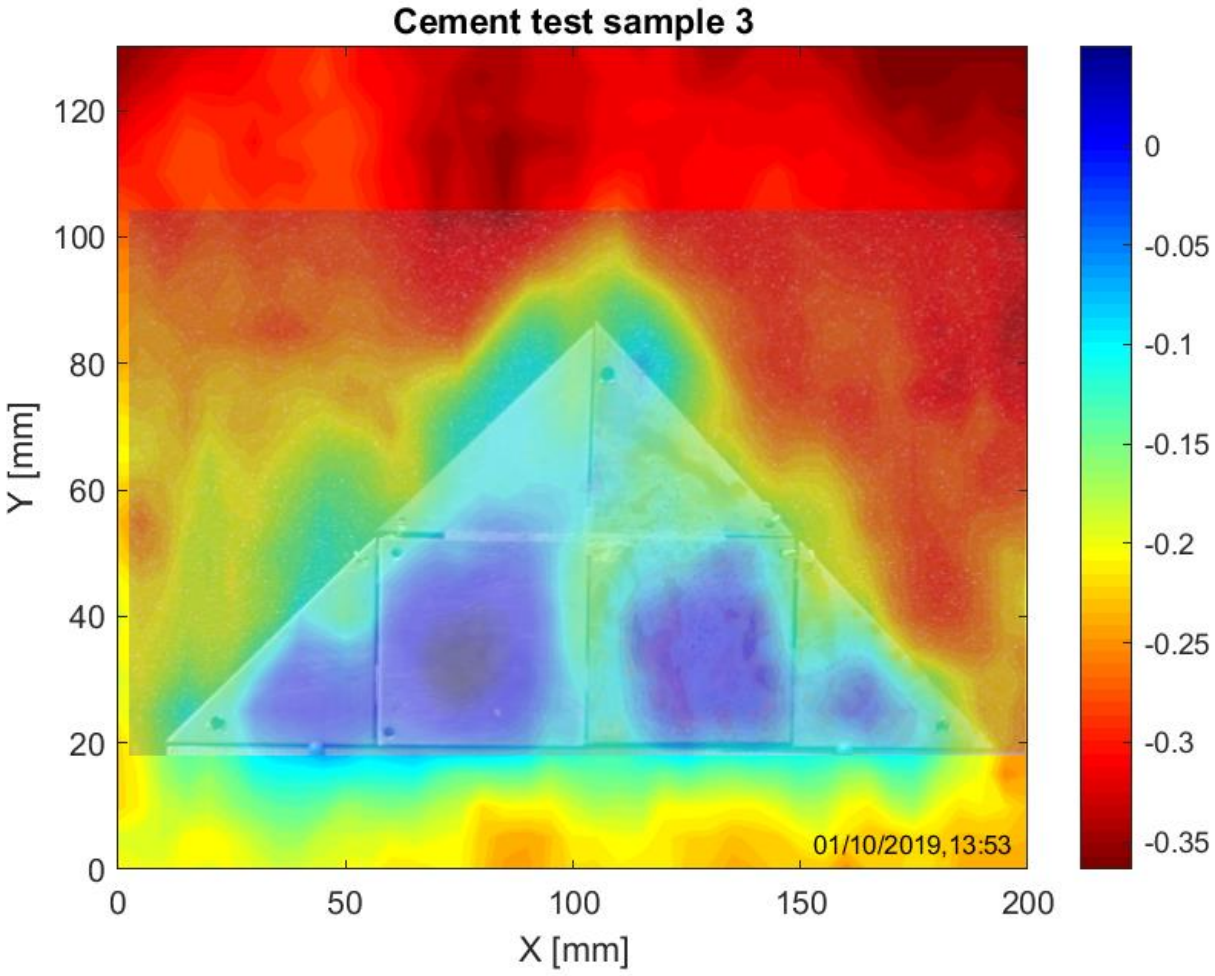

Figure 31: Image of the contents of cement stone test sample 3 overlaid on the heatmap from the scan.

Although this test sample did not provide the expected result, which was seeing a distinction between pristine and corroded steel, it did provide another interesting result. After the sample had outlived its intended purpose and no more scans seemed useful, it was used to test a commercial $CuSO_4$ reference electrode in a half-cell potential measurement to hopefully compare our results with a commercial technique. The test was unsuccessful, but several weeks later another scan was done with the FKP. The resulting scan showed a big spike matching the size and shape of the reference electrode plug, that completely drowned out any other contrasts, in the spot where the electrode had been placed. This could provide some support to the idea that utilizing a reference electrode for half-cell potential measurements contaminates the concrete and alters its chemistry. The heatmap from the scan showing this result is shown in Figure 32 and the surface plot is shown in Figure 33.

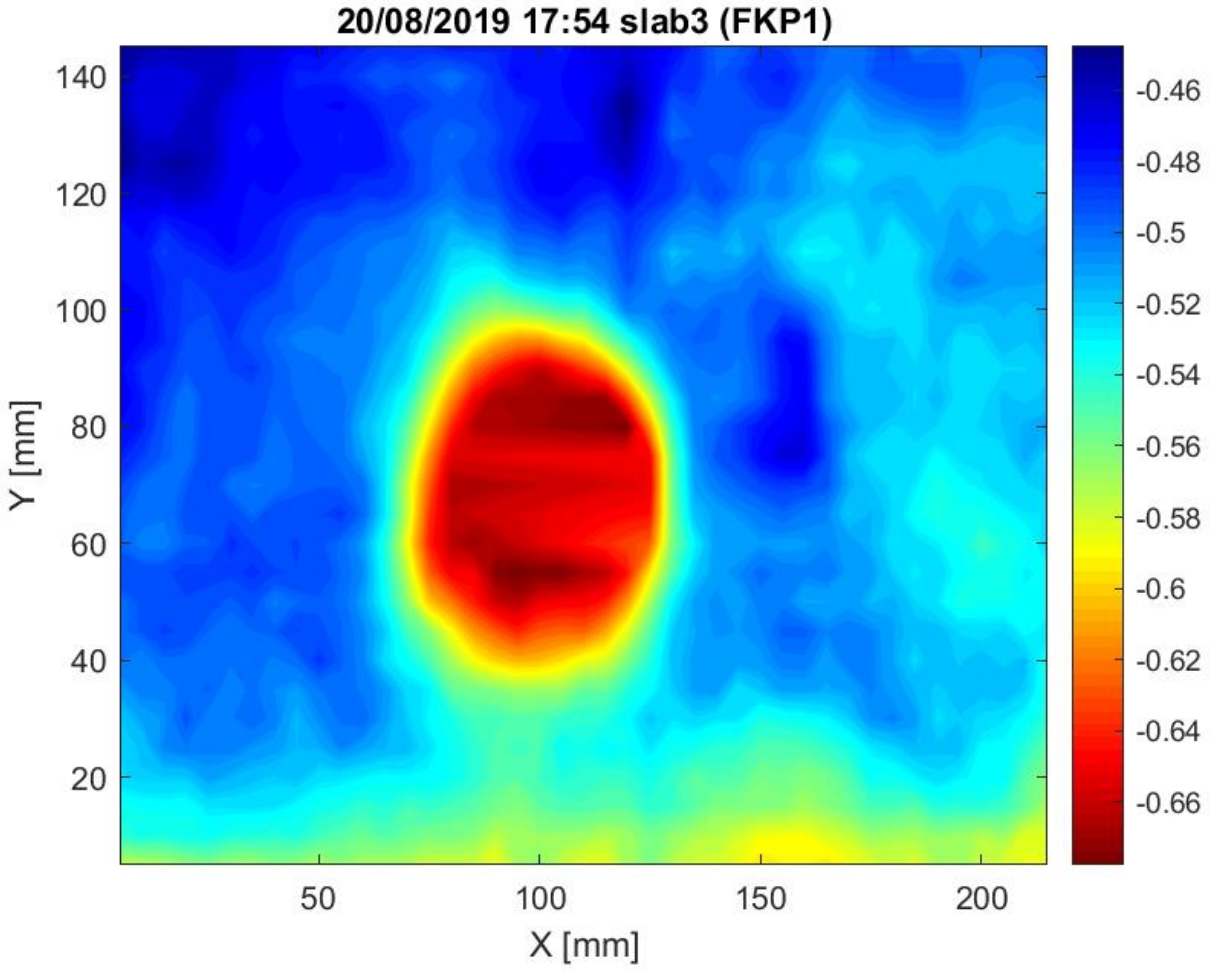

Figure 32: The heatmap from the scan of cement stone test sample 3 suggesting that the $CuSO_4$ electrode had contaminated the sample so that measurements with the FKP were no longer possible. The shape and size of the spike matches that of the electrode.

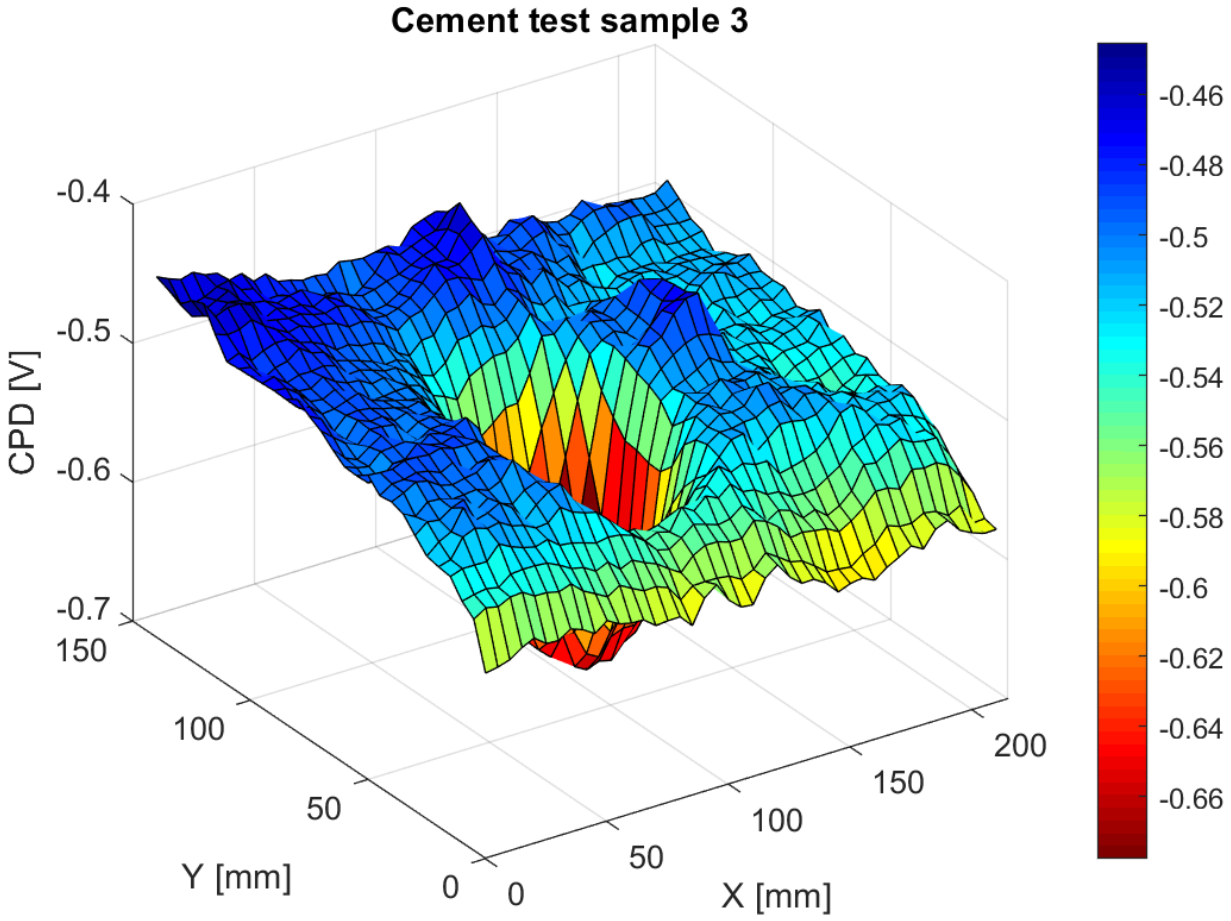

Figure 33: Surface plot of the sample presented in Figure 32.

Cement stone test sample 3 did not provide any support to the idea that pre-corroded steel could be distinguished from pristine steel with the FKP. The conclusion drawn from this at the time was that pre-corroded patterns may not be distinguishable at all and that an active corrosion situation was needed.

3.3.5 Cement stone test sample 4

The three previously described test samples were made with steel plates as they are larger and thus easier to detect with FKP. As the tests showed that the plates are detectable with the FKP, the next natural step was to make a sample with rebars (12mm diameter, commercially available rebar). The fourth cement stone test sample was made to both test the FKP's ability to detect rebars and attempt to create a distinction between a pristine and an actively corroding rebar. A 300x150 mm^2 two-in-one sample with two identical rebars separated by a wood divider was made. Since the rust pattern in cement stone test sample 3 was indistinguishable from the pristine steel, the idea here was to instead invoke active corrosion in one of the rebars. One of

the rebars was wrapped in gauze that had previously been soaked in 3.5% NaCl solution and left to dry. The idea was that the NaCl, when exposed to added water from the wet cement, would induce corrosion in the rebar, while the other rebar would be protected by the wood divider and remain unaffected. Cement stone test sample 4, before and after casting, is shown in Figure 34. The depth of the rebars was 5mm.

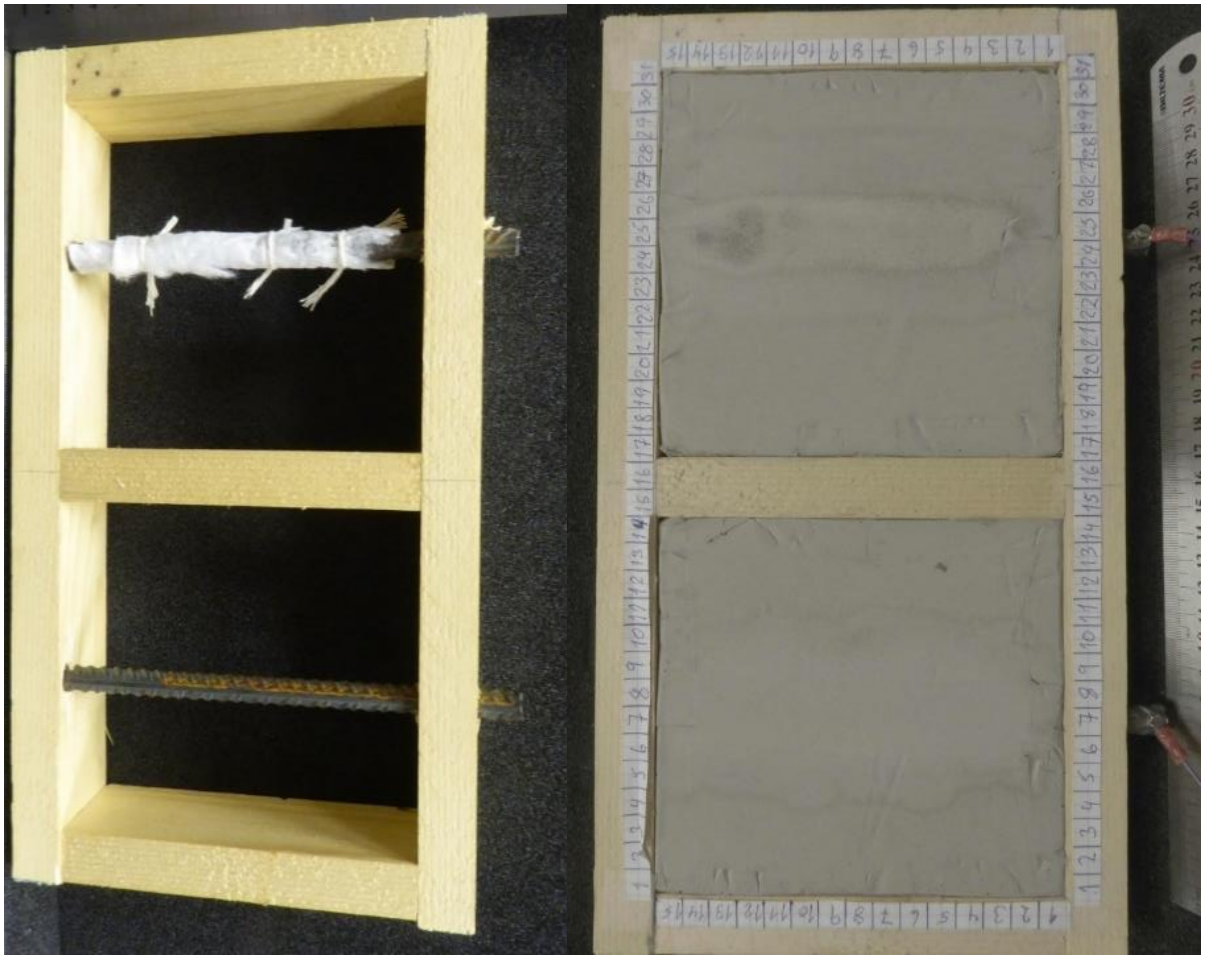

Figure 34: Cement stone test sample 4, before and after casting. The top rebar was wrapped in NaCl soaked gauze prior to casting. The wooden divider protects the other rebar, which is unaltered.

There was a stain visible on the cement surface over the corroded rebar. Looking at the stain through a video microscope revealed that the stained area had a much rougher surface than the rest of the sample. This could suggest that a layer of salt has formed on the surface during casting (instead of the cement mixture) and was since washed away, leaving a rougher surface. Sandpaper was used to sand a small area of the sample surface to compare the two, revealing that the areas look much alike. Figure 35 shows microscope pictures of the area above the corroded rebar, the sanded area, and an area with a smooth surface for comparison. From the microscope images, it seems clear that the pattern on the surface above the corroded rebar is

simply a rougher surface compared to the rest of the sample. This in itself should not influence the measurements to the degree seen in the scans (Figure 36 and Figure 37).

Figure 35: The surface of cement stone test sample 4 under a microscope. Three different areas are shown. Left: Smooth surface (untouched). Middle: Sanded surface. Right: The pattern above the corroded rebar.

Scans of the test sample showed that the unaffected rebar was visible (it can be seen as a small bump in Figure 37 around X=50mm) with a contrast of around 50mV, and the (potentially) corroded rebar showed up in great contrast to the surrounding cement stone, with a contrast of around 150mV. The rough surface may have had an influence on the contrast seen in the scans, but previous experience from the lab suggests that it should not make such a profound difference. The heatmap from the scan is shown in Figure 36 and the surface plot is shown in Figure 37. It seems likely that the stark contrast (around 150mV difference) seen in the scans is indeed caused by ongoing corrosion of the rebar. From the scan it is also clear that the whole cement stone bulk containing the corroding rebar has a lower potential than the bulk containing the unaffected rebar. A possible explanation for this could be that the salinity of the cement stone (from the gauze wrapped around the rebar) influenced the moisture content of the cement stone bulk, decreasing the resistivity of the cement stone, leading to a greater (more negative) measured potential. The full effects of the moisture conditions in the cement stone on FKP measurements is not presently known and requires further investigation.

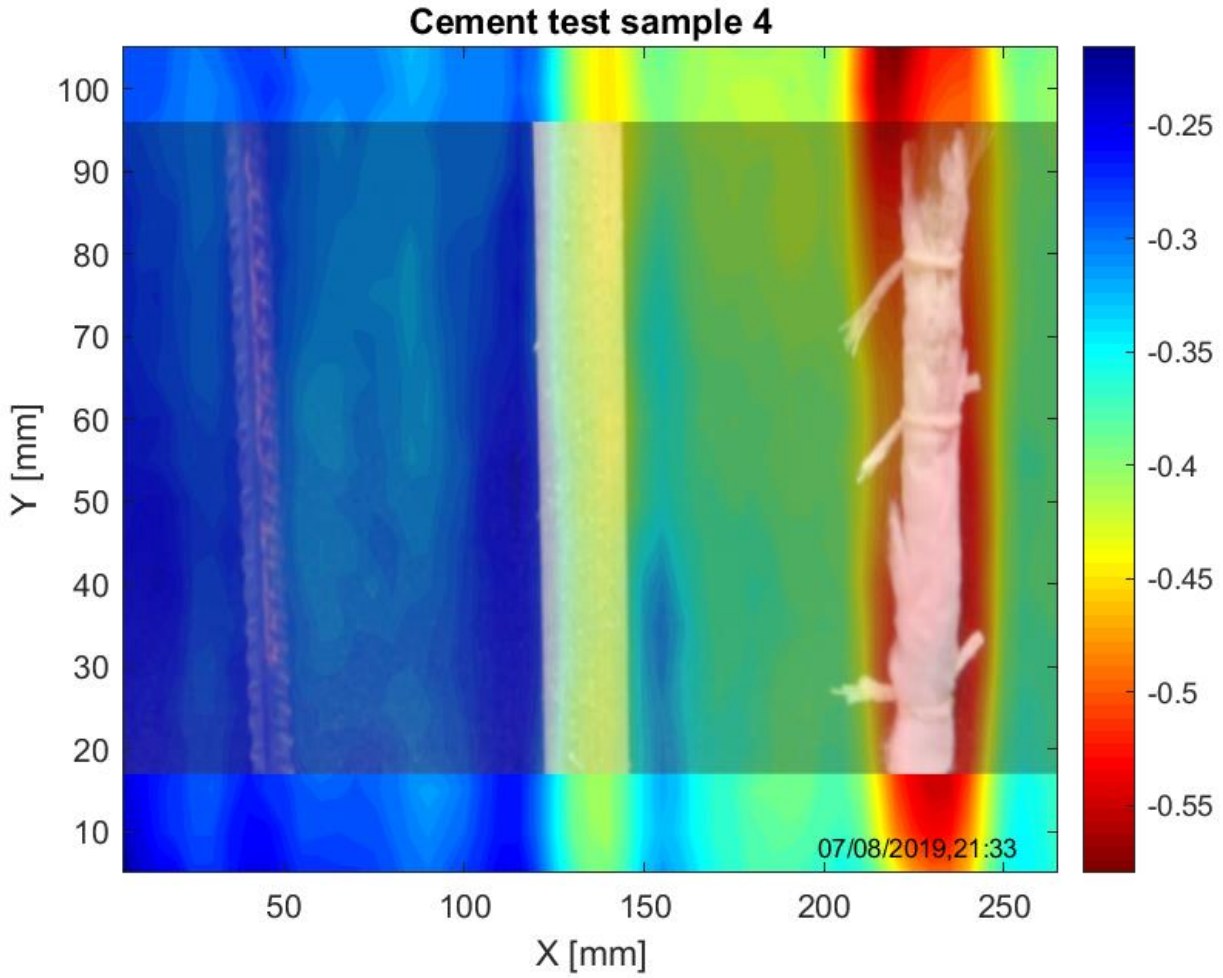

Figure 36: Heatmap from the scan of cement stone test sample 4. Image of a portion of the embedded rebars and wooden divider overlaid. The right rebar is wrapped in NaCl soaked gauze, while the left rebar is unaltered. The area matching the corroding rebar shows up in great contrast to the surrounding cement stone.

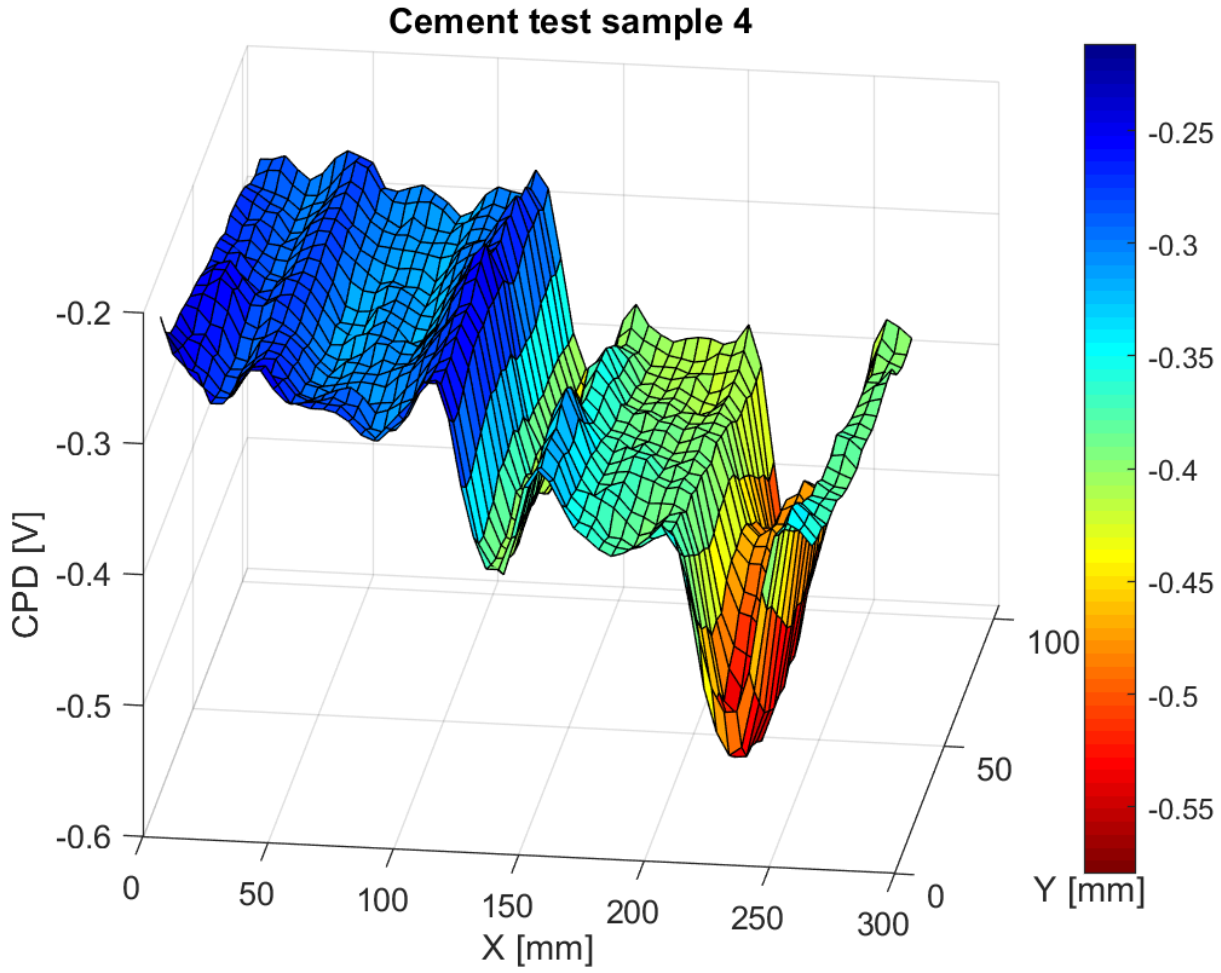

Figure 37: Surface plot from the scan of cement stone test sample 4. The difference in CPD between the corroding rebar and the surrounding cements stone is clearly seen, as in Figure 36. The pristine rebar is better seen in this plot, around X=50mm.

Scans of cement stone test sample 4 show that rebars embedded in cement stone are detectable with the FKP. In addition to the fact that the FKP can detect the rebars, the results from cement stone test sample 4 seem to suggest that the FKP can distinguish between a corroding and a pristine rebar.

3.3.6 Cement stone test sample 5

Now that there were encouraging results indicating that corroding rebars are detectable, the idea was to produce corrosion on the rebar and experiment with polarization (applying voltages between the different contents of the test sample). The fifth cement test sample was a 150x150mm^2 cement stone slab. In the slab, a rebar was embedded, at 5mm depth, in the middle of the frame as well as two carbon steel plates at the edges, one on each side of the rebar. The rebar was not parallel to the sides of the frame but was mounted at an angle of around 3^o. The

carbon steel plates would serve as counter electrodes to polarize the rebar, meaning to apply a voltage across the rebar and either electrode. The rebar was set at an angle to test the effect of distance on the polarization. The contents of cement test sample 5 prior to casting is shown in Figure 38.

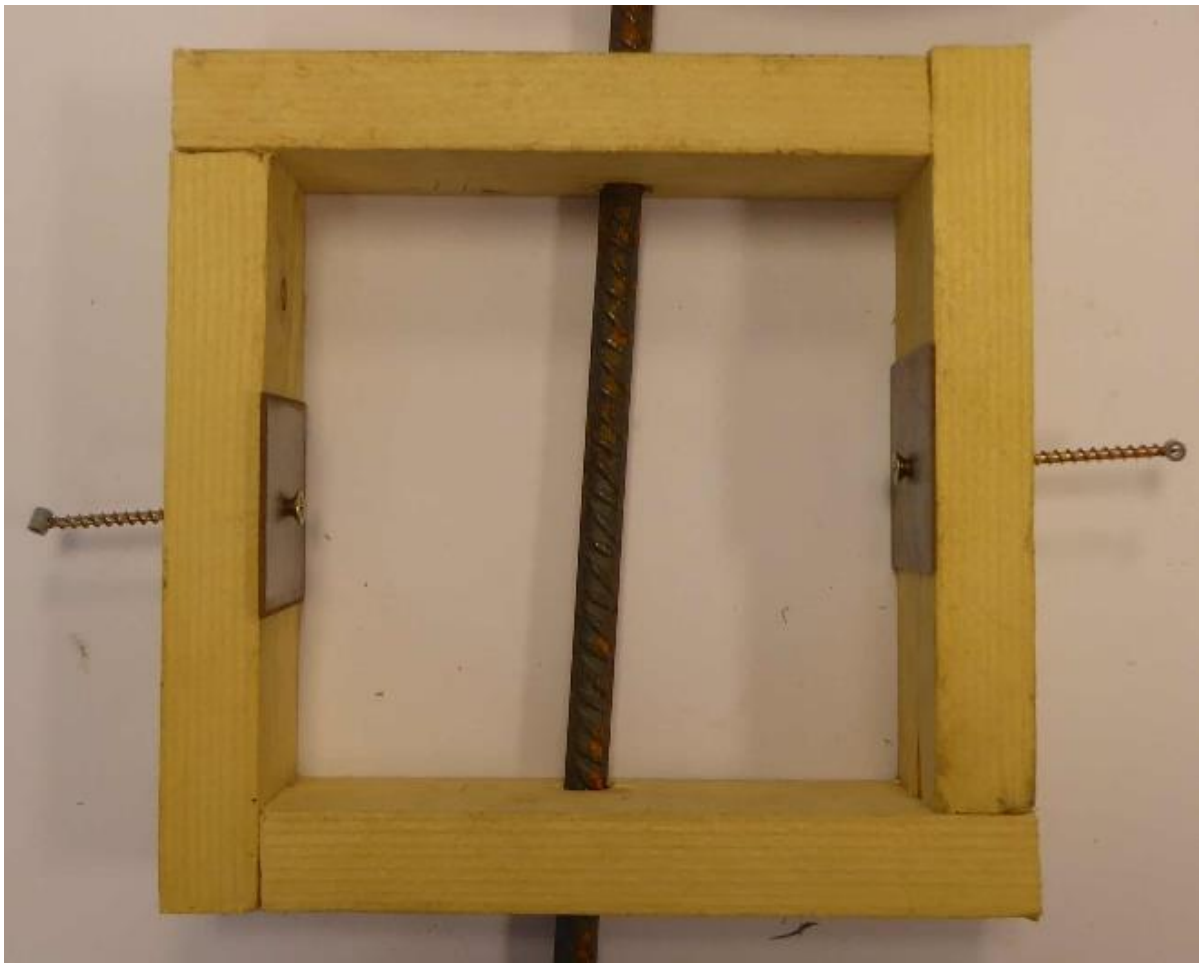

Figure 38: The contents of cement stone test sample 5.

While the polarization of the rebar in this sample proved fruitless, scans of the slab showed a curious feature on the rebar. In the middle of the rebar there seems to be a missing piece, which obviously could not be the case. This was first thought to be an effect caused by the resolution (grid size) of the scan (5mm) in combination with the angle of the rebar, but a scan with 1mm step size revealed the same feature again, proving that it was a real effect. Unfortunately, a picture from the top of the rebar was not taken prior to casting, making it impossible to know if there was some defect responsible for the feature that showed up in the scans. There are also some quite prominent features on both sides of the rebar, which could warrant further investigation. The heatmap from the scan with 1mm steps is shown in Figure 39.

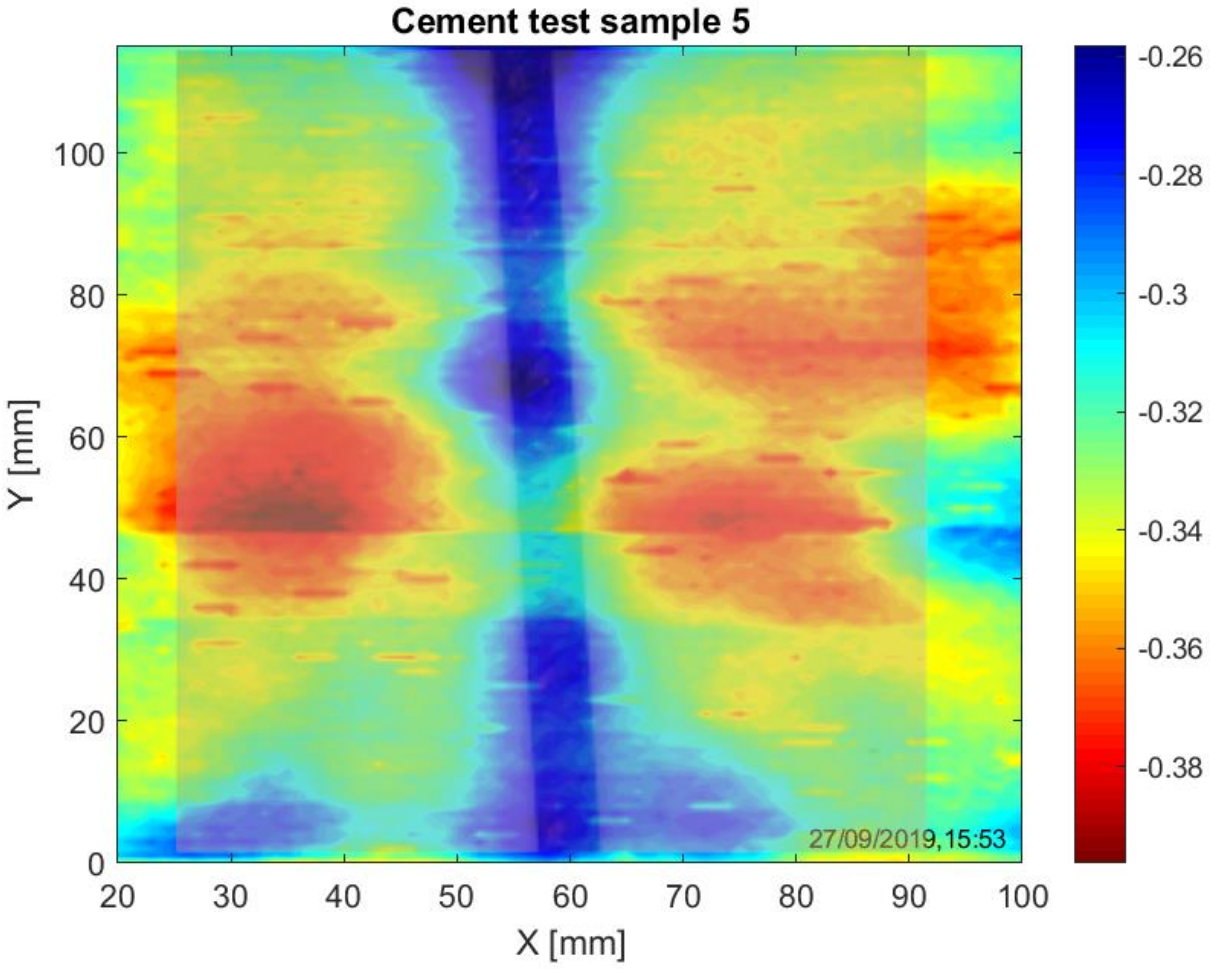

Figure 39: Heatmap from the scan of cement test sample 5 with image of the embedded rebar overlaid. The rebar seems to have a different potential near its centre (ca. X=60, Y=50).

While the rebar and the defects are clearly seen in the heatmap in Figure 39, the surface plot shown in Figure 40 makes it even clearer that the rebar does not have a uniform contact potential along its length. Quite prominent features along the rebar can be seen, especially the seemingly missing piece around Y=50. This feature, along with the other potential gradients along the rebars length could suggest active corrosion, or at least some defect on the rebar.

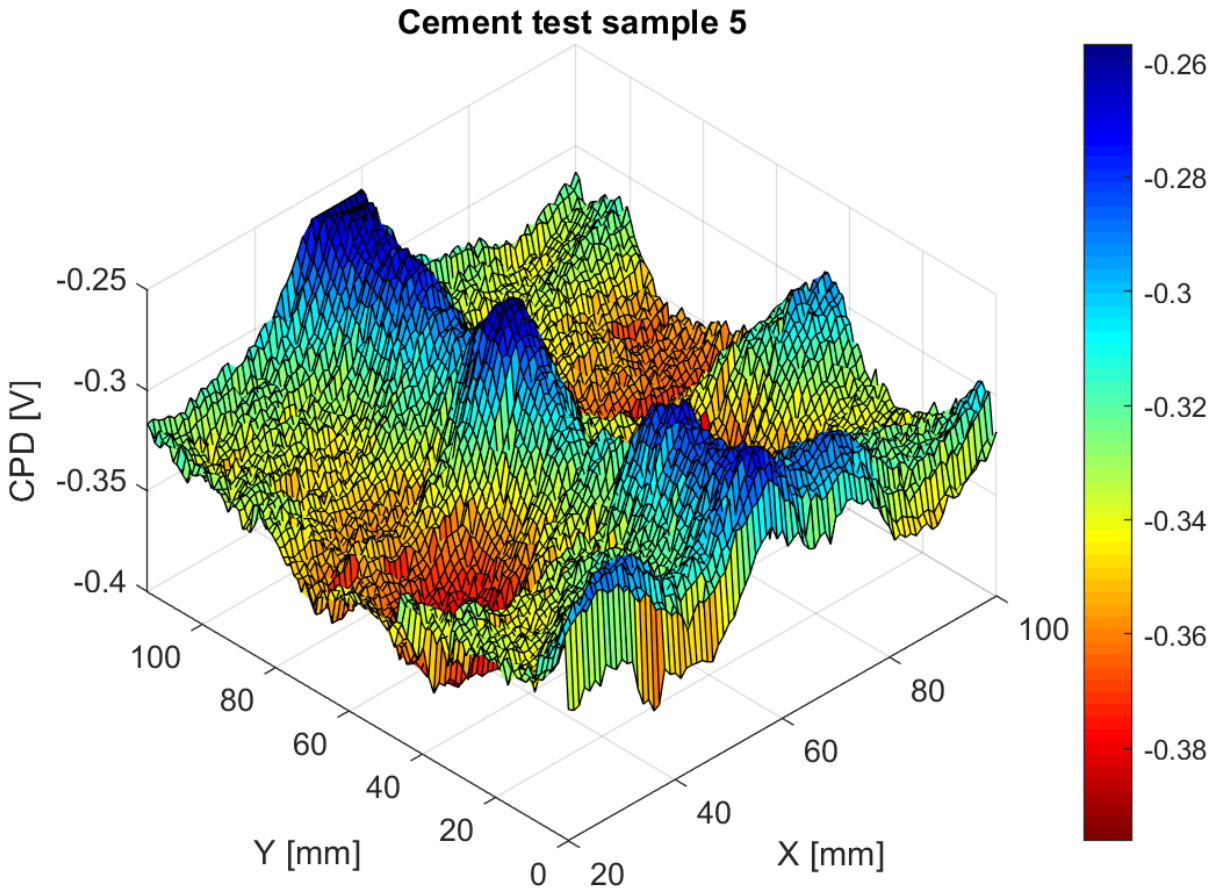

Figure 40: Surface plot from the scan of cement test sample 5.

Scans of cements stone test sample 5 did not specifically support the idea of corrosion detection. The results do however show that the FKP can pick up defects along the rebar in high detail, which would aid the detection of localized corrosion spots. If the spots with high potential gradients are not caused by active corrosion, it could suggest that stable (i.e. not actively corroding, but corrosion products etc.) defects are indeed detectable, contrary to what was found in the previous attempts (section 3.3.3-3.3.4). Because of this, yet another attempt was made with pre-corroded steel.

3.3.7 Cement stone test sample 6

A final attempt at distinguishing pre-corroded steel from pristine steel was made with cement test sample 6. Four carbon steel plates were connected in two pairs, one of them was sandblasted and the other was heavily rusted with 3.5% NaCl solution. The plates were screwed into a piece of wood which was then used to hold them in place during casting in a 185x150mm^2 wooden frame, so the depth was around 7mm. The contents of the sample are shown in Figure 41.

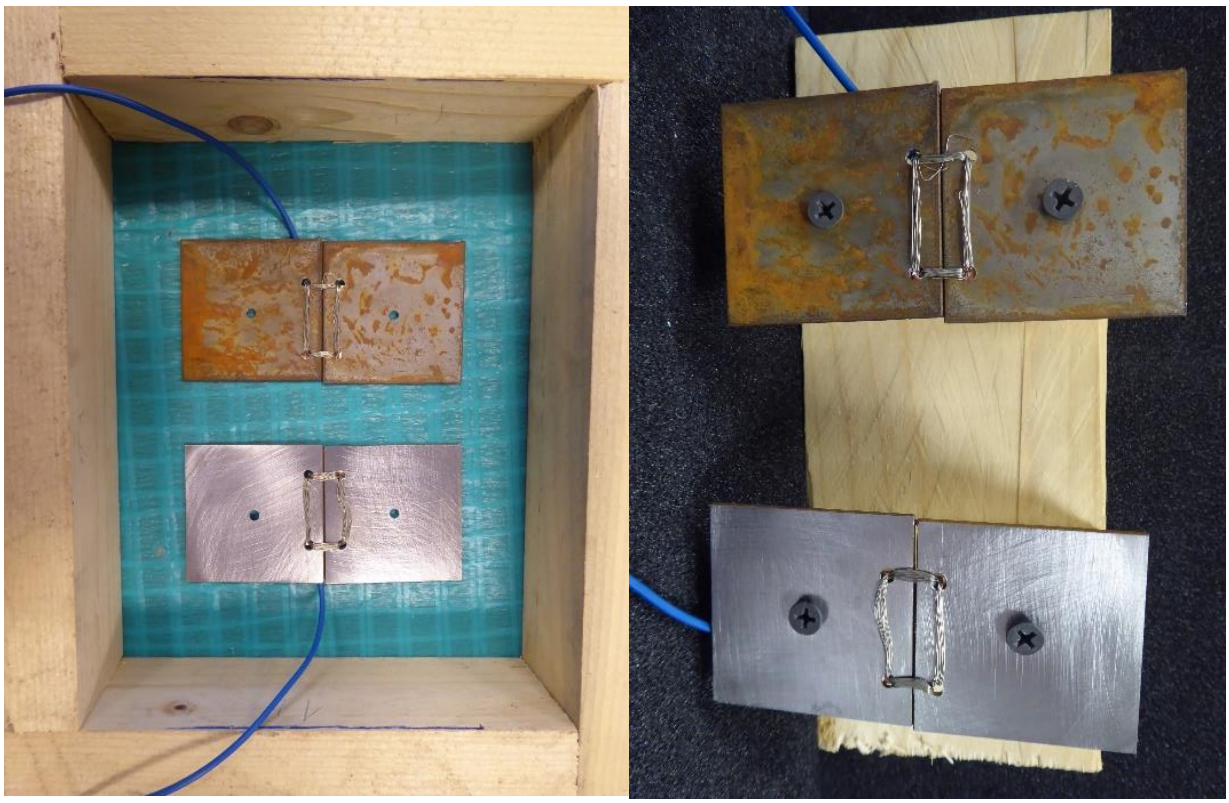

Figure 41: The contents of cement test sample 6. Four carbon steel plates connected in two pairs, one sanded and one heavily rusted.

As before, scans showed that the steel plates were clearly distinguishable from the surrounding environment and as before, no distinction between the pristine and corroded steel was apparent. The heatmap and surface plot from the scans are shown in Figure 42 and Figure 43, respectively.

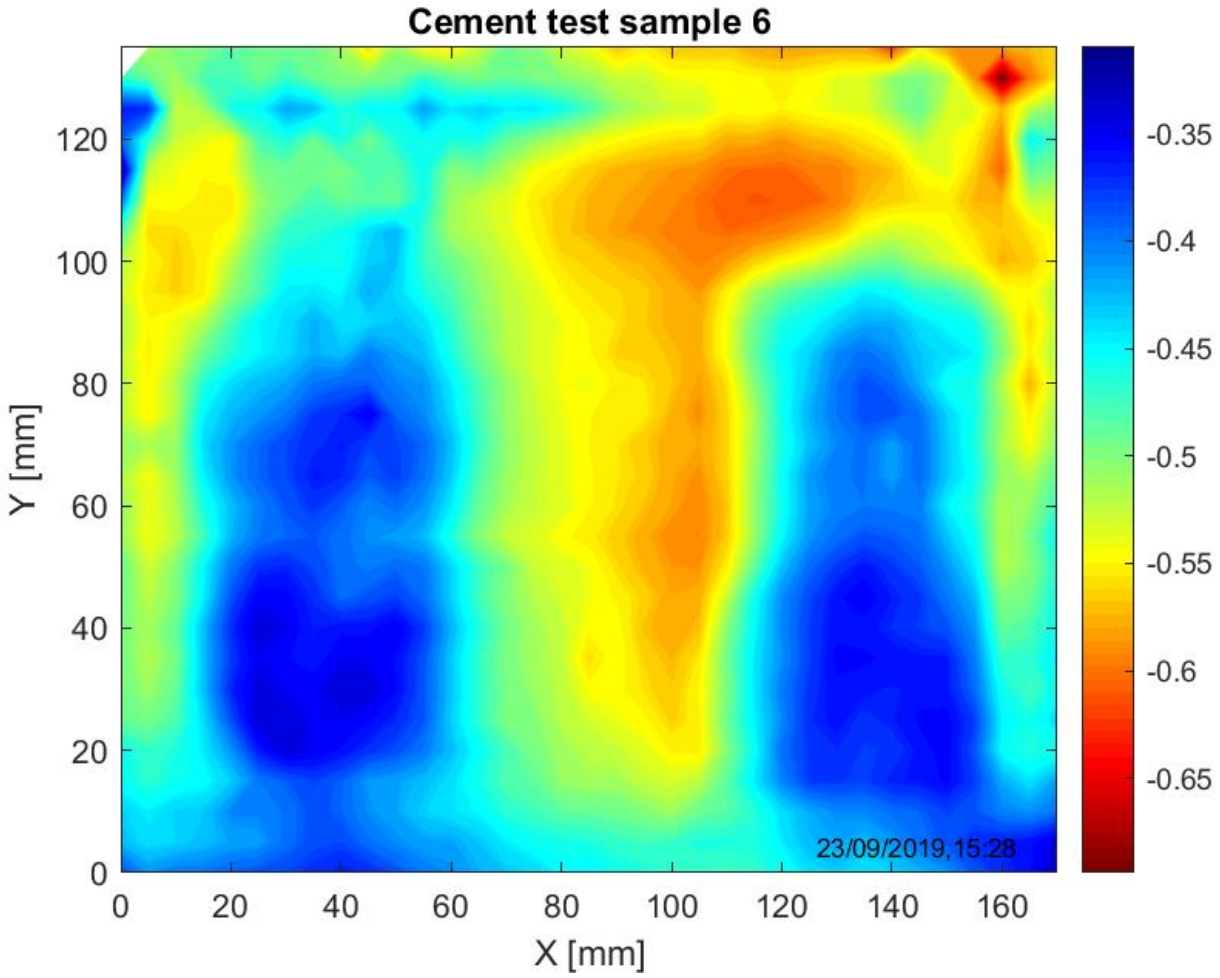

Figure 42: Heatmap from the scan of cement test sample 6. The two sets of carbon steel samples are basically indistinguishable, even though one was corroded and the other was pristine prior to sample casting (see Figure 41).

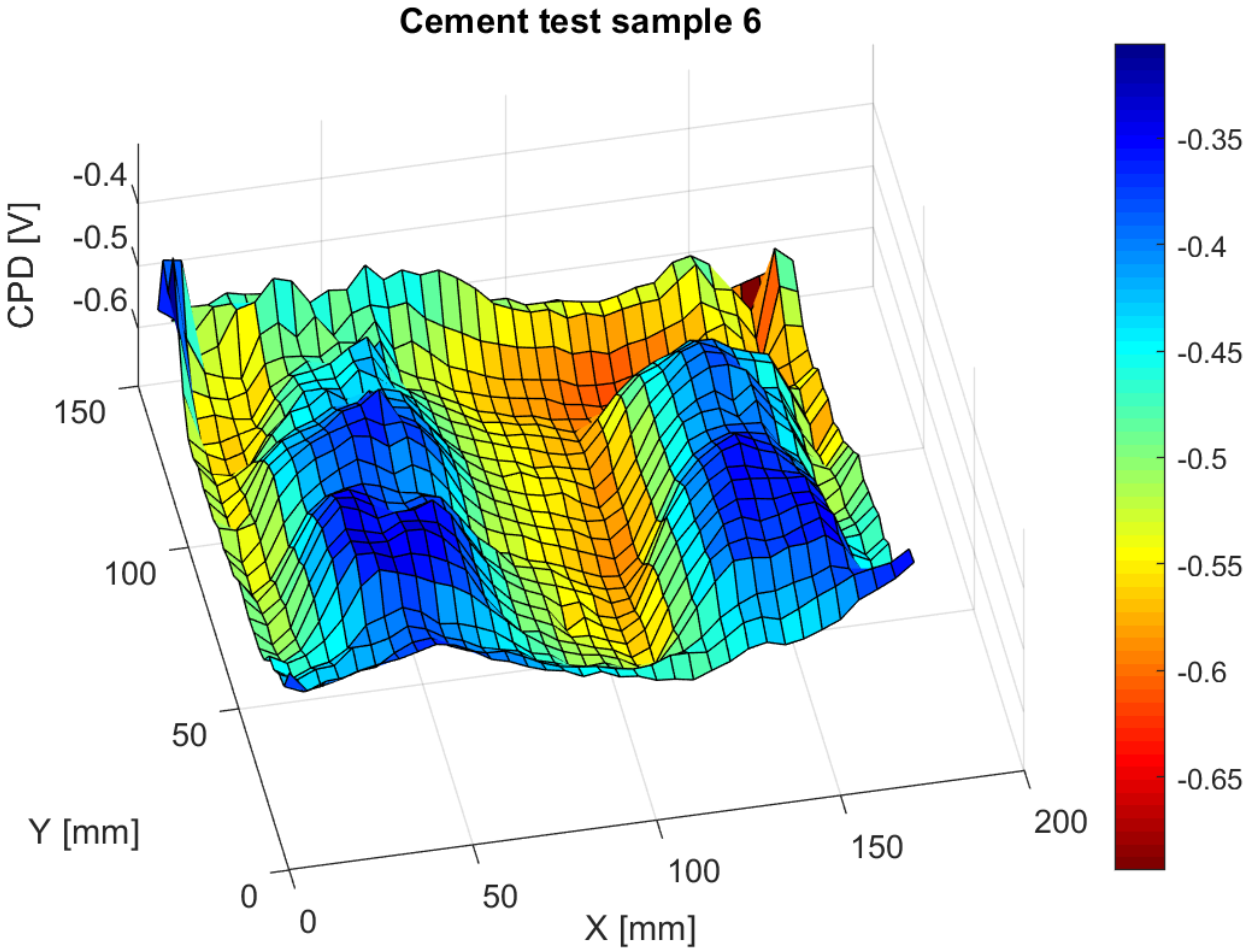

Figure 43: Surface plot from the scan of cement test sample 6.

The results from cement stone test sample 6 show yet again that pre-corroded steel is not distinguishable from pristine steel using the FKP. This suggests that the defects on the rebar in cement stone test sample 5 (section 3.3.6) are something else, possibly active corrosion. It is however difficult to say much about what has happened below the sample surface after casting.

3.3.8 Cement stone test sample 7 – The Cemwich

The results from cement test sample 2 gave some indication that it could be possible to distinguish a pre-corroded pattern from pristine steel. The subsequent results, however, seems to indicate that it is not. It seems likely that during casting and curing, some chemical reactions happen that equalize the electric potential of the steel plates, quite possibly forming the same oxide layer on all embedded steel (passivation – section 1.2.1). To counteract the uncertainties related to the condition of the steel embedded in the cement stone, a reopenable "cement sandwich" (Cemwich), was created. The aim was to make a cement brick which could be

opened multiple times, making it possible to control the condition of the steel that was placed inside the slot. Wires were split and cast into both parts of the Cemwich, to create a common connection to the FKP for the cement stone and the steel. A schematic drawing of the Cemwich is shown in Figure 44.

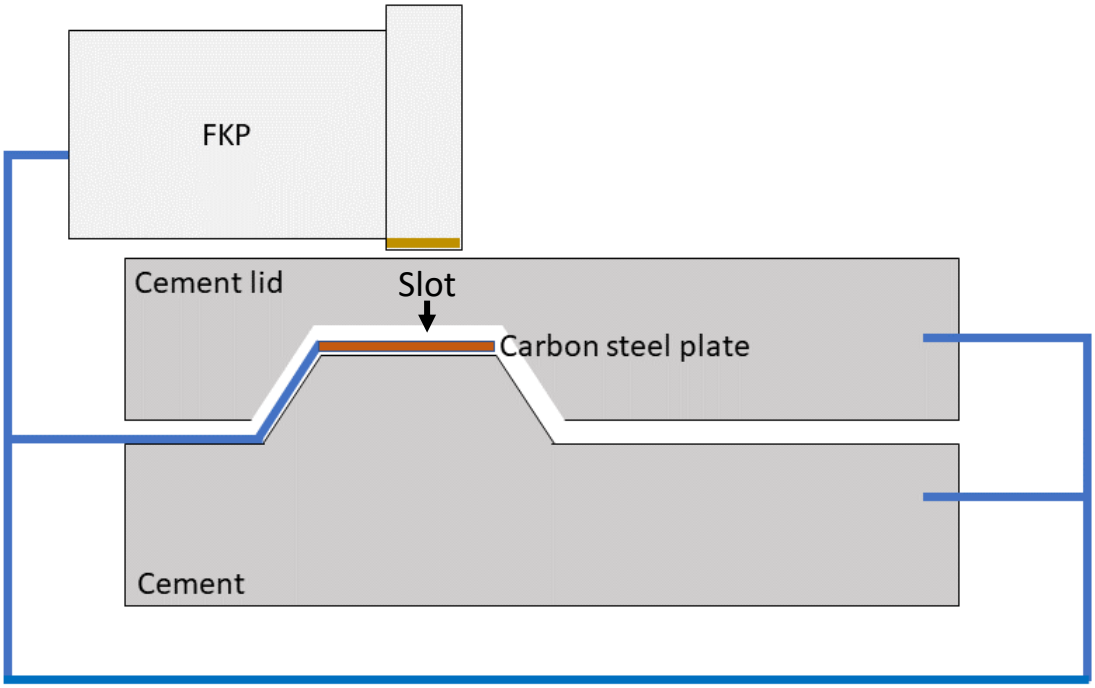

Figure 44: Schematic drawing of the Cemwich, a cement stone brick in two parts. The idea was that a steel plate could be placed inside the slot and its corrosion conditions could be controlled by e.g. adding NaCl.

Three versions of the Cemwich was made. The first two had structural problems and broke easily if not handled with extreme care. The third and last Cemwich was sturdy enough to withstand the measurement process. Pictures of the three versions of the Cemwich are shown in Figure 45.

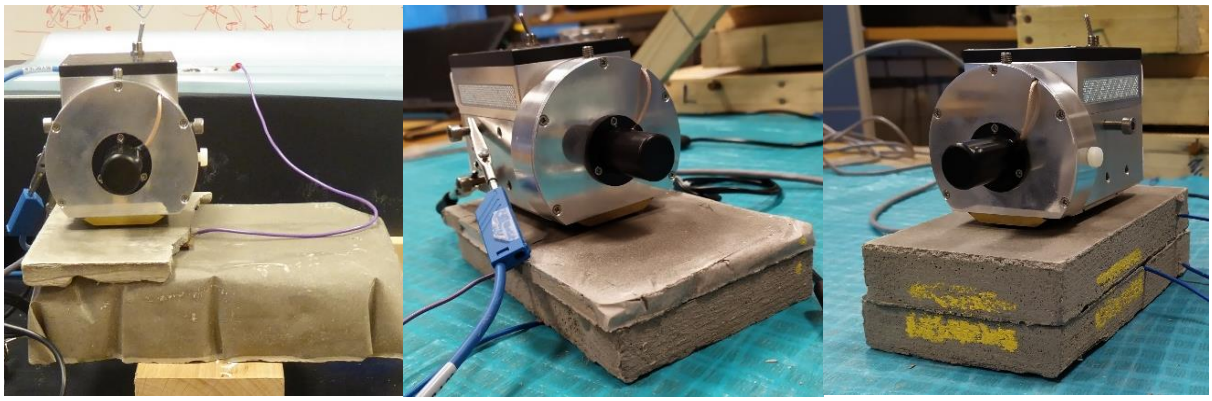

Figure 45: The three versions of the Cemwich, in chronological order from left to right. The lid of the first two versions was too thin and broke during the measurement process. The final version is the one that was ultimately used.

Measurements on the Cemwich were done without the scanning robotic stage setup (section 3.1), in a single spot right above the slot. Measurements were taken when the slot was empty, then with a carbon steel plate (the same kind as in cement stone test sample 1 – section 3.3.2). This was done once then repeated before 3.5% NaCl solution was added on the steel to induce corrosion. The results are shown in Figure 46.

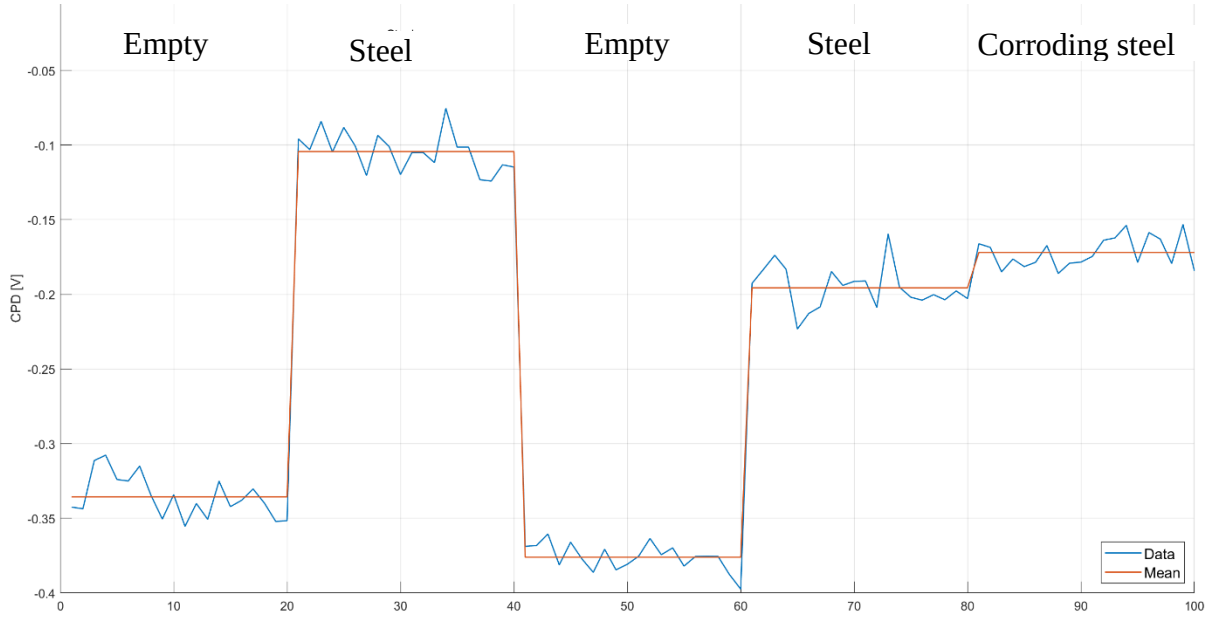

Figure 46: Spot measurements on the Cemwich, right above the "slot". Measurements were done with the slot empty and then with a steel sample in. This step was repeated before adding NaCl to the steel plate to induce corrosion. X-axis has arbitrary units (number of measurement).

There is a clear difference between when the slot is empty and when the carbon steel plate is placed inside. There also seems to be a slight difference between pristine and corroded steel, but the difference is quite small, and does not land outside the spread of the measurements. This

result showed some promise, but subsequent tests showed a high degree of randomness in the measurements when steel with and without active corrosion were added and removed. This could be due to the slowly changing humidity in the cement stone (as the water/NaCl solution diffuses) or some other effect. As a result, the Cemwich experiments were abandoned. They did show some promise and could warrant further experimentation, but due to time constraints and the emergence of another idea, it seemed logical to move on to the next test sample.

3.4 The final concrete testing design – The interrupted rebar

From the previously described experiments, it became clear that real corrosion is difficult to produce in a controllable way. Pre-corroding the samples before casting produced no tangible results, and the Cemwich experiments were inconclusive. The conclusion from this was that a different approach was needed.

3.4.1 Concept and design

A solution was suggested by Prof. Sylvia Keßler, to imitate corrosion by applying a voltage between a portion of the rebar and a stainless-steel mesh or another rebar (to imitate the anodic and cathodic regions – section 1.2.1). A rebar was cut into three pieces, two big and one small, and reassembled with plastic tubes and X60 quick glue to ensure no electrical contact. A stainless-steel mesh was placed at the bottom of the frame, to serve as both a counter electrode for applying a voltage and to serve as a possible connection point for the FKP. Wires leading out of the frame were connected to the small rebar piece and the mesh, while the other rebar pieces were sticking out of the frame. The test sample was then cast in cement stone. A schematic of the interrupted rebar setup is shown in Figure 47.

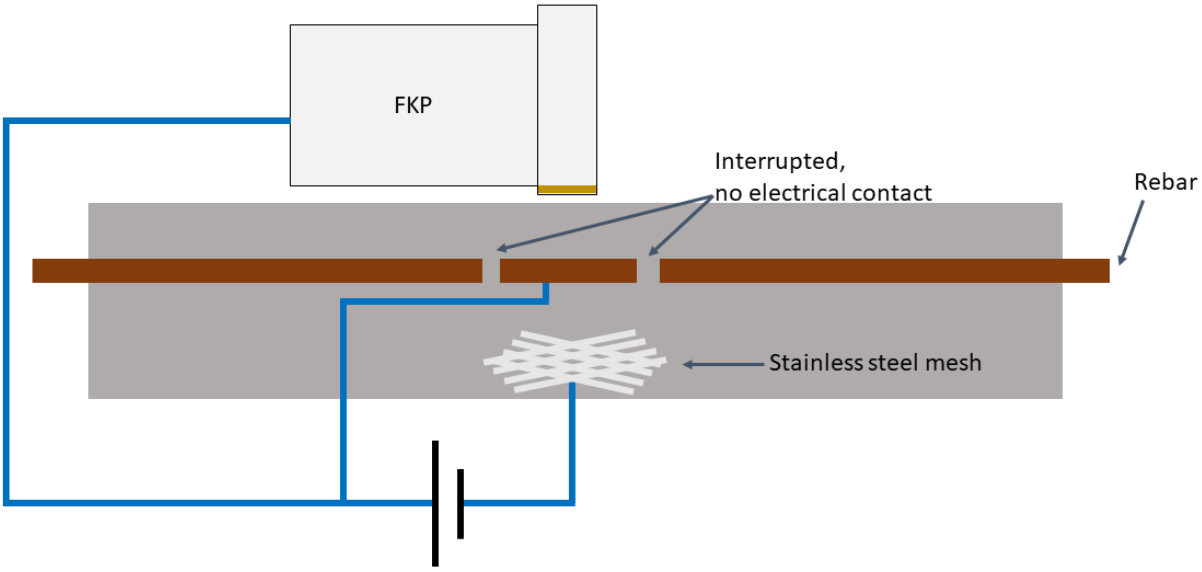

Figure 47:Schematic of the experimental setup with the interrupted rebar design to imitate corrosion on a portion of the rebar, by polarizing against a stainless-steel mesh.

Images of the contents of the interrupted rebar test sample before casting are shown in Figure 48.

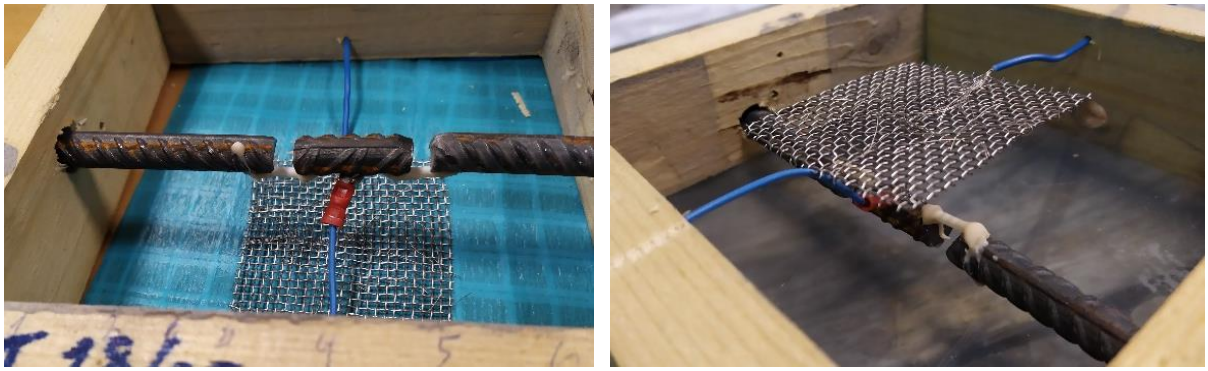

Figure 48: The inside of the interrupted rebar test sample, seen from the top (left) and bottom (right). (The mesh is leaning on the wire from the small rebar piece but they are not electrically connected).

3.4.2 Parallel plate capacitor model of the interrupted rebar test sample

For the purpose of creating a simple simulation of the measurements on the interrupted rebar test sample presented in sections 3.4.4 and 3.4.6, the parallel capacitor model presented in section 2.3.2 was modified slightly. The difference from the original model is that the rebar is now split into three parts where the voltage U_0 is applied between the two outer rebar pieces and the centre piece in such a way that the centre piece has zero potential and the two side pieces have the potential $-U_0$.

The basis of the simulation is equation (8) from section 2.3.2, where $\epsilon_{concrete}$ and ϵ_{air} are the relative dielectric constants for concrete ($\approx 4.5\epsilon_0$) and air ($\approx 1\epsilon_0$) respectively[26] (the dielectric constant for cement stone was not found, so concrete was used instead). *t* and *d* are the thicknesses of the cement stone cover and the work distance (probe-sample distance) of the FKP, respectively.

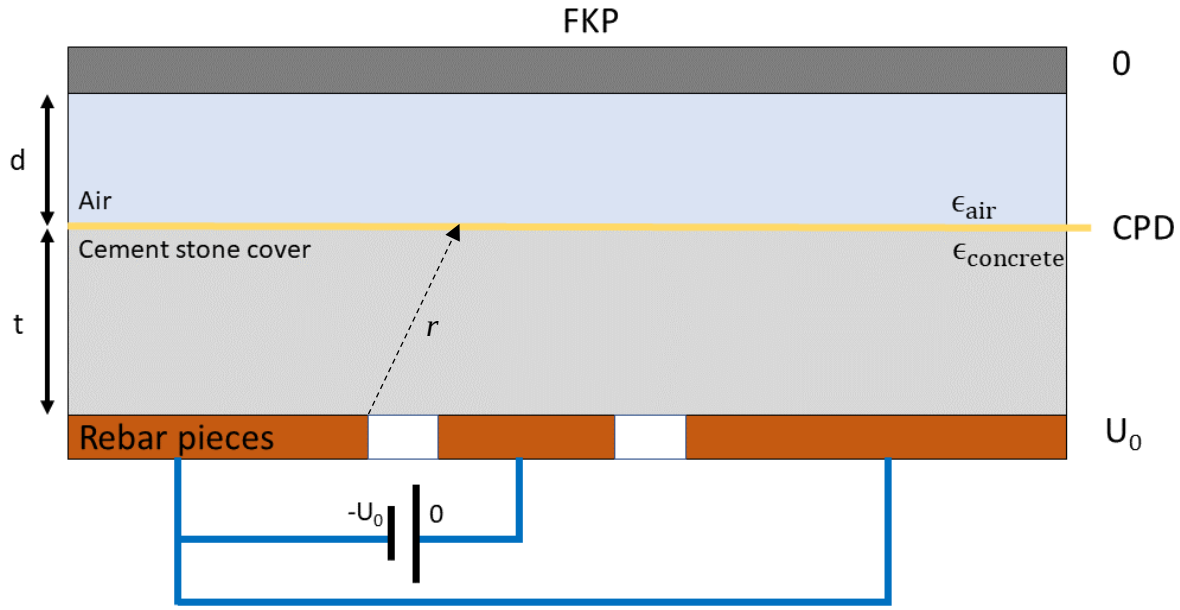

Figure 49: A simple model of the FKP-rebar system. The FKP and rebar form the two parts of a parallel plate capacitor. In between are two different dielectrics, the cement stone and air. By assuming that the potential U_0 is the same as the applied voltage and the potential at the FKP is zero (i.e. the potential difference between them is U_0), the potential at the cement stone-air interface can be calculated. The voltage was applied in such a way that the middle rebar piece sits at zero potential and the two side pieces sit at U_0.

This approximation in equation (8) seems reasonable right above the source of the potential U_0, i.e. the two side pieces. When moving along the rebar across the cement stone surface, towards the middle (from either side), it was assumed that the potential drops as *1/r*, where *r* is the distance from the potential source to the spot in question on the surface. Adding this to equation (8) yields the following for the contact potential difference *CPD*:

$$CPD(r) = \frac{\epsilon_{concrete} d}{\epsilon_{air} t + \epsilon_{concrete} d} U_0 \frac{t}{r} \tag{11}$$

In addition to this, comes the fact that the cement stone surface itself has its own electrochemical potential relative to the FKP. By looking at the data from the uncertainty test (Figure 61), and looking at the peak values for the lines, it can be assumed that the cement stone

has a potential of around -0.3V relative to the FKP. Adding these to equation (11) yields the following for the interface potential:

$$CPD(r) = -0.3V + \frac{\epsilon_{concrete} d}{\epsilon_{air} t + \epsilon_{concrete} d} U_0 \frac{t}{r}$$

Testing of the model revealed a systematic error in the contrast (max-min value) of each line of 100-200mV. The following was observed: The centre of the zero applied potential line in Figure 61, where the potentiostat was disconnected, is shifted from the 100mV line by a disproportionately large margin compared to the other cases. It seems likely that simply connecting the potentiostat alters the measured potential. Investigation of the data revealed that the centre point of the lines shifts by an average of 22mV between steps, except the zero line, which shifts by 162mV. By assuming that the line would have shifted by the average, had it still been connected to the potentiostat, the influence of connecting the potentiostat is 140mV. This value is therefore added to the applied potential U_0, resulting in the final expression for the interface potential:

$$CPD(r) = -0.3V + \frac{\epsilon_{concrete} d}{\epsilon_{air} t + \epsilon_{concrete} d} (U_0 + 0.14V) \frac{t}{r} \quad (12)$$

Plotting the interface potential from equation (12) with $\epsilon_{concrete} = 4.5\epsilon_0$, $\epsilon_{air} = 1\epsilon_0$, $d = 1mm$, $t = 5mm$, and U_0 decreasing from 0.5V to 0.1V in 0.1V steps produced the plot shown in Figure 50.

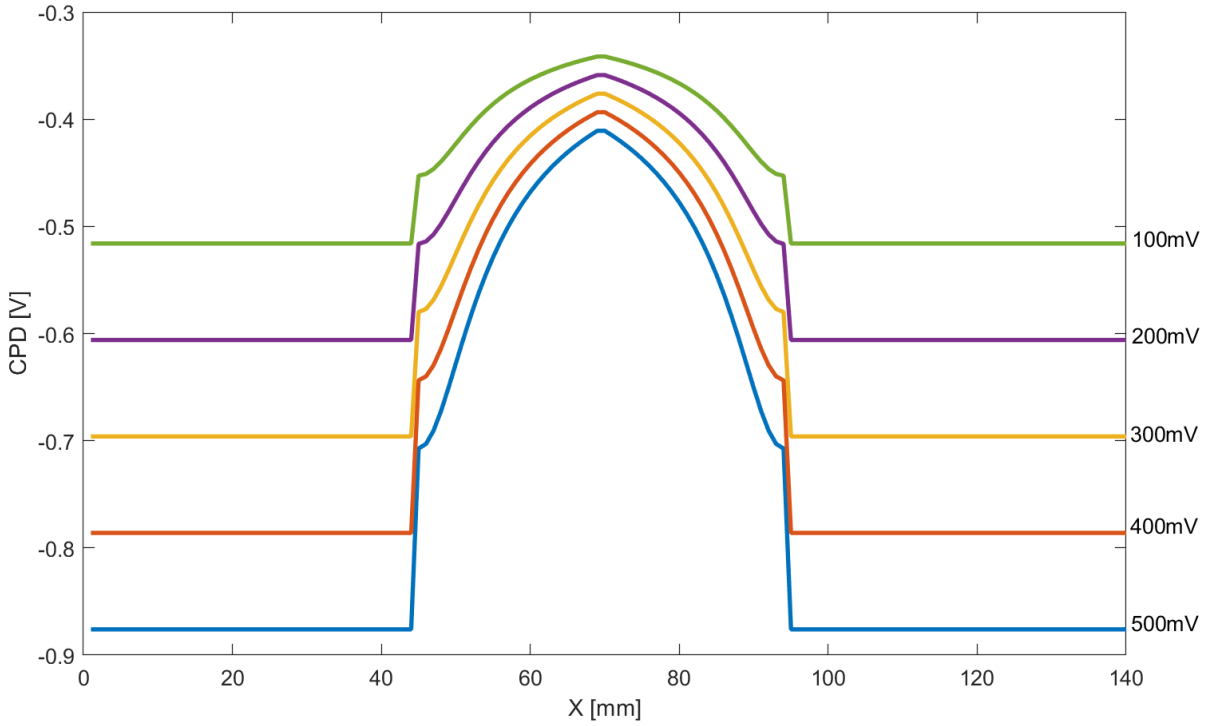

Figure 50: Plot of the simple model of the FKP-interrupted rebar system with applied voltages from 500-100mV.

The model was compared with two experiments, presented in sections 3.4.4 and 3.4.6. The results, presented in Figure 56 and Figure 62, show a very good agreement between the experimental data and the theoretical model regarding the linear relationship between the contrasts (maximum value - minimum value) and the applied voltage.

3.4.3 Polarization against stainless steel mesh

A “proof of concept” test was done by connection a 1.5V battery between the stainless steel mesh and the middle rebar piece. As seen in Figure 51, the rebar piece clearly shows up as a sharp peak in contrast to the surrounding environment. The increasing CPD towards lower X values is most likely due to the test sample not being completely level on the stage and the rebars being embedded at a slightly uneven depth, since the FKP is quite sensitive to small differences in work distance.

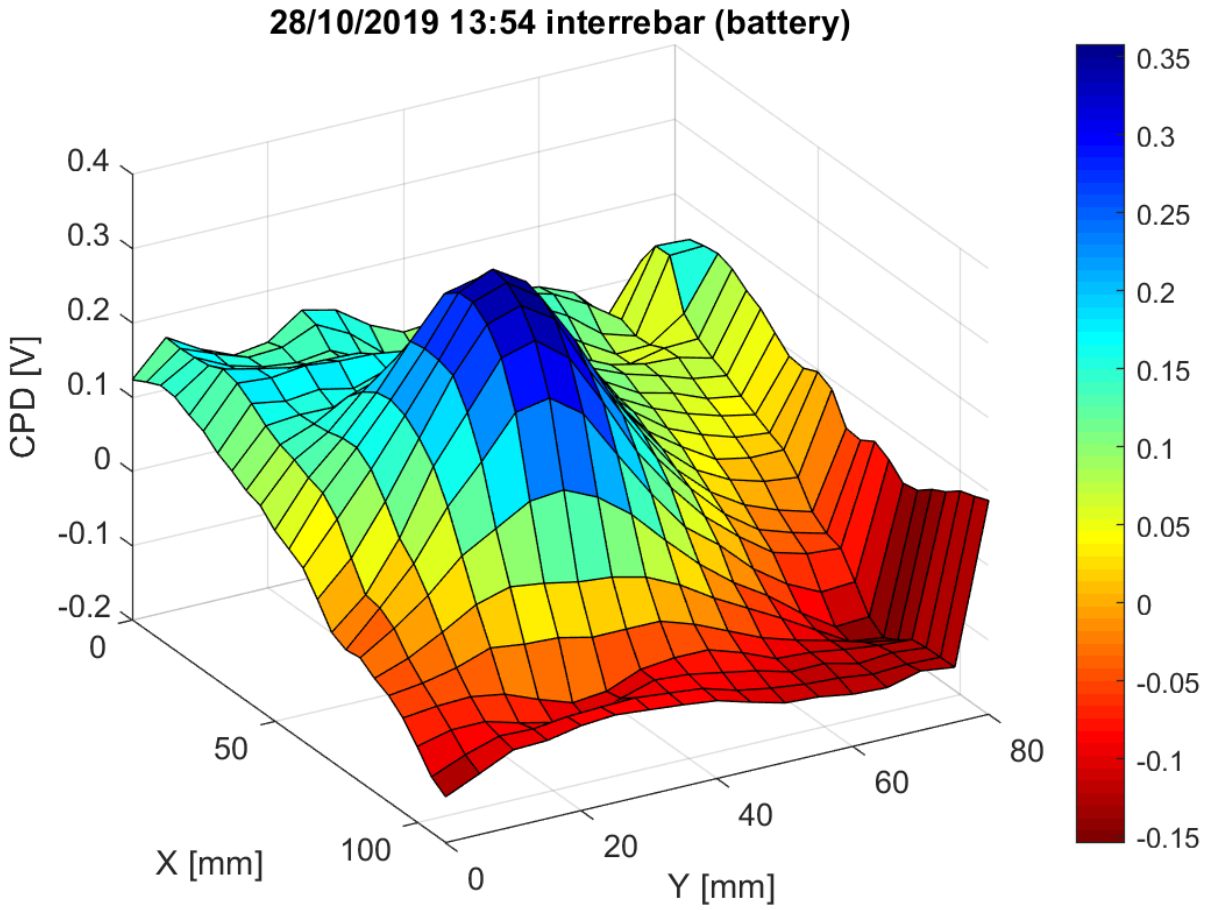

Figure 51: Surface plot from scanning the interrupted rebar when polarized with a 1,5V battery. The bump in the plot coincides with the location of the small rebar piece (X=50mm, Y=40mm).

3.4.4 Polarization against rebar

This encouraging result prompted further experiments on the interrupted rebar test sample. In the case of active corrosion, distinct CPD gradients are a good indicator pinpointing the corrosion spots. The question now was: How small such gradients are observable with the FKP? A potentiostat was connected between the small rebar piece and the two longer pieces on the sides, as shown in Figure 52. Scans of the test sample were done with the potentiostat applying decreasing voltages in 50mV steps from 500mV to 0mV over the course of around 20 hours. The first scan, with an applied voltage of 500mV, is shown in Figure 53.

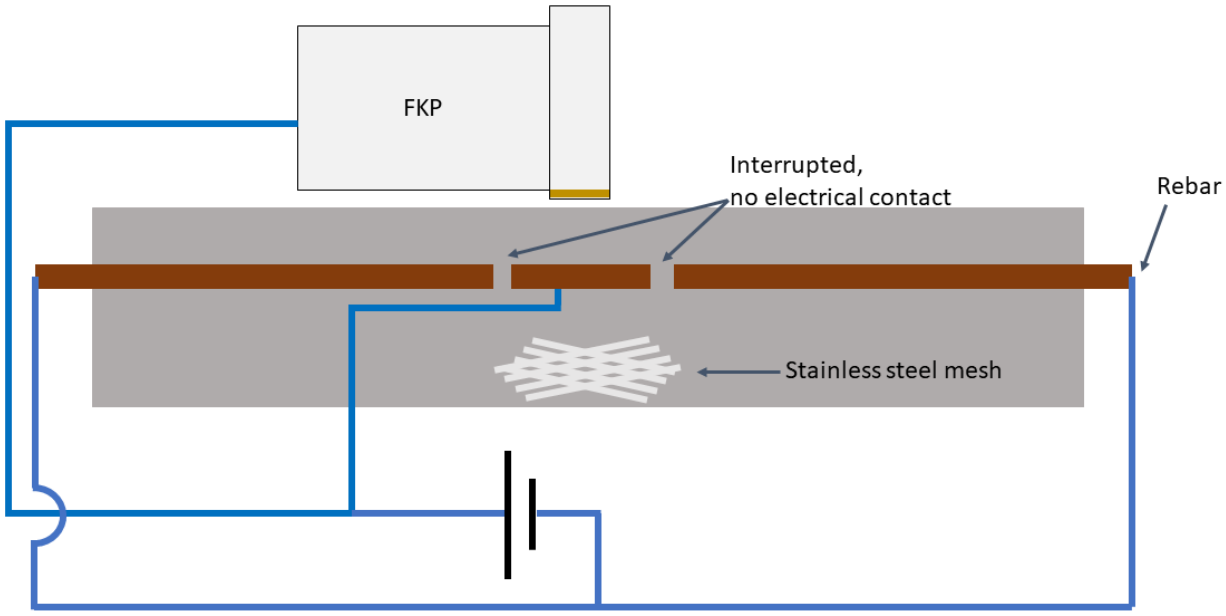

Figure 52: Schematic drawing of the setup of the interrupted rebar test sample. Small rebar piece polarized against the two larger rebar pieces and connected to the FKP. The potentiostat is indicated by the battery symbol. Note: The connections are different than in Figure 47.

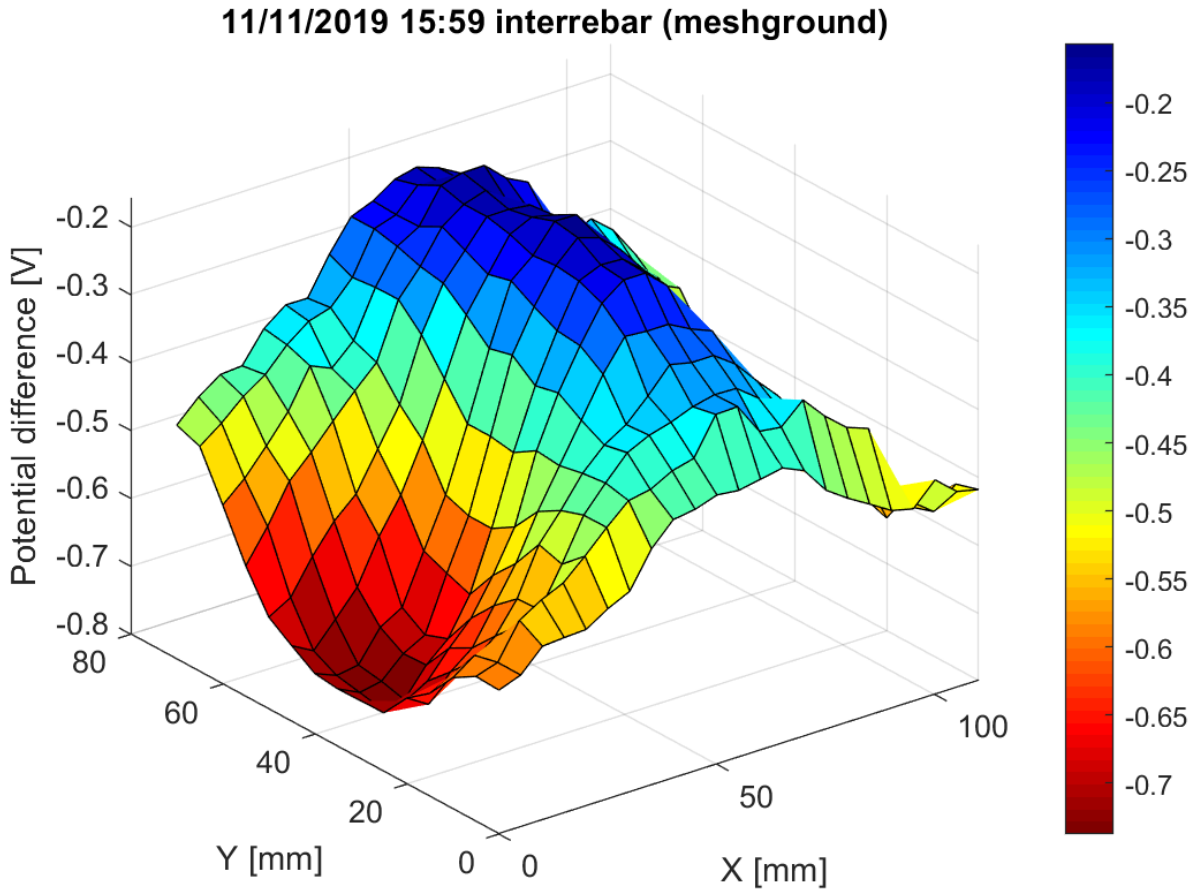

Figure 53: Surface plot of the interrupted rebar test sample with a 500mV voltage applied across the rebar piece and the mesh.

Due to the connection of the different pieces of the sample, with the small rebar piece and FKP sitting at the ground potential, the picture is opposite to the one in Figure 51 (in Figure 51, the middle rebar piece had an elevated potential. Here, the two side pieces have a lower potential). The longer side rebar pieces sit at a lower potential than the surrounding environment, including the small piece.

To show a representation of how the scans change with the applied voltage, cross-sectional surface scans were taken in the X-direction, through Y=30mm which is the line with the biggest potential gradient (maximum to minimum) as shown Figure 53. There was a slight drift in the measurement results over the 20 hours, most likely due to the temperature changes in the room (the temperature was regrettably not recorded). To factor out this drift, the cross-sectional profiles were normalized in the following way: The CPD value of the centre point of each profile was subtracted from every point on that profile, so that the centre point has a CPD value of zero (The raw data can be seen in Appendix I). Since the centre point is located at the small

rebar piece, which sits at the ground potential with the FKP, it should be unaffected by the applied voltage. Figure 54 shows the normalized cross sectional profiles as a function of applied Voltage. The same cross-sectional profiles are shown in Figure 55, superimposed on each other in a 2D-plot.

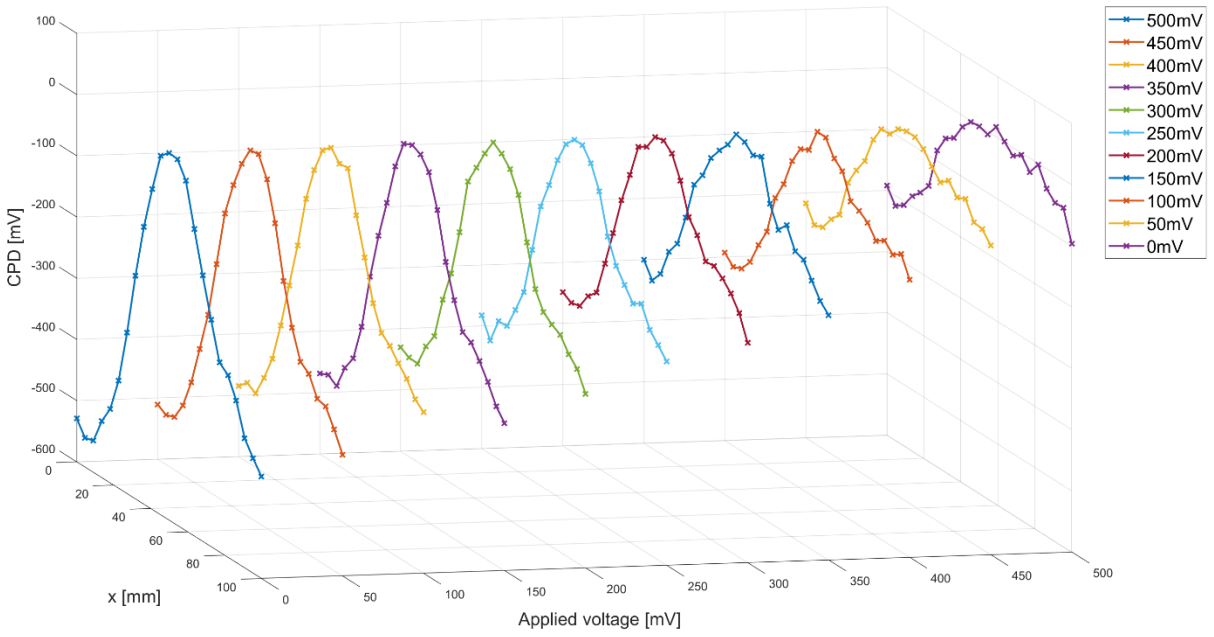

Figure 54: 3D- plot of the cross-sectional profiles as a function of applied voltage. The profiles have been normalized to account for drift in the measurement data.

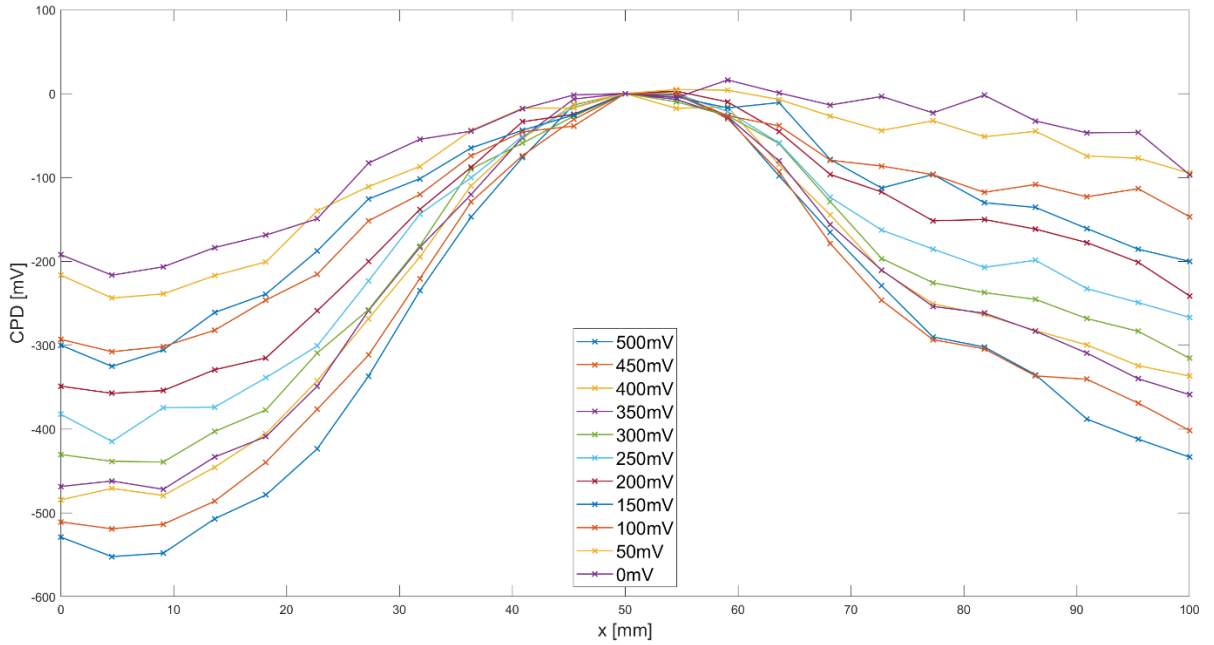

Figure 55: 2D-plot of the cross-sectional profiles shown in Figure 54 as a function of applied voltage. The profiles have been normalized to account for drift in the measurement data. There is a general tilt

in the measurement, i.e. higher values on the right. This is probably due to both uneven depth of the rebar and levelling of the sample on the stage.

From Figure 54 and Figure 55 it becomes clear that the changes in the CPD profiles, as a consequence of applying an external voltage between the small and the two large rebar pieces, is measurable with the FKP. There is a tilt in the measurements, i.e. the values are higher on the right side than the left. It is likely that this is caused both by uneven depth of the rebar and the levelling of the test sample on the stage as previously discussed. In Figure 56, the results are compared with the theoretical model described before (section 3.4.2). The difference between the maximum and the minimum CPD, or "contrast", of the 11 cross-sectional profiles are plotted, showing a linear relationship between the contrast and the applied voltage that matches well with the theoretical model (section 3.4.2), although the slope is slightly off. There is a systematic shift of 50-100mV between the experimental and theoretical contrasts. It could be that the line (Y=30) slightly misses the rebar as this experiment was not originally intended to show single lines. This experiment was also performed several months prior to the one in section 3.4.6, and the conditions in the cement stone has likely changed in that time (changing the permittivity etc.), which this simple model does not account for. A better representation of the of the model is presented in Figure 62 in section 3.4.6.

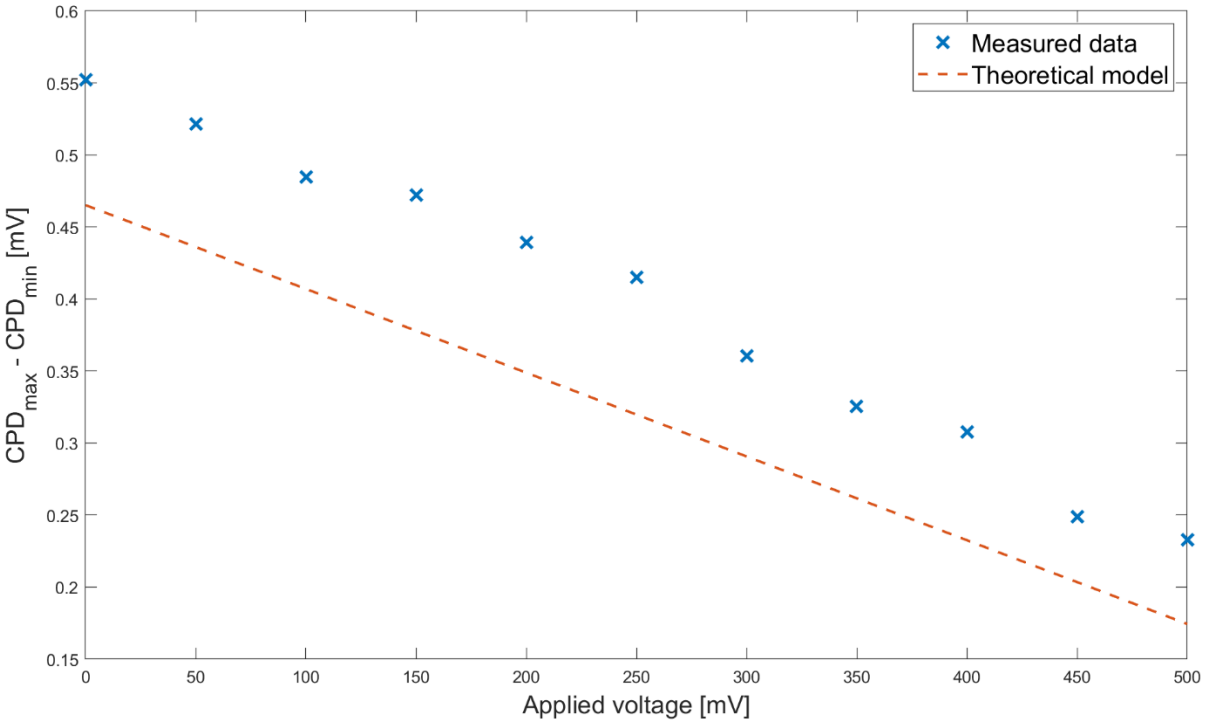

Figure 56: The difference between maximum and minimum CPD, or "contrast", for the cross-sectional profiles as a function of applied voltage. The linear trend is well produced by theoretical model from

section 3.4.2, although the slope is slightly off. There is a systematic shift of 50-100mV between the experimental data and the theoretical model. The slope and systematic shift are likely a result of the model not taking into account the changes in the cement stone humidity conditions at the time of the experiment.

3.4.5 Coating

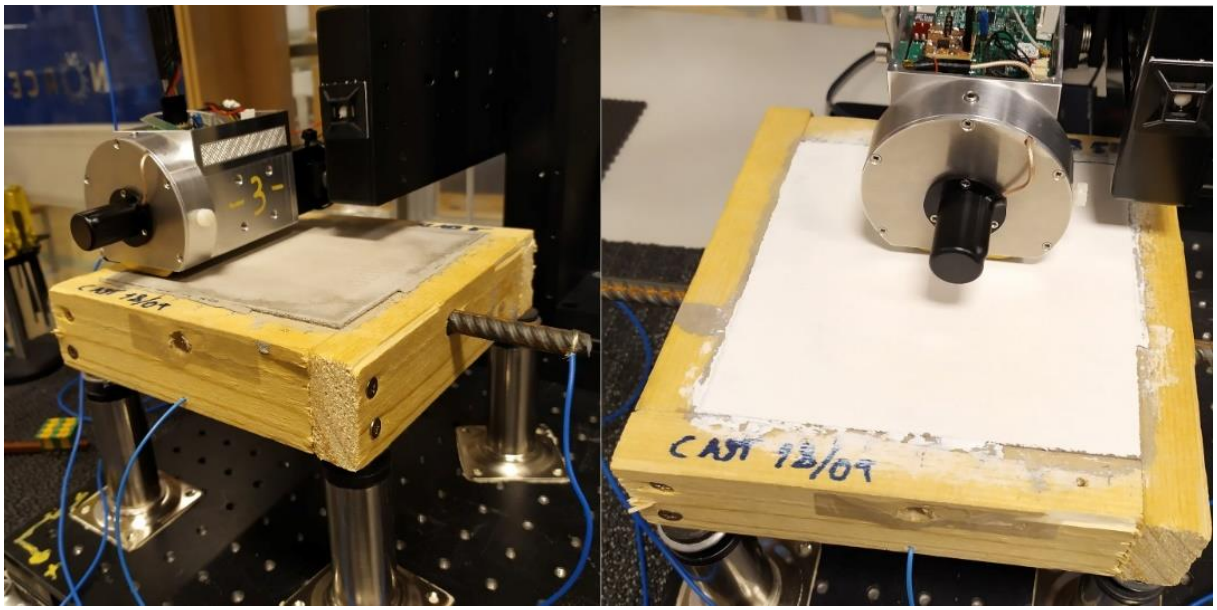

Figure 57: The interrupted rebar test sample before (left) and after (right) coating with Bengaläck.

As discussed in section 3.2, previous testing on non-concrete samples have been done, demonstrating that the FKP can measure CPD through non-conducting coatings. To test whether this also applies to concrete, two scans were done. A voltage of 500mV was applied in the same way as before and the sample was scanned. A coat of Bengaläck was then applied and the procedure was repeated. Figure 57 shows pictures of the test sample before and after the coating was applied. The two resulting scans are shown in Figure 58 and the cross sectional profiles of the two are shown for comparison in Figure 59.

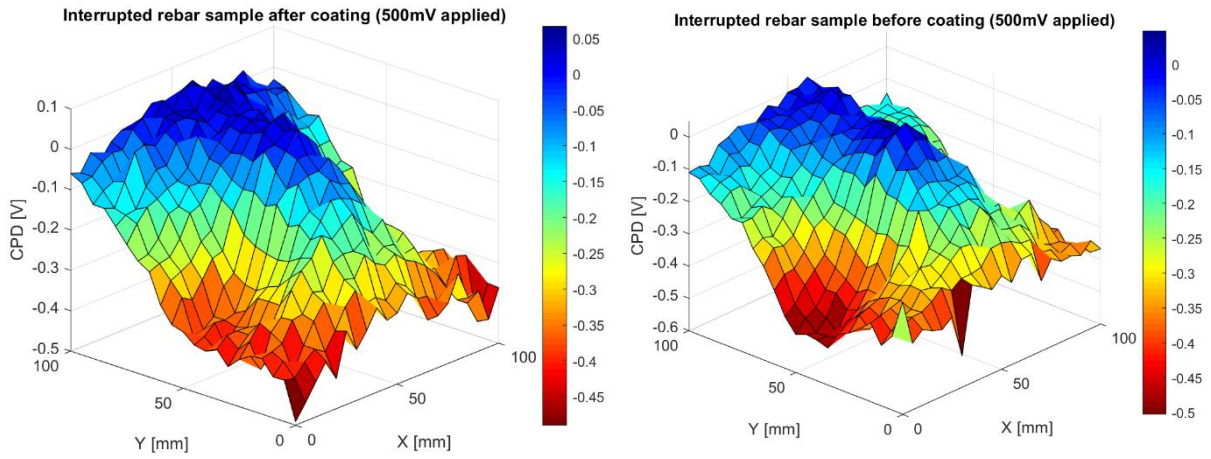

Figure 58: Surface plot of the measured CPD on the interrupted rebar test sample before and after coating with Bengalack with an applied voltage of 500mV.

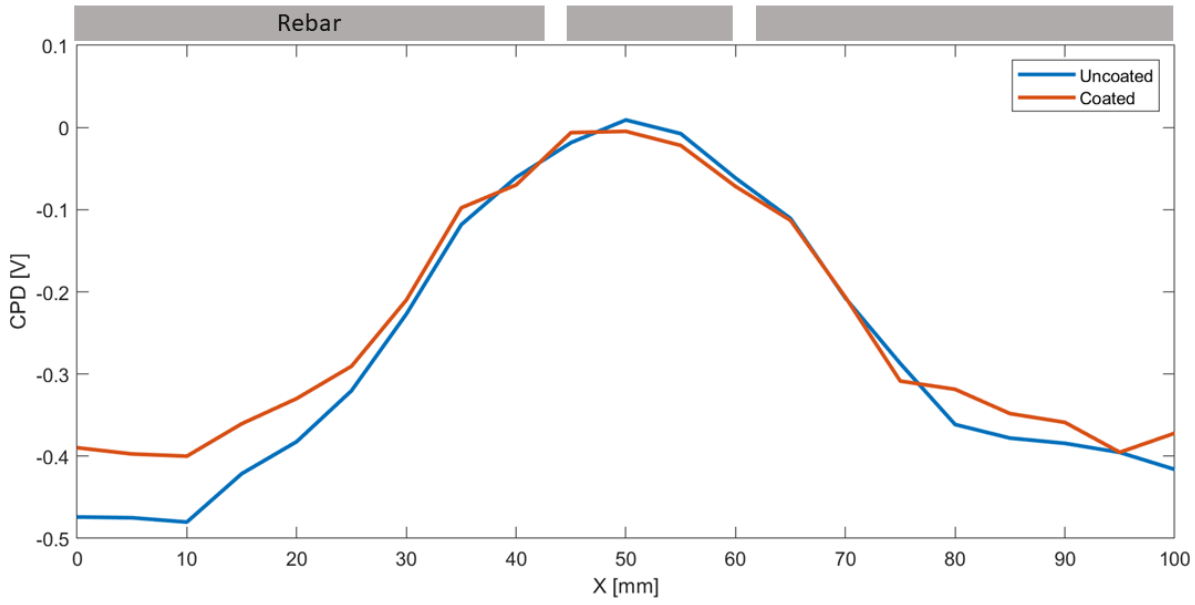

Figure 59: Cross-sectional profile of the two scans of the interrupted rebar test sample before and after coating with Bengalack with an applied voltage of 500mV. A drawing of the rebar matched with the scan locations is shown above.

No extensive analysis of this result seems necessary, as it is intended to show that even with a coating applied on the surface, measurements with the FKP can be carried out as expected. There is a slight difference in the maximum and minimum CPD values, as seen in Figure 59, but these could be due to several factors including humidity and temperature or the distance between the sensor and the test sample. Regardless of the small differences between the two, the features, e.g. the contrasts, seem well preserved.

3.4.6 Measurement uncertainty/spread for the FKP

As mentioned in section 2.4, quantifying the measurement uncertainty of the FKP is difficult at this time. The data acquired from the FKP is given as the average measured value in each spot, with no information about the spread. The following test was performed to at least get an idea of the reliability and repeatability of the FKP measurements, as well as to test a more remote connection between the FKP and the test sample. The potentiostat was connected between the small and large rebar pieces and the FKP was connected to the stainless steel mesh, i.e. no direct contact to the rebar pieces, as shown in Figure 60.

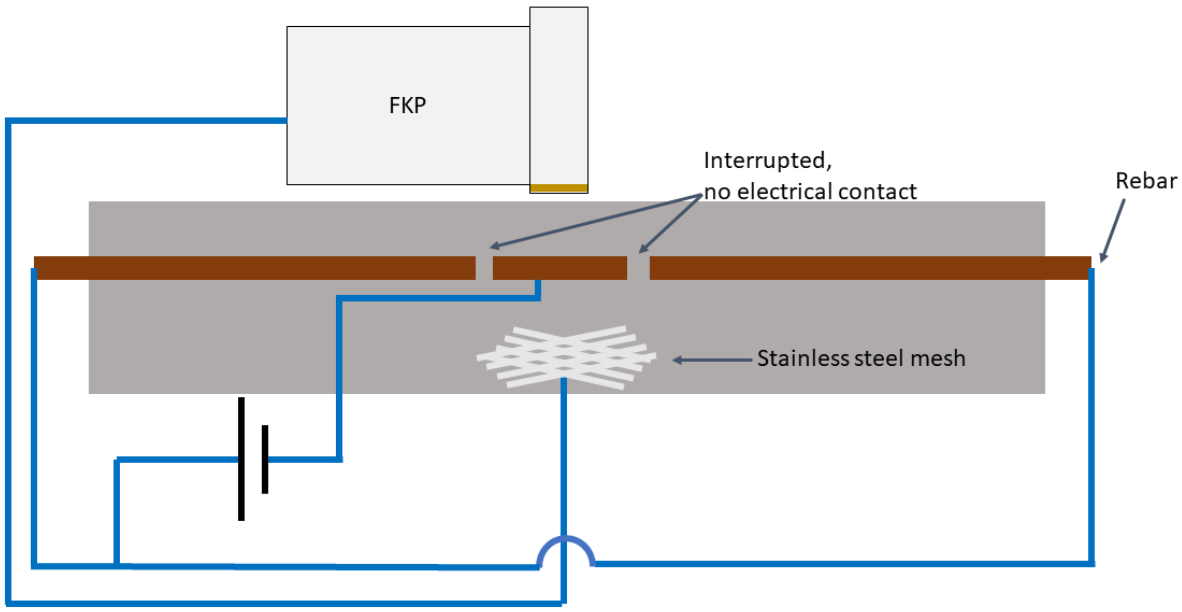

Figure 60:Schematic drawing of the setup of the interrupted rebar test sample. Small rebar piece polarized against the two larger rebar pieces. The FKP is only connected to the sample via the stainless steel mesh. The potentiostat is indicated by the battery symbol. The connections are different than in Figure 47 and Figure 52.

A total of 30 line scans were performed on the now coated interrupted rebar test sample, along the three rebar pieces. Five different voltages were applied across the rebar pieces, from -500mV to -100mV, each with five line scans performed over the course of around 30 minutes. Temperature and humidity were not recorded. Finally, the potentiostat was disconnected and another five line scans were performed. The average of the five line scans for each applied voltage are shown in Figure 61, with errors bars denoting the mean absolute error. For a plot with the raw data, see Appendix I – Raw data.

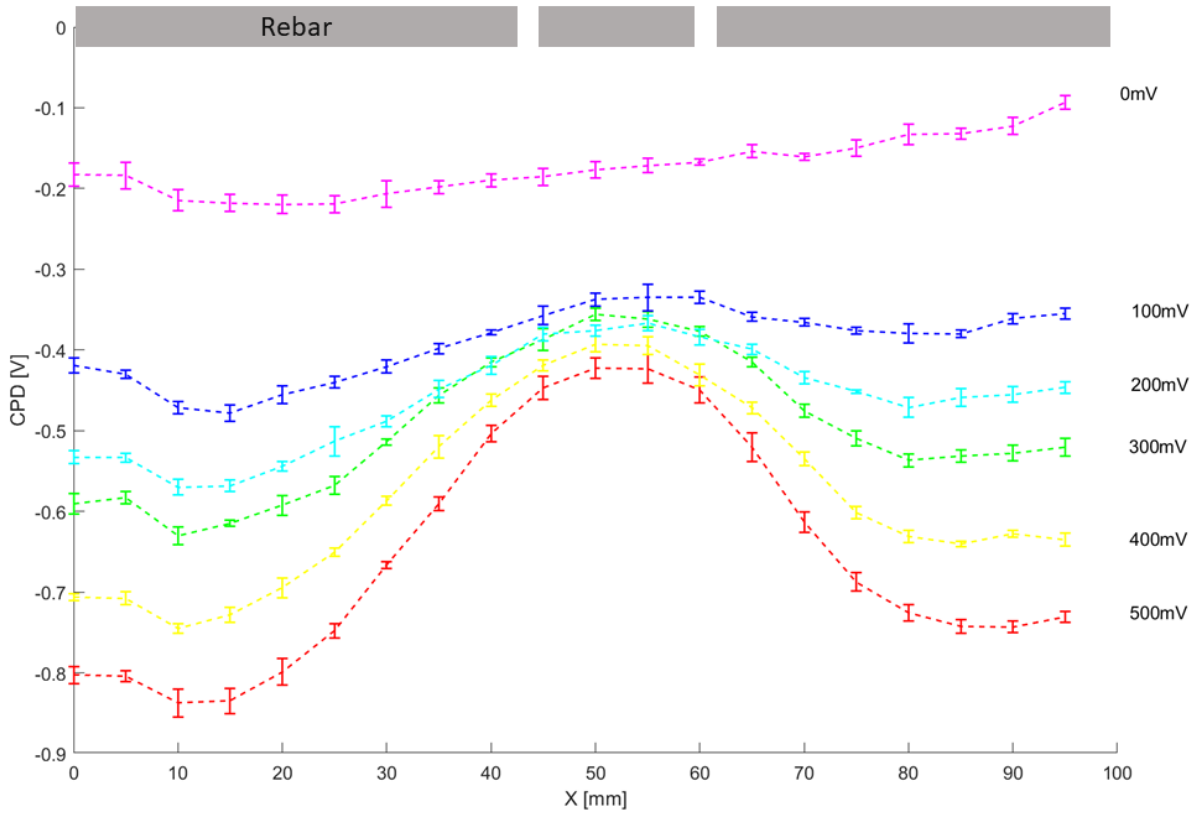

Figure 61:Five line scans along the three rebar pieces for 5 applied voltages from 500-0mV applied between the small rebar piece and the two larger pieces. A drawing of the rebar pieces matched with the scan locations is shown above.

These results show the following: i) There is some deviation between each individual line scan, but it is reasonably small, and the gradients seen are larger than the error. ii) Potential gradients of less than 100mV are still distinguishable by the FKP, confirming yet again that the FKP has no problem measuring through a coating. iii) The FKP can measure the potential drop over the rebar without direct contact to the rebar itself, any connection to the cement stone bulk will do.

The result from simulating the parallel capacitor model of the interrupted rebar presented in Figure 50 shows quite good agreement with the measurement data presented in Figure 61. Especially the baseline values for each applied voltage (the flat lines on each side of the peak in Figure 50) seem to match very well with the measurements, while the peaks are a little lower than the measured values. In order to further compare the experimental data with the theoretical model, the largest difference for each line (i.e. maximum value minus minimum value) was plotted for both. Again, the zero applied potential line is not included, as it provides no information from the theoretical model. The resulting plot (Figure 62) shows a good agreement between the experimental data and the theoretical model.

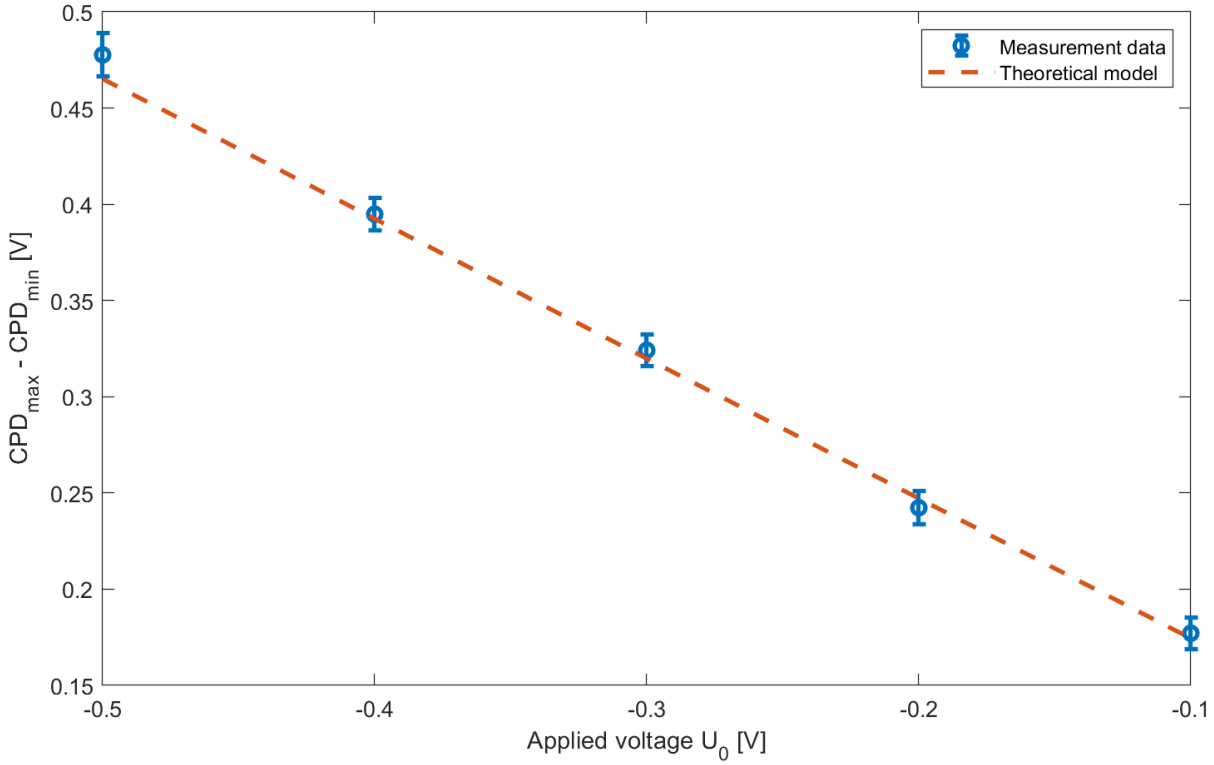

Figure 62: Comparison between the measurement data shown in Figure 61 (the zero applied voltage line is excluded, as the model would naturally return zero) and the theoretical model shown in Figure 50. There is a very good agreement between experimental and the theoretical model.

3.4.7 Summary – interrupted rebar test sample

The results from tests on the interrupted rebar test sample show the following:

- Connecting the FKP directly to the small rebar piece and polarizing the piece against the stainless steel mesh at a voltage comparable with what one would expect from corrosion, leads to a clear increase in measured CPD at the location of the small rebar piece. The increase in measured potential matches quite well with the expected values obtained from a simple theoretical model (section 3.4.2, equation (12)).
- Connecting the FKP directly to the small rebar piece and polarizing the piece against the two larger pieces, with voltages down to 50mV, produces a measurable potential gradient between the rebar pieces comparable to what one would expect from corrosion hot spots. This, along with the first point, shows that the FKP can be used to measure corrosion in a rebar embedded in cement stone.
- Applying a coating to the cement stone surface makes no difference to measurements with the FKP. This shows that the FKP could be used to measure corrosion under coated surfaces, which is a point of great importance.

- The FKP can measure the potential of a rebar embedded in cement stone with a remote ground, i.e. no direct electric contact to the rebar. This was shown by using the stainless steel mesh in the interrupted rebar test sample as a ground for the FKP while measuring potential gradients in the rebars from an externally applied voltage (see section 3.4.6).
- Modelling the FKP as a parallel plate capacitor produces a good agreement between experimental and theoretical data, although the model should be expanded to account for e.g. moisture conditions in the test sample.

4 Field tests

A number of field tests were performed over the course of the work presented in this thesis, both on concrete and non-concrete surfaces, with varying degree of success. While most of these tests did not produce much in the way of proving the FKP can detect corrosion, they did provide answers to some questions on the FKP's performance in the field. Plots of the measurement results will not be presented for all of these, but rather a description of what was done and the experience that was gained from it.

The first field test was performed early in the project, on a concrete building with heavily corroded rebars exposed by cracks in the wall, as shown in Figure 63. Different rebars were used as a grounding point for the FKP. Designed as a quick test, this did not produce much in terms of actual results as not everything was recorded. What was demonstrated, however, was that the FKP produced a quite steady and equal signal no matter which rebar was chosen as ground, giving the first indication that a remote ground might be used.

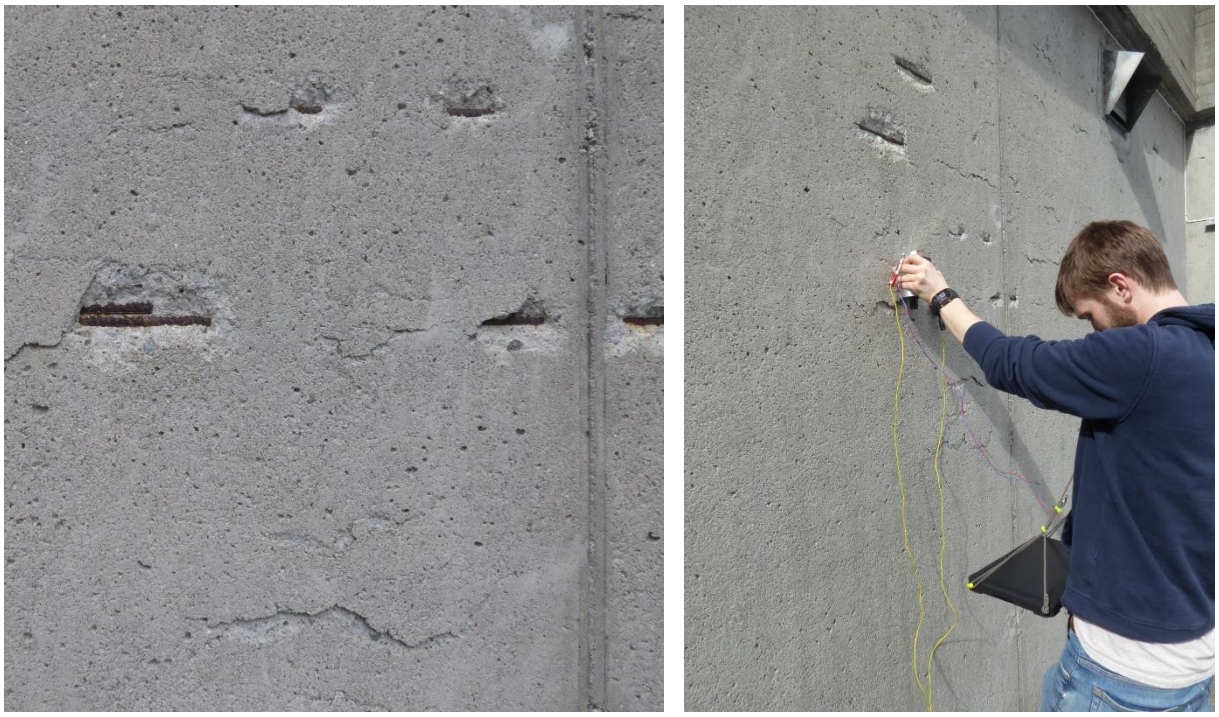

Figure 63: The first outdoors test of the FKP on a concrete wall with cracks and heavily corroded rebars. The FKP being controlled via Bluetooth from a tablet is shown in the picture to the right.

Another field test was performed just outside the NORCE building at Fantoft, with the aim of further investigating the use of a remote grounding point. A long rebar was hammered into the ground and connected by a wire to the FKP, as shown in Figure 64. The FKP was then used to measure in a single spot on cement test sample 3 (section 3.3.4), which was connected to the (actual) ground by burying the wire from the sample under the rocks seen in the picture.

Figure 64: Field test outside NORCE, Fantoft. With the aim of testing measurements with a remote ground, a rebar was hammered into the ground and connected to the FKP. The FKP was then tested on cement stone test sample 3, which was connected to ground via a wire buried under the stones seen in the picture, producing a steady signal.

This test showed once again that the FKP produces a steady signal even with a remote ground connection. The effect of the grounding was tested by disconnencting the wire, which led to a very noisy signal.

A field test to further demonstrate the use of remote ground and perhaps produce some corrosion measurements was performed in a parking house. The temperature during this test was around zero degrees celsius. The concrete floor of the parking house had some exposed, heavily corroded rebars. The FKP was connected to ground via a distant pole, as shown in Figure 65.

Figure 65: Field test in a parking house with corroded rebars on the concrete floor. The picture to the left shows the ground connection and the picture to the right shows the FKP and the measured area.

A 8x4 grid of 10x10mm^2 squares was drawn on the concrete floor, over the exposed rebar, and spot measurements were done. The grid and the resulting plot is shown in Figure 66. While the results shown might not indicate corrosion, there does seem to be a spike at A5 and C5 that matches the brown spots seen in the picture of the grid, however it is difficult to draw any conclusions from this alone. The measurements were again steady in each spot, showing that the FKP works with a remote ground connection. The FKP has also now been shown to work well even at low temperatures.

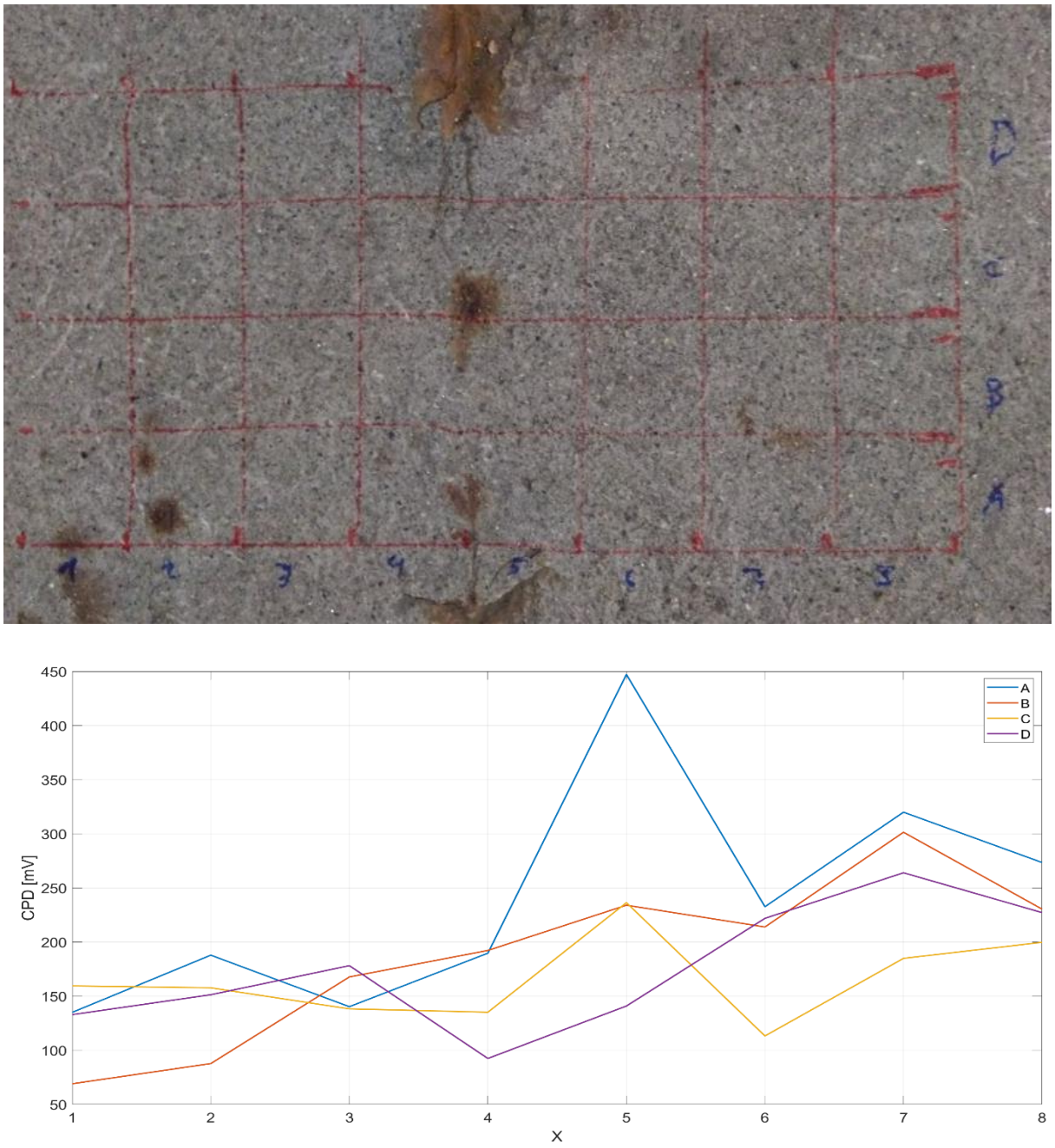

Figure 66: The 8x4grid marked on the parking house floor and the resulting plot from FKP spot measurements. Each line in the plot is one horizontal line (A, B, C, D) of the grid.

Two more field tests were carried out, on coated metal surfaces. One field test was on the inside of a tank at an oil terminal, shown in Figure 67, and the other was on the deck of "MS Miljødronningen", a research and conference vessel operated by Norges Miljøvernforbund (NMF), shown in Figure 69. The temperature was around zero degrees celsius in both field tests. Both field tests once again demonstrated that the FKP can be used in cold and humid conditions.

Figure 67: The FKP being used for measurements on the painted (and unpainted) metal surface on the inside of a large storage tank at an oil terminal.

The coating on the inside of the tank was unevenly applied and the thickness varied greatly. Paint sagging made the surface uneven, making it difficult to place the FKP steadily on the surface. The results in Figure 68 show large differences (sometimes several thousand mV) in the measured CPD values from one spot to the next. The exact reason for the large differences is not easy to pinpoint but it seems likely that the uneven coating surface is one of the main reasons, as moving the FKP mid measurement, even slightly, causes quite noisy signals. In other words, the FKP must be held steady for the duration of each measurement.

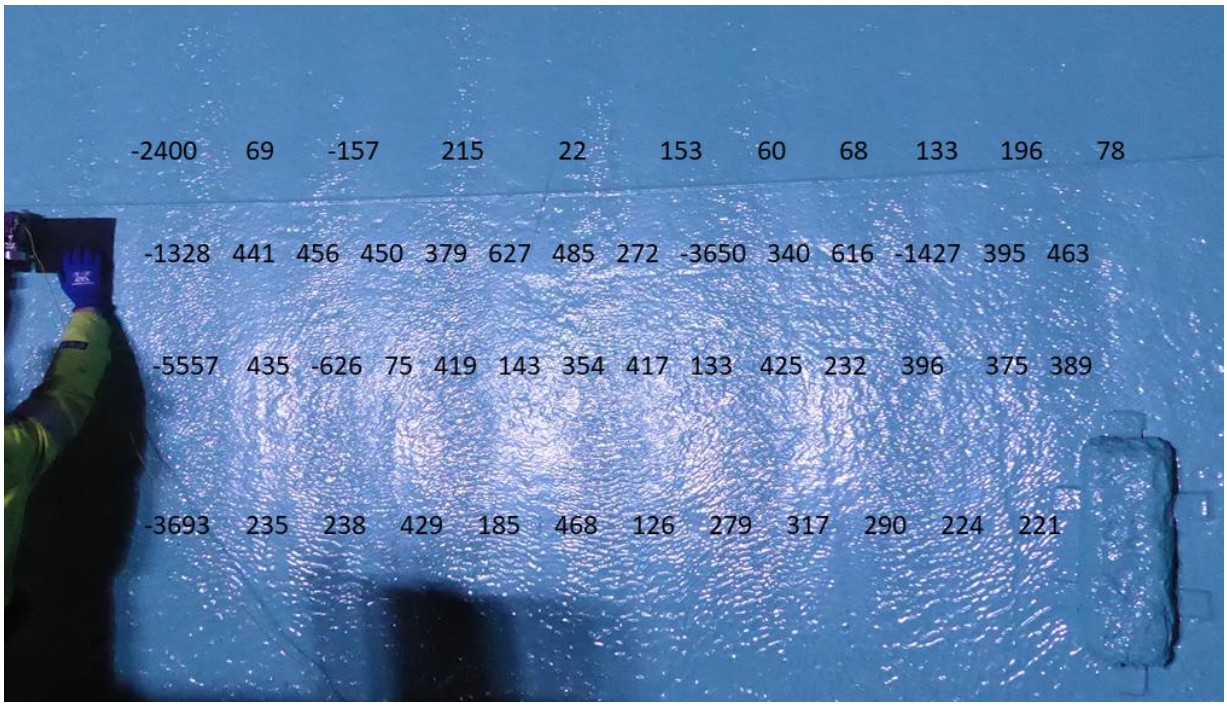

Figure 68: FKP measurements from a portion of the inside of the oil terminal tank. The measured values are presented in mV and are matched to the measurement location. Unusually high values of more than thousand mV are a result of the uneven surface making the FKP unsteady during the measurement.

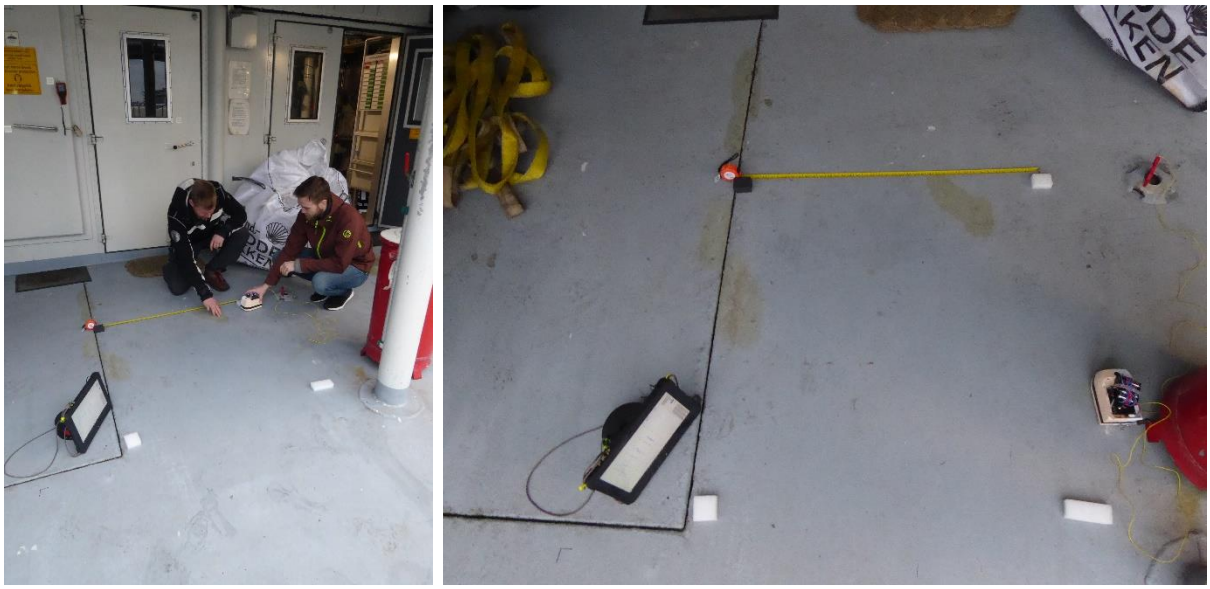

Figure 69: The FKP being used for measurements on the painted deck of MS Miljødronningen.

The results from the deck of MS Miljødronningen, shown in Figure 70, show reasonable values from the FKP, meaning values in the same range as what has been measured in the lab on other metal surfaces, normally in the range of tens-hundreds of mV. Potential gradients of more than 100mV are observed on the deck, which could indicate corrosion. There is however a lack of comparison with state-of-the-art inspection methods, as well as not enough knowledge on other

factors (coating thickness etc.) and their exact effect on the FKP, making it difficult to draw conclusions on the condition of the metal.

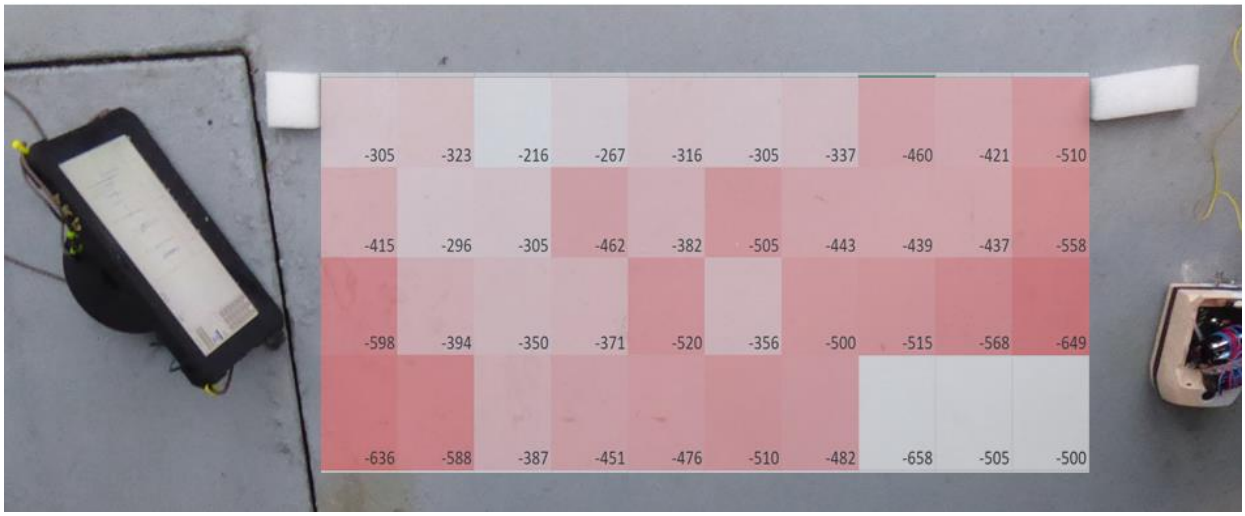

Figure 70: FKP measurements from the coated metal deck of MS Miljødronningen. The measured values are presented in mV and are matched to the measurement location. Potential differences of more than 100mV could indicate corrosion but could also be caused by other factors. More experimentation with the FKP is needed to know for sure.

As mentioned at the start of this chapter, the field tests did not provide any evidence for or against the detection of hidden corrosion in concrete. What the field tests did show, was that the FKP can be operated outside in the field, in cold and humid environments, and with a remote ground connection.

5 Conclusion

The application of Kelvin Probes to corrosion studies was introduced by Walsh and Sagüés in 2013 (see section 2.2.1). The Kelvin Probe in its original form is however unfit for field work, as discussed in section 2.2.3. The purpose of the project presented in this thesis was to evaluate a new technology based on the Kelvin Probe but designed as a field instrument, the Field Kelvin Probe (FKP), for inspection of reinforced concrete.

Proof that the FKP can distinguish between pristine steel and corroding steel and other defects was first acquired on non-concrete test samples, as presented in section 3.2. A comparison test showed a good agreement between the CPD measured with the FKP and the Scanning Kelvin Probe (Figure 21). Pristine steel and various defects were clearly distinguishable, even after a coating was applied to the metal surface (Figure 22 and Figure 23).

A total of 11 cement stone test samples were designed and made from scratch as described in chapter 3, including three generations of the new Cemwich design(section 3.3.8) and finally the interrupted rebar test sample (section 3.4). Experiments on the cement stone test samples showed that the FKP can:

- Detect various metal samples embedded in cement stone, at a depth of around 5-10mm. (All cement stone test samples described in section 3.3).
- Most likely distinguish between a pristine and a corroding rebar in cement stone (section 3.3.5). The measured difference was probably caused by corrosion in the steel, but other effect could be the cause making the result somewhat inconclusive, as discussed.
- Reproducibly detect and measure potential gradients in concrete of less than 100mV (potential gradients of 100mV or more are expected in a real corrosion scenario) (section 3.4.6). This was shown using the interrupted rebar test designed for the experiments presented in section 3.4.
- Very importantly: Measure CPD through a protective coating applied to the cement stone surface, with little to no effect on the measurement.
- Operate outside in a cold and humid environment, and with a remote ground connection.
- As an additional, unexpected result, the FKP could detect what was likely leakage from a CSE in cement stone, as discussed in section 3.3.4 and shown in Figure 32. This result seems to indicate that using a CSE to perform half-cell potential measurements contaminates the sample.

The results presented in this thesis give an indication to the potential of the Field Kelvin Probe. The potential gradients measured in the interrupted rebar sample, when a voltage was applied externally, match the expected potential gradients in a real corrosion scenario. It seems likely that more testing will reveal that the FKP can be a powerful handheld non-intrusive inspection tool and could eventually be the trusted technique for inspection of reinforced concrete.

6 Outlook

In this project, it was shown that the FKP can detect potentials and potential gradients in a cement stone test sample, which are similar to what one would expect to get from real corrosion. The next step is to be able to test the FKP in real corrosion. As a first step, experiments with a controlled corrosion process in concrete should be carried out. A possibility for this could be using a setup similar to the Cemwich (section 3.3.8), which had to be abandoned due to time

constraints but still seems worth pursuing. The key to making the Cemwich design work is finding a reliable connection (electrolyte bridge) between the concrete and the whole metal sample placed inside, so that there are no air gaps. A suggestion could be to use agar gel, which is conductive and can be shaped at will.

Having successfully detected controlled corrosion processes in concrete in the lab, the next step is to move to real field conditions, ideally somewhere where the conditions are known due to a prior industry standard inspection. This would allow for reliable comparison between the FKP and state-of-the-art inspection methods. In order for field tests to be performed properly, a slight redesign of the FKP to allow it to remain steady on rough surfaces during measurements may be necessary (this was a problem on the oil terminal tank interior, see chapter 4, Figure 67 and Figure 68). When the positioning system mentioned in section 2.3.4 is in place, repeated field measurements over time on corroding rebars could be easily performed to monitor the corrosion progression.

References

1. Revell, T. *Genoa bridge collapse – what went wrong and are other bridges at risk?* 2018 22.08.2018; Available from: https://www.newscientist.com/article/2176962-genoa-bridge-collapse-what-went-wrong-and-are-other-bridges-at-risk.
2. Øderud, H.T. and R.S. Nordahl. *Bro*. 2019 31.10.2019 [cited 2020 29.01]; Available from: https://snl.no/bro.
3. Koch, G., et al., *International measures of prevention, application, and economics of corrosion technologies study*. NACE International, 2016: p. 216.
4. NACE International. *NACE study estimates global cost of corrosion at $2.5 trillion annually*. 2016 08.03.2016; Available from: https://inspectioneering.com/news/2016-03-08/5202/nace-study-estimates-global-cost-of-corrosion-at-25-trillion-ann.
5. Guilbert, J.M. and C.F. Park, *The geology of ore deposits*. 1999, New York: W.H. Freeman.
6. Roberge, P.R. and Wiley InterScience (Online service), *Corrosion inspection and monitoring*, in *Wiley series in corrosion*. 2007, Wiley-Interscience,: Hoboken, N.J. p. viii, 383 p.
7. Gräfen, H., et al., *Ullmann's encyclopedia of industrial chemistry*. 2003.
8. Walsh, M.T. and A.A. Sagüés, *Kelvin probe electrode for contactless potential measurement on concrete : properties and applications*. 2013, University of South Florida. p. 1 online resource (73 pages).
9. Revie, R.W., *Uhlig's Corrosion Handbook 2nd edition*. Journal of applied electrochemistry, 2000. **30**(Part 10): p. 1189-1190.
10. Claisse, P.A., *Chapter 25 - Durability of concrete structures*, in *Civil Engineering Materials*, P.A. Claisse, Editor. 2016, Butterworth-Heinemann: Boston. p. 259-274.
11. Kessler, S. and C. Gehlen, *Reliability Evaluation of Half-Cell Potential Measurement Using POD*. Journal of Infrastructure Systems, 2017. **23**(2): p. B4016007.
12. Stern, H., D. Sadoway, and J. Tester, *Copper sulfate reference electrode*. Journal of Electroanalytical Chemistry - J ELECTROANAL CHEM, 2011. **659**: p. 143-150.
13. Giatec Scientific. *HALF-CELL POTENTIAL TEST*. 2016 [cited 2020 10.02]; Available from: https://www.giatecscientific.com/wp-content/uploads/2013/06/XCell-HalfCell-report.pdf.
14. Giatec Scientific. *iCor - Wireless NDT Corrosion Detection*. [cited 2020 08.03]; Available from: https://www.giatecscientific.com/products/concrete-ndt-devices/icor-rebar-corrosion-rate/.
15. Fahim, A., et al., *CEPRA: A new test method for rebar corrosion rate measurement*. ASTM International, 2018.
16. Wittstock, G., *Fundamentals of Electrochemistry Electrochmical Society Series, 2nd Edition Edited by Vladimir S Bagotsky*. Chemphyschem : a European journal of chemical physics and physical chemistry, 2006. **7**(9): p. 2022-2023.
17. Emmenegger, L.P. and A.A. Sagüés, *Kelvin probe electrode for field detection of corrosion of steel in concrete*. 2015, University of South Florida. p. 1 online resource (56 pages).
18. Thomson, W., *On a Method of Measuring Contact Electricity1*. Nature, 1881. **23**(598): p. 567-568.
19. Kelvin, L., *V. Contact electricity of metals*. The London, Edinburgh, and Dublin Philosophical Magazine and Journal of Science, 1898. **46**(278): p. 82-120.
20. Zisman, W.A., *A NEW METHOD OF MEASURING CONTACT POTENTIAL DIFFERENCES IN METALS*. Review of Scientific Instruments, 1932. **3**(7): p. 367-370.

21. Parker, J.H. and R.W. Warren, *Kelvin Device to Scan Large Areas for Variations in Contact Potential.* Review of Scientific Instruments, 1962. **33**(9): p. 948-950.

22. Mäckel, R., H. Baumgärtner, and J. Ren, *The scanning Kelvin microscope.* Review of Scientific Instruments, 1993. **64**(3): p. 694-699.

23. Stratmann, M. and H. Streckel, *On the atmospheric corrosion of metals which are covered with thin electrolyte layers—I. Verification of the experimental technique.* Corrosion Science, 1990. **30**(6): p. 681-696.

24. Yee, S., R.A. Oriani, and M. Stratmann, *Application of a Kelvin Microprobe to the Corrosion of Metals in Humid Atmospheres.* Journal of The Electrochemical Society, 1991. **138**(1): p. 55-61.

25. Rohwerder, M., *Scanning Kelvin Probe and Scanning Kelvin Probe Force Microscopy and their Application in Corrosion Science*, in *Corrosion Science and Technology: Mechanism, Mitigation and Monitoring*, U.K. Mudali and B. Raj, Editors. 2008, Taylor & Francis London, UK. p. 468-499.

26. Wikipedia contributors. *"Relative Permittivity"*. Wikipedia, The Free Encyclopedia 2019 [cited 2020 16.03]; Available from: https://en.wikipedia.org/wiki/Relative_permittivity.

Appendix I – Raw data

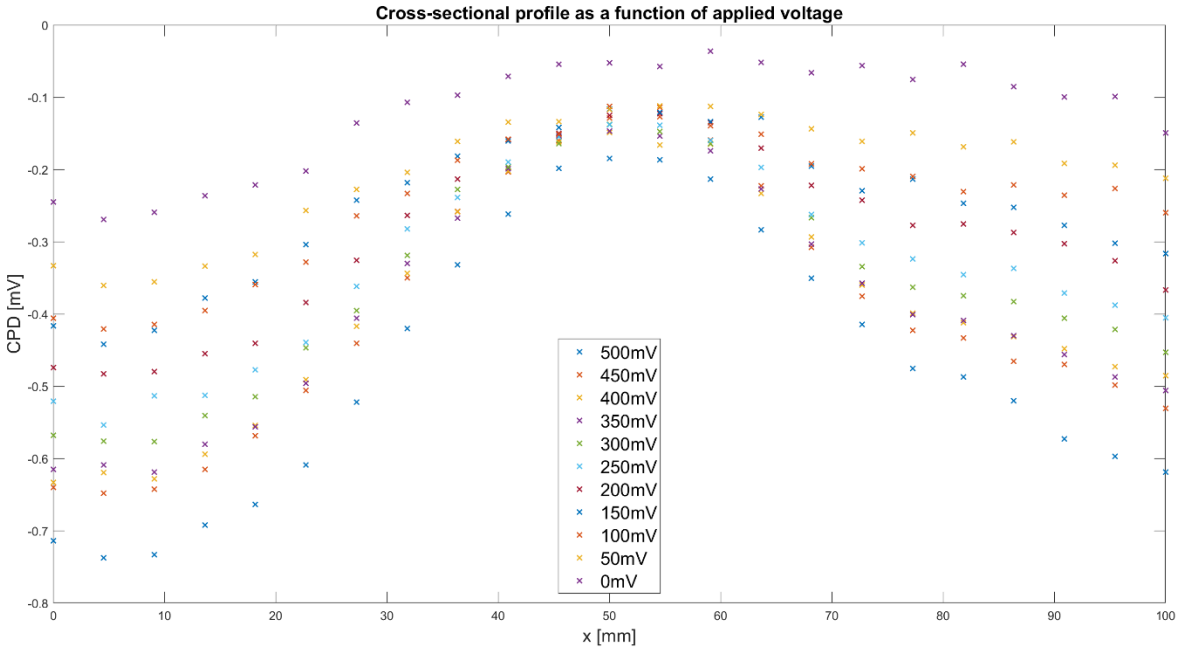

Figure 71: The non-normalized data from the stepwise applicatipon of voltage on the interrupted rebar sample. Normalized data in Figure 55.

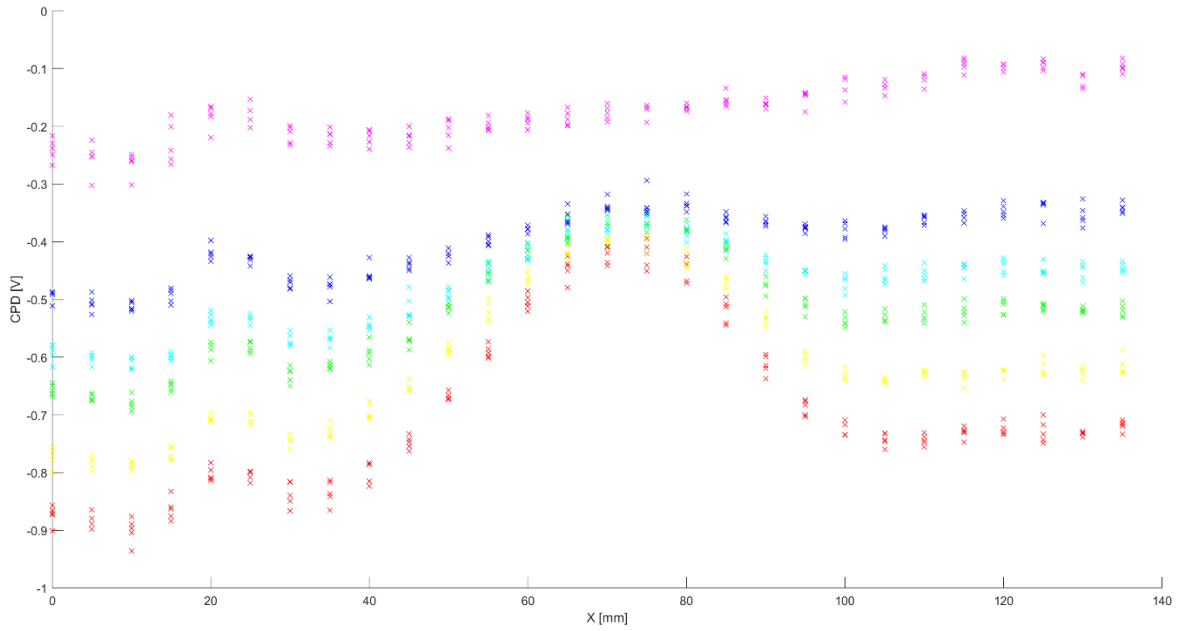

Figure 72: The raw data for the error plot in Figure 61.

Appendix II – Conference contributions

I presented parts of the results in this thesis as an oral contribution at Eurocorr 2019 in Seville, Spain. The conference paper is shown below.

A poster was also presented at Overflate 2019 in Bergen, Norway, using some of the results in this thesis. The poster is also presented in this section, after the Eurocorr conference paper.

Non-contact corrosion monitoring of steel reinforcement

Simen Kaasa HELLNER[1], Bodil HOLST[2], Eugen Florin TURCU[3]

[1]IFT / UiB, Bergen, Norway, Simen.Hellner@student.uib.no
[2]IFT / UiB, Bergen, Norway, bodil.holst@uib.no
[3]Norce, Bergen, Norway, fltu@norceresearch.no

Abstract
We have evaluated the possibility of monitoring the corrosion of concrete reinforcement (rebar) with the Field Kelvin Probe (FKP) technology.
Unlike the traditional half-cell potential mapping, which requires direct contact to the test sample and some surface preparation, the corrosion potential of the rebar is readily accessible to the FKP without any direct contact. Preliminary data show that the potential of steel is measurable from a distance of several mm.

Keywords
Kelvin Probes, contactless detection, rebar corrosion

Introduction

The condition of the steel reinforcement in concrete structures is critical for safe operation of large, load-carrying concrete structures. Road bridges, offshore oil and gas platform legs or concrete storage tanks rely on the steel reinforcement for preserving their structural strength. Norway alone has over 17 thousand road bridges of which many are concrete-based. Currently, the condition of the reinforcement is evaluated by measuring the potential of the steel versus a reference electrode (typically $Cu/CuSO_4$). This methodology is rather slow and it alters the chemistry of the concrete as it promotes the absorption of Cu^{2+} ions into the concrete bulk.

Instrumentation

Earlier work from Sagüés and Walsh [1] shows that a Kelvin Probe (KP) can successfully measure the corrosion potential of a steel test sample embedded in concrete. The laboratory testing was carried out with a modified KP on small concrete blocks. Nevertheless, the instrument envisioned by them lacks the compactness, robustness and the self-calibration ability which are be desirable for a field instrument.

The Field Kelvin Probe (FKP) does not have these limitations. The non-contact corrosion potential measurement of a steel is derived from the contact potential difference naturally established between the grounded FKP and the steel. The principle is well known from the widely used Scanning Kelvin Probes (SKP). In order for any KP to continuously generate data, the electrical capacity of the probe-sample must periodically vary in time. The SKP and FKP achieve this in different ways: 1) the SKP vibrates a fine tip on a direction perpendicular on the sample, with a displacement of several tenths of microns; 2) the FKP, rotates a probe around an axis parallel to the sample. The advantages emerging from a rotating probe are schematically presented in Fig. 1.

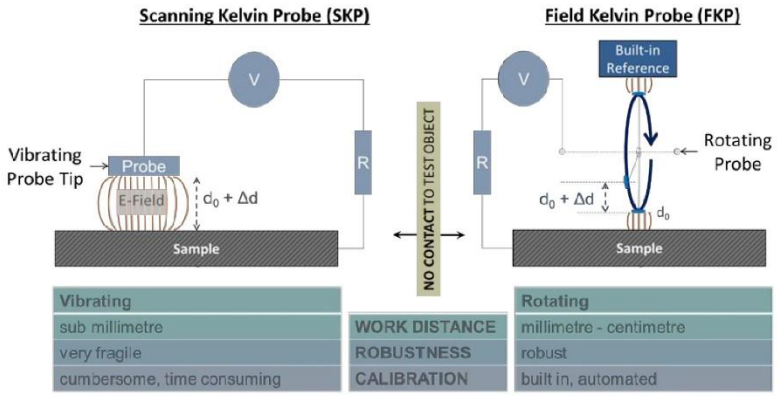

Fig. 1 – Operation principle and comparison of the vibrating and rotating probe. The rotation of the probe comes with several advantage: i) mechanical robustness, ii) larger sensor area and therefore larger work distance and iii) self-calibration / self-diagnosis.

The FKP operates at a rotation frequency of ca. 50 Hz. The three sensors on the probe (ca. 1 cm^2 each) are mounted on the shaft at 120° angular spacing (Fig. 2B). Thus, the actual signal frequency is three times higher than the actual rotation frequency. During a complete probe revolution, any of the sensor successively move over the test sample and the reference surface. The probe carrying the three sensors is shielded against electromagnetic noise and mechanical stress with a box-in-box system. The test sample connects periodically to the nearest sensor through the opening made in the metallic cases protecting the probe. A connection to the

reference is established within the inner box since the reference is mounted flash with it and at 180° from the opening to the test sample. Therefore, in one single rotation the FKP records and analyses six signal peaks (Fig. 2C) from which it determines the sample potential and evaluates the quality of the measurement. If the inner reference is calibrated against a potential benchmark (e.g. saturated $Cu/CuSO_4$ electrode), the FKP displays standard corrosion potentials.
A stable reference signal is crucial for the quality control of the FKP measurements. Figure 2D shows little variation of the reference signal (red curve) when the FKP is moved over various test samples. As expected, there are significant changes (ca. 1V) in the sample signal (blue curve). The noise level for both signals is ca. ±10 mV.
All data processing is performed on the FKP instrument. A low energy Bluetooth ensures a two-way communication between the FKP and a computer tablet. The test results are displayed in real-time, by the FKP app, on a tablet / laptop. Depending on the instrument configuration, one single measurement takes now up to 5 seconds but it is possible to speed it up at least by a factor of ten.

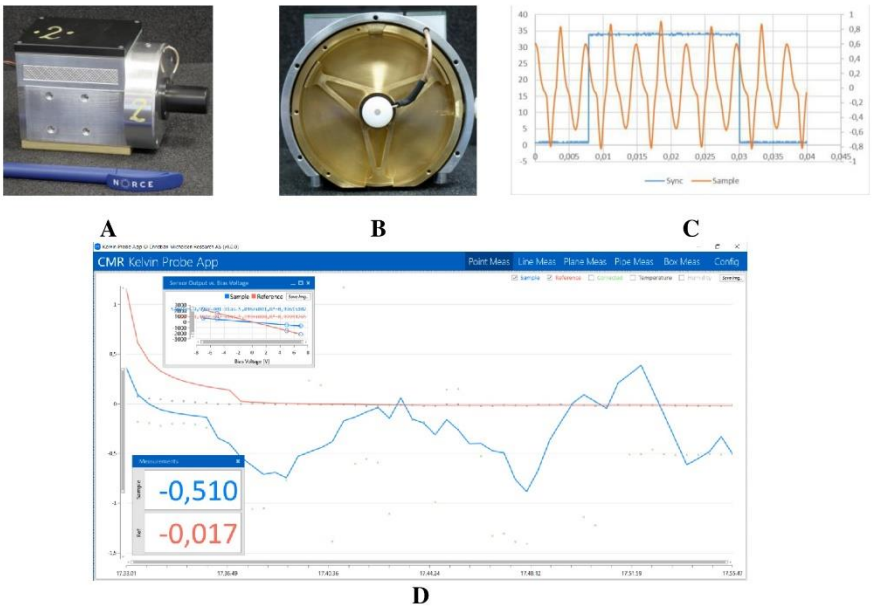

Fig. 2 – [**A**] An FKP ready for use. Size and weight without batteries 130x80x70 mm and 650 grams respectively. The black plastic cover conceals the Bluetooth antenna. [**B**] A front view of the FKP with the two cover plates removed. The three interconnected sensors are visible together with the built-in reference and the opening at the bottom. Sensor area is ca. 1 cm^2. [**C**] Oscillogram showing an example of sync (blue) and raw signals (orange). One revolution corresponds to one period of the sync signal and encompasses six raw signal peaks (three from the sample and three from the built-in reference). [**D**] Sample (blue) and reference (red) signals displayed on the FKP app. For this particular FKP demonstrator, both signals stabilize within 2-3 minutes from the start of the measurement. Large changes (ca. 1V) of the sample signal have no influence on the reference. Noise level for both signals is ca. 0.01 V.

Experimental

Test samples

Before attempting to ascertain the condition of a real rebar, we sought to test the FKP on samples with gradually increasing complexity, that is on samples with:
- steel sections larger than typical rebar (i.e. > 12 mm)
- different mortar / concrete compositions
- steel buried at various depths in the concrete
- different geometries / shapes.

All test slabs were prepared by pouring the mortar / concrete in rectangular frames in which one or several steel samples were fixed at predetermined depths (Fig. 3A). We have used an off the shelf cement mix and a quantity of water corresponding to the 1/7 of the cement mix. Electric wires connected to the steel samples ensured individual or grouped ground connections.

Measurements

The FKP can be used as a hand-held instrument or attached to a scanning device (Fig. 3A, B). In any case, the distance between the FKP sensor and the slab surface can be easily adjusted from ca 0.25 mm to 10 mm or higher. It must be noted however, that the signal strength drops as the distance increases.

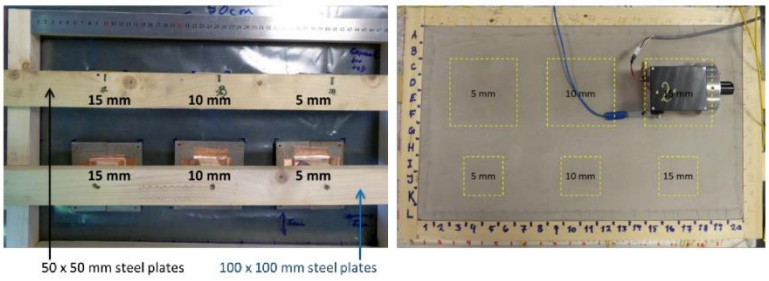

A

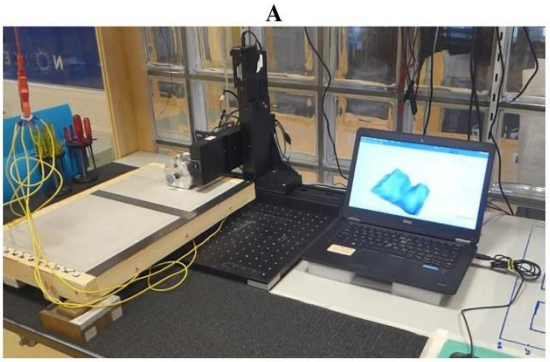

B

Fig. 3 – [**A**] Left: Preparation of the test sample. The steel plates fixed, at various depths in the frame (5, 10 and 15 mm). Right: Finished slab. An FKP is used manually to measure the steel plates. [**B**] A version of the FKP is mounted on a scanning XY stage. The laptop screen shows a partial 3D scan of the test sample.

Bare steel plates (with no visible rust) mounted at a depth of 5 mm are clearly visible in the 2D scan (Fig. 4). The FKP was positioned at 1 mm over the slab surface.

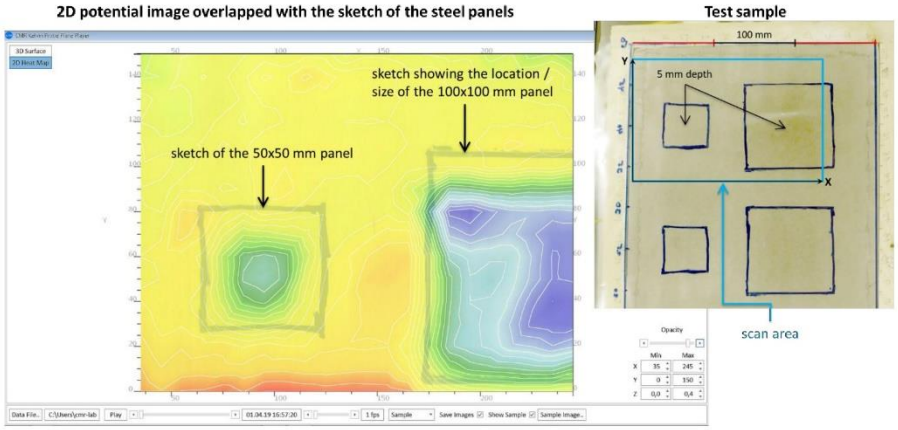

Fig. 4 – A 2D scan showing two steel plates. The 5 x 5 mm plate appears smaller than its actual size; this effect is caused by the rather high scanning step (10 mm).

By scanning embedded steel samples with certain rust patterns, we could demonstrate that the non-contact FKP measurement can differentiate the bare and rusted steel (Fig. 5). To create the rust pattern, the blast-cleaned steel plates were wetted, on predefined areas, with salt water (3.5% NaCl).

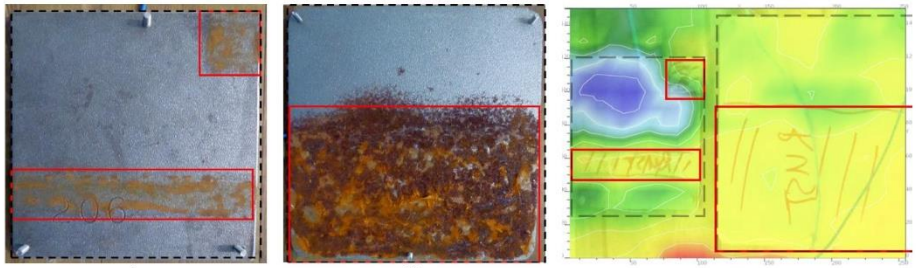

Fig. 5 – 2D scans of partly rusted steel plates. **[A]** and **[B]** The two plates with blast-cleaned and rusted areas. **[C]** An overlap of the 2D scan and the plates shows a good match between the rust boundaries and higher potentials (relative values). The red lines help identify the rusted areas within the 2D scan. Interrupted grey lines show plate boundaries.

To test the influence of sand (grain size ca. 3 mm) in the mortar composition, we have manufactured one slab with the following weight ratio: cement : sand : water = 2.8 : 1.2 :1.0. With the triangular shape of this steel sample (Fig. 6A) we tested the FKP's ability to detect small features on the sample. Figure 6 present the results of two scans performed over the same slab area: 2D scan in Fig. 6B was obtained with 3 mm scan steps and with the FKP sensor 3 mm from the slab; in Fig. 6C the step size was 10 mm scan steps with the sensor 10 mm from the slab surface. Surprisingly, the amount of details captured from a distance of 10 mm to the

slab (and 17 mm to the steel) makes the identification of the shape straightforward. However, the potential map losses contrast and thus the corroded areas become practically undistinguishable from the non-corroded steel.

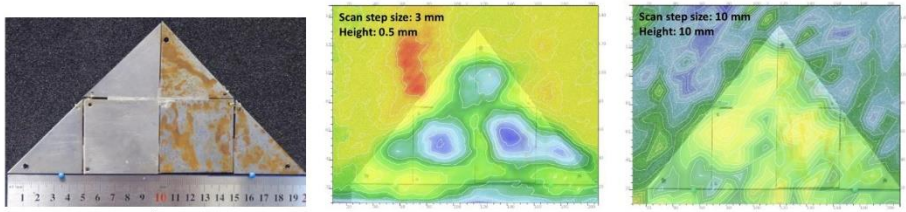

Fig. 6 – **[A]** A triangular steel sample with rust on one half. The FKP measured the sample with different scan step sizes and from different heights: **[B]** 3 mm steps and 0.5 mm above the slab. **[C]** 10 mm steps and 10 mm above the slab. The steel plate was located at a depth of 7 mm in the slab.

Discussion and outlook

Preliminary laboratory testing of the Field Kelvin Probe (FKP) suggest that such a technology can measure the electric potential of steel test samples embedded in mortar / concrete. The measurement is contactless and can be carried out even with the probe 10 mm above the concrete surface. A unique built-in reference system ensures the quality of the measured data.

More testing and refinements of the probe will be necessary to increase the measurement sensitivity and measurement speed. Although the instrument is already hand-held (Fig. 7), its size and weight could be farther reduced. An ergonomic design will make the outdoor utilisation easier and safer.

Fig. 7 – A possible way to deploy the FKP on real concrete structures. Here we show an attempt to measure a concrete wall with visible cracks along the rebars. The red-blue wire is used to power the *instrument (battery pack in the operator's* pocket). The yellow wire connects the FKP to the ground (i.e. one of the rebars).

References

1. A. A. Sagüés and M. T. Walsh, Corrosion Science, **56** (2012) 26-35.

Field Kelvin Probe – selected applications

Authors: Eugen Florin Turcu[a,b], Kjetil Daae Lohne[a,b], Inge Klepsvik[b], Gaute Lied[b], Simen Hellner[c]

Affiliation: [a] – INDIKEL AS / Norway, b – NORCE, c – UoB

Introduction

The Field Kelvin Probe (FKP) is a rugged Kelvin Probe for non-contact measurement/detection of surface potentials. For corrosion related applications, it can distinguish the bare metal from corroding and corroded (already rusted) surface. Its compact size enables hand-held operation in addition to the possibility to be interconnected in an FKP array.

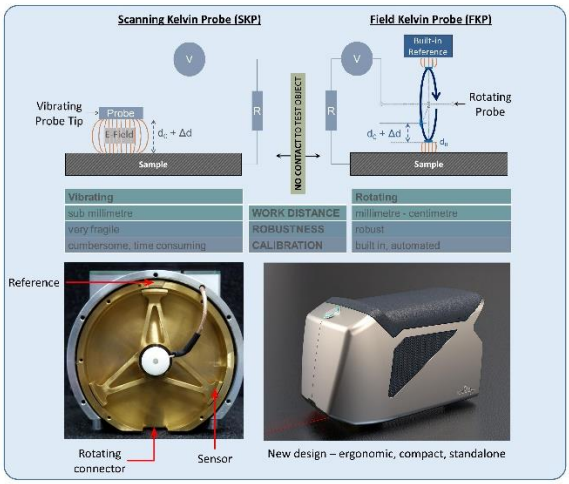

For easy FKP control and access to measurement data

Data storage & availability

All FKP data can be stored on the device. At the same time, all measured data can be accessed remotely, via a remote server.

FKP

This can be presented in real-time in an Excel sheet for example.

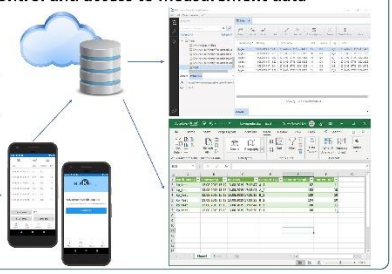

Examples of field test on coated vessels

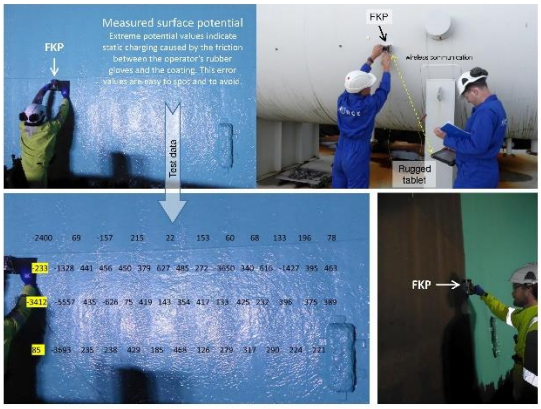

Technology GAP

Coated metallic surfaces often undergo (slow) corrosion which can results in delamination and blisters. When such tell-tale signs are noticeable, the damage to the metal can be significant, especially if the items have significant value (e.g. heritage objects) or when safety is at risk (e.g. OG installations, infrastructure). FKP detects the very onset of the corrosion thus allowing the preparation of the maintenance and repair.

Coated test sample with rust patterns

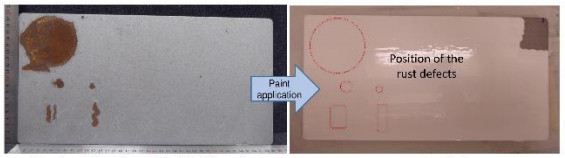

Blast cleaned steel panel (3x200x400 mm)
- surface profile 30-75 µm ; rust patterns

Protective coating – 2x Bengalack, DFT ca. 120 µm

FKP measurements through coating - 1

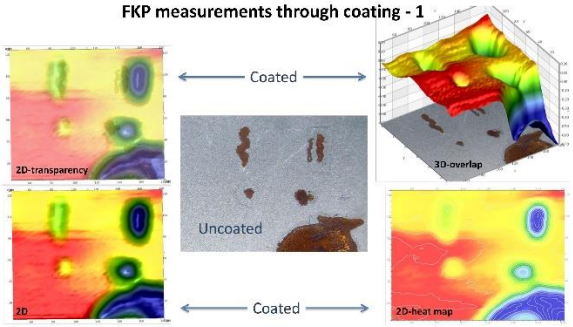

FKP measurements through coating - 2

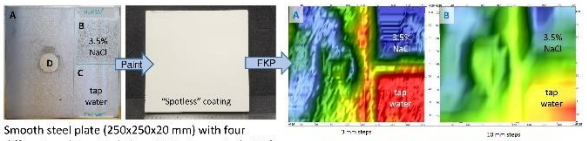

Smooth steel plate (250x250x20 mm) with four different regions: **A** pristine, **B**,**C** 2 x pre-rusted, **D** Pd

Scan detail level = f(step size): A 3 vs B 10 mm

Other applications

Internal corrosion
Mock-up to test the corrosion detection inside a pipe (lab trial)

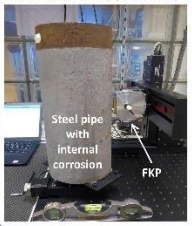

Corrosion on reinforcement
The FKP could replace the traditional half-cell electrode (outdoor test)

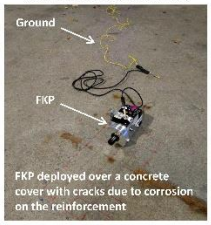

Historical heritage artefacts
Checking the condition of the patina on a bronze relief (indoor)

Outlook

- Decrease measurement time from 1 sec to 0.1 sec.
- Reduce size and weight of the hand-held FKP with ca. 50% - 75%.
- Enable the positioning system for accurate spatial and potential mapping of the test item.
- Produce and deliver FKP units to the R&D and industrial companies.